Contract No:

This document was prepared in conjunction with work accomplished under Contract No. 89303321CEM000080 with the U.S. Department of Energy (DOE) Office of Environmental Management (EM).

Disclaimer:

Sludge Batch 10 Flowsheet Testing with Non-radioactive Simulants

W. H. Woodham

A. M. Howe

M. J. Siegfried

September 2021

SRNL-STI-2021-00349, Revision 0

DISCLAIMER

Printed in the United States of America

Prepared for
U.S. Department of Energy

SRNL-STI-2021-00349
Revision 0

Keywords: *DWPF, REDOX, CPC*

Retention: *Permanent*

Sludge Batch 10 Flowsheet Testing with Non-radioactive Simulants

W. H. Woodham
A. M. Howe
M. J. Siegfried

September 2021

Savannah River National Laboratory is operated by Battelle Savannah River Alliance for the U.S. Department of Energy under Contract No. 89303321CEM000080.

REVIEWS AND APPROVALS

AUTHORS:

_____
W. H. Woodham, Chemical Flowsheet Development

_____
A. M. Howe, Chemical Flowsheet Development

_____
M. J. Siegfried, Chemical Flowsheet Development

TECHNICAL REVIEW:

_____
S. C. Hunter, Chemical Flowsheet Development, Reviewed per E7 2.60

APPROVAL:

_____
G. A. Morgan, Jr., Manager
Chemical Flowsheet Development

_____
F. M. Pennebaker, Director
Chemical Processing

_____
R. T. McNew, Manager
Flowsheet Development and Facility Integration

_____
T. H. Huff, Manager
DWPF Facility Engineering

ACKNOWLEDGEMENTS

The authors would like to thank the following personnel for roles played in the completion of this work:

- Meagan Kinard, Katherine Miles, Tyler Ellis, Daniel Jones, and Matt Alexander for their diligent work in executing the CPC demonstrations discussed herein
- Whitney Riley, Kandice Miles, and Kim Wyszynski for their efforts in performing analysis on the hundreds of samples submitted as a result of this program
- Matt Williams and John Pareizs for overseeing the calibration and operation of off-gas analytical equipment
- Holly Hall for coordinating the timing and colocation of experiments
- Dan Lambert and Chris Martino for their valuable insights in the preparation, execution, and documentation of these experiments

The authors would also like to express sincere gratitude to all of those who helped to navigate the especially challenging trials associated with conducting research during a pandemic. We live in exceptional times, and it is because of exceptional people that we are able to perform our work to the same standards of quality and accuracy that have come to be expected of SRNL.

To all of you, we wish to say “Thank you”.

EXECUTIVE SUMMARY

Fourteen Chemical Processing Cell (CPC) simulations were performed with nonradioactive sludge simulants at the Aiken County Technology Laboratory in Aiken, SC. Four of these experiments were performed with Tank 51 sludge simulant. The remaining ten were performed with Tank 40 sludge simulant. The purpose of these experiments was to elucidate the chemistry and characteristics of Sludge Batch (SB) 10 as anticipated in the Defense Waste Processing Facility (DWPF). Experiments were performed at acid stoichiometries between 76% and 138% of the Koopman Minimum Acid requirement (85% - 144% of the Hsu acid requirement) and at REDuction/OXidation (REDOX) targets between 0.1 and 0.3. Testing examined the impact of coupled operations and sludge-only operations during Sludge Receipt and Adjustment Tank (SRAT) and Slurry Mix Evaporator (SME) processing at both design basis and nominal boilup rates.

The following conclusions are made as a result of this testing. Conclusions applicable to only one sludge type (Tank 40 or Tank 51) are indicated as needed.

- Acid stoichiometries as low as 76 % KMA (86% Hsu) are too low to effectively process SB 10 sludge. This stoichiometry leads to rheologically thick SRAT products that are prone to fouling, poor heat transfer, and poor mixing (Tank 51 sludge).
- The concentration of glycolate in condensates being sent to the Slurry Mix Evaporator Condensate Tank (SMECT) is expected to be <50 mg/L.
- Peak hydrogen generation rates observed in SB 10 testing are 3.90×10^{-4} lb h^{-1} and 6.04×10^{-4} lb h^{-1} during SRAT and SME processing, respectively. These values are well below the proposed SRAT and SME DWPF limits of 2.4×10^{-2} lb h^{-1}.
- CH_4 was observed during SB 10 simulant testing. Peak CH_4 production was shown in one experiment to coincide with the SRAT dewater stage of CPC processing. The appearance of CH_4 was confirmed by GC and FTIR. The presence of CH_4 has not been shown to be representative of expected CPC processing at the DWPF. Furthermore, observed concentrations of CH_4 (<100 ppm) do not indicate flammability hazard.
- Coupled operations processing may be responsible for a departure from previously observed glycolate destruction factors from SRAT processing, yielding a melter feed that is more glycolate-rich than would be expected in sludge-only processing (Tank 40 sludge).
- An assumed steam stripping factor of 750 g H_2O per g Hg appears to be adequate to achieve Hg concentration targets of 0.8 and 0.45% of total solids in SRAT and SME products, respectively.
- Methylmercury was observed during the SRAT and SME cycles. Evidence suggests that this reaction occurs in the reaction vessel itself, not exclusively downstream in condensate collection vessels. Furthermore, concentrations in condensates appear to be related to Hg concentrations in sludge.
- REDOX predictions made by the Jantzen equation correlate linearly with REDOX measurements in SB 10, indicating qualitative validity.
- No NH_4^+ was noted in the performance of SB 10 simulant experiments, indicating a lack of ammonia production during CPC processing.
- Acid stoichiometries greater than 100% and less than 110% (104% - 115% Hsu) are expected to yield an optimal yield stress during SRAT processing (Tank 40 sludge).
- Acid stoichiometries less than 110% (115% Hsu) are expected to yield an optimal viscosity during SRAT processing (Tank 40 sludge).
- Antifoam Y-17112 mitigated foaming in all SB 10 simulant experiments with no detectable evolution of antifoam degradation products.

The following recommendations are made as a result of this testing.

- SRNL may benefit by investigating alternative methods of heating to allow for maximum concentration of dilute sludge batches in future SB studies.
    - The SRNL Shielded Cells qualification experiment is expected to target lower total solids during SRAT and SME processing, so over-concentration is not anticipated.
- Testing in the SRNL Shielded Cells should include capabilities to quantify methylmercury in liquid samples and methane in gas samples. Laboratory personnel should take sufficient sample to ensure adequate organomercury analyses and handle organomercury samples according to best practices.
    - Upon completion, organomercury results from the Shielded Cells qualification experiment should be compared to results obtained from simulant testing to determine similarities.
- SRNL should add glycolate at the beginning of future SRAT experiments (either as a trim chemical or as part of simulant development) to allow for an understanding of glycolate volatility during caustic boiling (recommended for Tank 40 sludge).
- Future CPC tests should include additional methylmercury analysis to assist in the understanding and closure of organomercury mass balances and amounts.
- SB 10 REDOX measurements should be compared against previous SB data sets to determine if changes to REDOX prediction methodology are merited.
- SRNL should investigate methods to determine Hg concentration and speciation in off-gas leaving the CPC condenser train.
- An acid stoichiometry of 105% is recommended for initial SB10 processing with Tank 40 material in the DWPF. At this stoichiometry, the glycolate destruction factor for coupled operations and sludge-only operations are expected to be 11.8% and 27.2%, respectively. At this stoichiometry, nitrite-to-nitrate conversions are expected to be between 8% and 94% (recommended for Tank 40 sludge).
- If future operational changes are made to increase the sludge solids output from SWPF, a separate investigation into the impacts of this increased sludge solids concentration on CPC chemistry should be performed.
- Additional rheology data gathered during SB 10 simulant testing should be documented and compared with rheological measurements that will be performed in the SRNL Shielded Cells (recommended for Tank 40 sludge).
- Additional SB 10 simulant samples should be submitted for methylmercury analysis to better elucidate the mechanism of methylmercury formation.
- SB 10 processing should be conducted with the antifoam addition strategy developed by Lambert.

TABLE OF CONTENTS

LIST OF TABLES

LIST OF FIGURES

LIST OF ABBREVIATIONS

ACTL	Aiken County Technology Laboratory
ADP	Antifoam Degradation Product
ARP	Actinide Removal Process
CPC	Chemical Processing Cell
CS	Calcined Solids
CSSX	Caustic Side Solvent Extraction
CSTF	Concentration, Storage, and Transfer Facilities
DAC	Data Acquisition and Control
DI	Deionized
DSA	Documented Safety Analysis
DWPF	Defense Waste Processing Facility
ELN	Electronic Laboratory Notebook
FAVC	Formic Acid Vent Condenser
FT-IR	Fourier Transform Infrared Spectroscopy
GC	Gas Chromatography
HMDSO	Hexamethyldisiloxane
IC	Ion Chromatography
ICP-AES	Inductively Coupled Plasma Atomic Emission Spectroscopy
IS	Insoluble Solids
KMA	Koopman Minimum Acid
LWO	Liquid Waste Operator
M&TE	Measuring and Test Equipment
MCU	Modular Caustic Side Solvent Extraction Unit
MS	Mass Spectrometry
MS&E	Measurement Systems and Equipment
MST	Monosodium Titanate
MWWT	Mercury Water Wash Tank
PRA	Percent Reducing Acid
PSAL	Process Science Analytical Laboratory
RCT	Recycle Collection Tank
SAC	Safety Administrative Control
SAM	Sensing and Metrology
SB	Sludge Batch
SCFM	Standard Cubic Feet per Minute (21.11 °C, 1 atm)

SEFT	Strip Effluent Feed Tank
SME	Slurry Mix Evaporator
SMECT	Slurry Mix Evaporator Condensate Tank
SRAT	Sludge Receipt and Adjustment Tank
SRE	Sodium Reactor Experiment
SRNL	Savannah River National Laboratory
SRR	Savannah River Remediation
SRS	Savannah River Site
SS	Sludge Solids
SWPF	Salt Waste Processing Facility
TIC	Total Inorganic Carbon
TMS	Trimethylsilanol
TOC	Total Organic Carbon
TS	Total Solids
TSR	Technical Safety Requirement
TTR	Technical Task Request

1.0 Introduction

The Savannah River Site (SRS) Liquid Waste Operator (LWO) Savannah River Remediation (SRR) has requested that Savannah River National Laboratory (SRNL) perform laboratory-scale simulations of the Defense Waste Processing Facility (DWPF) Chemical Processing Cell (CPC) operations to support development of Sludge Batch (SB) 10 under the nitric-glycolic flowsheet.[1-3] CPC simulations are conducted with nonradioactive sludge simulants and are performed to elucidate the processing characteristics of the Sludge Receipt and Adjustment Tank (SRAT) and Slurry Mix Evaporator (SME) cycles employed in melter feed pretreatment.

SB 10 will be a landmark sludge batch for a few reasons. First, it is the first sludge batch that will be executed in its entirety concurrently with operations in the Salt Waste Processing Facility (SWPF). While CPC simulations coupled with salt waste projected waste streams have been performed in the past (such as streams associated with the Modular Caustic Side Solvent Extraction (CSSX) Unit (MCU) and the Actinide Removal Process (ARP)),[4] the scale of projected SWPF operations are expected to necessitate a shift in DWPF operations such that the majority of SB 10 processing will be performed under coupled processing.

Furthermore, SB 10 will be the first sludge batch executed at the DWPF completely under the nitric-glycolic flowsheet. The nitric-glycolic transition is expected to be carried out near the end of SB9. By the time SB 10 processing begins, the facility will be beyond the transition state and fully under the nitric-glycolic flowsheet. Additionally, SB 10 will be the first sludge batch operated entirely with the support of the new antifoam agent Y-17112 from Momentive Performance Materials. In previous sludge batches (up to and including SB 9),[5] Antifoam 747 has been used to mitigate foaming in the CPC. While Antifoam 747 is an effective antifoam for brief periods of time in the CPC, it is not chemically stable in the extreme pH ranges encountered during processing. This instability leads to increased antifoam addition and the presence of flammable volatile organic compounds.[6] Current DWPF flammability constraints account for the production of these flammable species. SB 10 will be the first batch in which the impacts of these volatile organic compounds may be reconsidered under the nitric-glycolic DSA.

Finally, SB 10 includes the remainder of the waste from the Sodium Reactor Experiment (SRE) into DWPF processing. Small amounts of SRE material were transferred from H-canyon into Tank 40 during SB 9; however, the amounts transferred into SB 9 were sufficiently small to avoid the need of additional manganese poison. The amounts of SRE transferred to Tank 51 for SB 10 preparation are much larger, such that sufficient manganese was added to poison the additional fissile load. The addition of this manganese triggered the generation of two Technical Task Requests (TTRs) from SRR; a first to develop the SB 10 flowsheet,[1] and a second to develop an SRE simulant capable of modifying Tank 51 and Tank 40 simulants to account for differences introduced by SRE material.[2]

To satisfy the requirements of these TTRs[1-2] and other ongoing work, fourteen CPC simulations were performed by SRNL at the Aiken County Technology Laboratory (ACTL). Ten of these experiments were performed using Tank 40 sludge simulant to better elucidate the anticipated conditions at the DWPF under SB 10 using both a coupled flowsheet and a sludge-only flowsheet.[7] The remaining four experiments were performed with Tank 51 sludge simulant to provide insight into the expected characteristics of the SRNL shielded cells qualification experiment.[8]

2.0 Experimental Procedure

2.1 Simulant Preparation

2.1.1 Tank 40/51 Sludge Simulants

SB 10 sludge simulant was prepared using the same procedures employed in previous testing campaigns.[4] Generally, preparation of Tank 40 and Tank 51 sludge simulants follows the steps listed below:

1. Precipitation of MnO_2 using sodium permanganate and manganese nitrate – sodium permanganate and manganese nitrate are combined at fixed volumetric rates at a temperature of approximately 40 °C to control particle size, resulting in a slurry mixture of MnO_2 in strong nitric acid.
2. Continuous coprecipitation of metal nitrates with sodium hydroxide – soluble metal nitrates are added to the acidic MnO_2 slurry generated in step 1. This stream is then combined with sodium hydroxide in a continuously-stirred tank reactor, resulting in a caustic slurry of insoluble metal oxides and metal hydroxides and a supernatant phase rich in sodium nitrate and sodium hydroxide (see Figure 2-1).
3. Conversion of soluble hydroxides to insoluble carbonates – sodium carbonate is added to precipitate insoluble carbonate species to limit losses during washing.
4. Supernatant phase washing to reduce sodium molarity – caustic slurry from step 3 is allowed to settle and the supernatant phase is decanted as much as practical. Inhibited water (0.01 M NaOH + 0.01 M $NaNO_2$) is then added to dilute salt component concentrations to below targeted values.
5. Addition of insoluble trim components – final additions of insoluble solid species (e.g., SiO_2, TiO_2, etc.) to match target solid compositions.
6. Addition of soluble trim components – final additions of soluble salt components are added to match target supernatant concentrations.

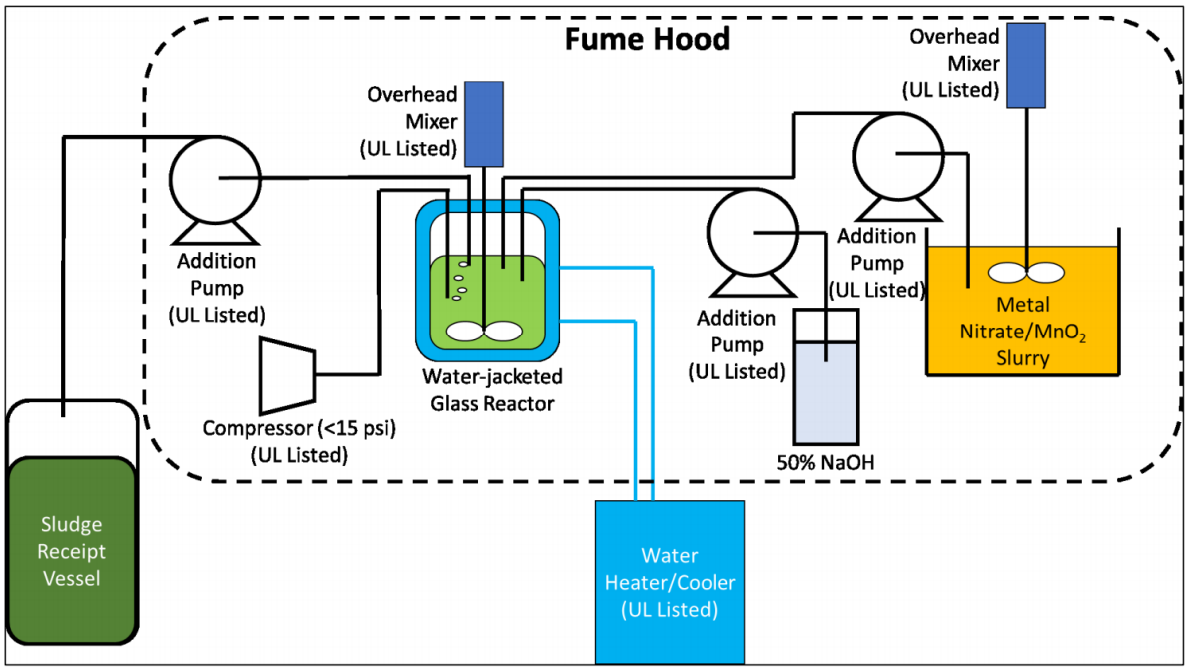

Figure 2-1. Diagram of Continuously-Stirred Tank Reactor Used in Simulant Preparation.

Amounts of chemicals added and phase removals made at each step of simulant preparation are dictated by the concentrations and solids targets specified in SB 10 projections provided by SRR.[9] Target and measured

concentrations of Tank 40 and Tank 51 sludge simulants are given in Table 2-1. Note that the values reported in Table 2-1 are the results of single samples and therefore have no applicable standard deviation. Target concentrations are derived from SRR projections.

Table 2-1. Tank 51 and 40 Sludge Simulant Compositions.

Parameter	Tank 51		Tank 40	
	Target	Measured	Target	Measured
wt% Insoluble Solids (IS)†	9.28	8.68	9.45	8.39
wt% Total Solids (TS)††	14.25	14.50	14.49	13.90
wt% Calcined Solids (CS)†††	9.77	11.00	10.52	10.60
Slurry Density (g/mL)	NR	1.119	NR	1.1102
Supernatant Density (g/mL)	NR	1.047	NR	1.0477
Al (wt% of CS)	1.84E+01	1.90E+01	1.63E+01	1.78E+01
Ba (wt% of CS)	7.93E-02	8.89E-02	8.29E-02	<1.00E-01
Ca (wt % of CS)	8.71E-01	1.23E+00	9.87E-01	1.18E+00
Cr (wt % of CS)	2.73E-01	4.61E-01	2.38E-01	3.40E-01
Cu (wt % of CS)	4.90E-02	4.92E-02	4.73E-02	<1.00E-01
Fe (wt % of CS)	1.34E+01	1.60E+01	1.51E+01	1.70E+01
K (wt % of CS)	8.50E-02	3.47E-02	9.41E-02	<1.00E-01
Mg (wt % of CS)	3.22E-01	3.58E-01	3.14E-01	3.39E-01
Mn (wt % of CS)	2.62E+00	3.40E+00	3.56E+00	4.31E+00
Na (wt % of CS)	2.16E+01	1.74E+01	2.14E+01	1.82E+01
Ni (wt % of CS)	4.34E-01	5.10E-01	6.46E-01	6.39E-01
S (wt % of CS)	5.91E-01	4.51E-01	5.38E-01	2.62E-01
Si (wt % of CS)	6.18E-01	8.02E-01	8.49E-01	2.85E-01
Zn (wt % of CS)	2.00E-02	NR	2.45E-02	<1.00E-01
Zr (wt % of CS)	2.56E-01	2.74E-01	2.10E-01	2.19E-01
Na^+ (M supernatant)	9.50E-01	9.87E-01	9.48E-01	1.01E+00
HCO_2^- (M supernatant)	NR	<2.22E-03	NR	<2.22E-03
Cl^- (M supernatant)	1.03E-03	<2.82E-03	1.06E-03	<2.82E-03
NO_2^- (M supernatant)	2.15E-01	1.96E-01	2.30E-01	1.94E-01
NO_3^- (M supernatant)	1.16E-01	1.71E-01	1.21E-01	1.19E-01
SO_4^{2-} (M supernatant)	1.76E-02	1.66E-02	1.64E-02	1.37E-02
$C_2O_4^{2-}$ (M supernatant)	6.53E-03	6.49E-03	1.04E-02	7.00E-03
PO_4^{3-} (M supernatant)	2.23E-04	<1.05E-03	3.69E-04	<1.05E-03
OH^- (M supernatant)	4.31E-01	2.58E-01	3.73E-01	2.19E-01
CO_3^{2-} (M supernatant)	3.78E-02	3.07E-02	5.66E-02	3.61E-02
Base Equivalents (M Slurry)	NR	7.11E-01	NR	5.85E-01

†Insoluble Solids is a calculated value that is dependent on the measured total solids and dissolved solids.
††Total Solids are those solids remaining in the sludge mixture after heating to a sustained temperature of 110 °C.
†††Calcined Solids are those solids remaining in the sludge mixture after heating to a sustained temperature of 1100 °C.
NR = Not Reported.

The data in Table 2-1 indicate reasonable agreement between Tank 40 and 51 projections (shown as target concentrations) and measured values. Per agreement with SRR, priority for simulant concentration targeting was given to total solids loadings such that simulant sludges should most closely match total solids targets. Given that radioactive waste is expected to contain significant amounts of uranium and thorium (not present in sludge simulants), the preference to match total solids targets inherently leads to higher concentrations of insoluble metals (e.g., Fe, Mn) and lower concentrations of soluble metals (e.g., Na) in simulant materials.

The lower concentrations of hydroxide observed in the prepared simulant are expected due to the increased solubility of aluminum. As both hydroxide and aluminum are expected to consume acid, this difference is believed to be negligible. The proximity of measured sodium supernatant concentrations to the targets indicates that washing endpoints were achieved successfully.

2.1.2 Monosodium Titanate/Sludge Solids Simulant

Monosodium Titanate (MST)/Sludge Solids (SS) simulant is used to simulate the addition of waste streams from the monosodium titanate strike and filtration process at SWPF. Under the ARP pilot program, titanate strikes were not employed in the recent sludge batches, resulting in a mostly homogeneous stream of salt solution waste being added to the CPC during treatment. However, SWPF is expected to operate with MST strikes at the beginning of SB 10. Therefore, it was necessary to add MST solids to coupled operations experiments to understand the impact of these solids on processing and rheology. Note that the amount of sludge solids expected in this waste is small compared to the amount of MST solids. For this reason, sludge solids were omitted in this simulant material. If the amount of SS in this waste stream is increased in future operations, a separate investigation into the impact of increased SS on CPC chemistry should be performed.

The scale of CPC experiments at SRNL (<4 L) is too small to adequately reproduce the slurried MST flow observed at DWPF with both representative solids suspension characteristics and representative volumetric flow rates (tubing sizes necessary to achieve sufficient Reynold's Numbers are too small to support MST particle sizes). Therefore, it was necessary to divide the MST/SS stream addition into two parts: 1) an addition of 15% MST in H_2O as a trim chemical before the experiment, and 2) a homogeneous solution accounting for the balance of the MST/SS expected compositions.[a]

The MST/SS targeted combined compositions were designed to match those employed in previous testing.[10] However, given the necessity of adding MST as a separate slurry, a new composition of salt supernatant was designed such that the combined masses of 15% MST slurry and salt solution would yield the appropriate concentrations of components in the CPC. The targeted and measured composition of this salt supernatant phase is given in Table 2-2. Note that no standard deviation is given because the reported values are the result of a single measurement.

Table 2-2. Composition of Salt Solution Component of SS/MST Simulant Addition.

Analyte	Target (mol/L)	Measured (mol/L)
Na	5.27E-01	5.37E-01
Al	3.18E-02	5.02E-02
K	5.35E-03	4.77E-03
HCO_2^-	1.81E-03	<2.22E-03
NO_2^-	9.08E-02	9.06E-02
NO_3^-	7.37E-02	6.45E-02
CO_3^{2-}	5.00E-02	5.05E-02†
OH^-	2.82E-01	2.64E-01†

†Carbonate and Hydroxide concentrations were calculated from known addition masses of Sodium Hydroxide, Sodium Carbonate, Potassium Carbonate, Sodium Nitrite, and Sodium Nitrate and measurements of Nitrite and Nitrate in solution.

Note that the concentrations given in Table 2-2 are approximately 30% higher than the concentrations employed in earlier testing by Lambert. This is due to the splitting of the stream into a 15% MST slurry and a soluble component, both of which are diluted upon combination to the appropriate concentrations. In

[a] MST/SS target compositions were based on CPC simulations performed to support the development of the Y-17112 antifoam flowsheet.

order to achieve the time at boiling expected in the DWPF, the caustic boiling stage was performed with a boilup rate higher than the salt solution addition rate. This allowed for continuous solution addition and boiling for the correct amount of time without the risk of line plugging via MST solids.

2.1.3 Strip Effluent Feed Tank Simulant

Strip Effluent Feed Tank (SEFT) simulant is used to reproduce the time at boiling and impacts of further chemical addition in the CPC when strip effluent is added from SWPF. At the time of this writing, SWPF uses dilute nitric acid (as part of the BobCalix flowsheet) to strip ^{137}Cs in the CSSX process. However, the majority of SB 10 processing is expected to occur under the Next Generation Solvent flowsheet in SWPF, which will employ MaxCalix and a dilute boric acid strip.[11] For this reason, boric acid was used to simulate the addition of strip effluent in SB 10 coupled operations experiments. Note that the trace organic components assumed to be present in the SEFT material were not included in this testing. The composition of this stream is given in Table 2-3.

Table 2-3. Composition of SEFT Simulant.

Component	Concentration (wt%)
Boric Acid, $(HO)_3B$	0.06
DI H_2O	99.94

2.1.4 Sodium Reactor Experiment Simulant

The addition of manganese-poisoned SRE is also a part of SB 10. The objective of the SRE simulant produced for SB 10 testing is to introduce a simulated waste stream representative of the manganese added to Tank 51 as a result of the transfer of SRE material from H-Canyon to the CSTF. Ideally, this addition should not significantly alter the composition of other components in the sludge simulant mixture such that the final blend is representative of the material expected in Tanks 51 and 40 after the addition of SRE. In order to accomplish this goal, SRE simulant was prepared by precipitating manganese solids in a process similar to that employed in H-Canyon. These solids were subsequently washed with DI H_2O and trimmed with soluble salt components to match the supernatant observed in Tank 40 and Tank 51 sludge simulants as closely as practical. Once trim additions were complete, a final supernatant phase decant was performed to increase the level of solids in the SRE simulant. The general steps used to prepare SRE simulant are given below:

1. 50% manganese nitrate solution was added to a solution of ~5 M nitric acid to simulate the conditions of SRE material in H-Canyon before neutralization and transfer.
2. 50% sodium hydroxide solution was metered into the neutralization vessel while the mixture was agitated. This process was controlled such that any temperature excursions above 60 °C would trigger a temporary cessation of sodium hydroxide addition (similar to the procedure used in H-Canyon). This resulted in a slurry mixture of light-colored solids (nearly 100% manganese(II) hydroxide) and a salt solution of sodium nitrate and sodium hydroxide.
3. The neutralized material was allowed to settle before being decanted and washed with DI H_2O to lower the concentration of soluble components.
4. Addition of trim salts and a final decant were performed to complete the preparation.

The targeted and measured composition of the SRE simulant is given in Table 2-4. Manganese(II) hydroxide was confirmed to be the only insoluble solid present in the mixture by solids and elemental analysis. Therefore, the insoluble solids may be assumed to be equivalent to the concentration of manganese(II) hydroxide. Note that two batches of SRE simulant were prepared for SB 10 testing. These

batches were prepared in an identical manner. Analyses given in Table 2-4 are from measurements of the first batch and are assumed to be applicable to the second batch.

Table 2-4. Composition of SRE Simulant.

Supernatant Component	Target	Measured
Insoluble Solids (wt.%)[b]	8.73	8.80
Density (g/mL)	N/A	1.11
Mn (% of IS)	61.8	66.8
Al (mol/L Supernatant)	3.78E-02	3.89E-02
K (mol/L Supernatant)	1.44E-03	7.69E-03
Na (mol/L Supernatant)	8.59E-01	8.12E-01
Mn (mol/L Supernatant)	0	<1.82E-05
F^- (mol/L Supernatant)	7.31E-04	<5.26E-03
Cl^- (mol/L Supernatant)	9.81E-04	<2.82E-03
NO_2^- (mol/L Supernatant)	2.13E-01	2.30E-01
NO_3^- (mol/L Supernatant)	1.12E-01	1.01E-01
SO_4^{2-} (mol/L Supernatant)	1.52E-02	1.43E-02
$C_2O_4^{2-}$ (mol/L Supernatant)	9.68E-03	9.35E-03
PO_4^{3-} (mol/L Supernatant)	3.40E-04	<1.05E-03
CO_3^{2-} (mol/L Supernatant)	5.21E-02	5.65E-02[†]
OH^- (mol/L Supernatant)	3.41E-01	3.47E-01[†]

N/A – Not applicable.
[†]Carbonate and Hydroxide concentrations were calculated from known addition amounts of Sodium Hydroxide and Sodium Carbonate in relation to the measured nitrite concentration resulting from an addition of a known amount of Sodium nitrite.

As Table 2-4 shows, the observed concentrations of SRE simulant closely match the targeted concentrations. Measurements of manganese in the slurry are consistent with the presence of $Mn(OH)_2$. As mentioned above, one of the primary goals of the SRE simulant was to resemble the Tank 51 and Tank 40 sludge simulants in solids loading and supernatant concentrations. By achieving similar concentrations in the SRE simulant, this material can be added to adequately increase the concentration of Mn in any CPC experiment without significantly affecting the overall insoluble solids loading or the supernatant chemistry. This allowed for the addition of SRE simulant such that varying levels of SRE addition campaigns could be evaluated (this flexibility was not needed during SB 10 flowsheet testing). SRE simulant was added to each batch of simulant to increase the total manganese concentration to levels predicted by SRR projections. Actual amounts added to each type of experiment are given in Section 2.3.

2.2 Experimental Apparatus

The apparatus used in SB 10 simulant testing was similar to equipment used in previous SB campaigns at SRNL.[5] The SRNL 4L reaction vessel consists of a ~5L glass kettle (approximately 6 inches in diameter) equipped with a stainless steel lid. The lid of the vessel was equipped with nine Ultra-Torr fittings and one ground glass adapter to allow the introduction of several pieces of equipment into the vessel headspace. The Ultra-Torr fittings were used to introduce: 1) two Incoloy fire rods to provide heating, 2) a Mettler-Toledo Autochem pH01 pH electrode for continuous pH monitoring of the reaction via a Thermo Scientific Orion 2-Star benchtop pH meter (initial tests used a specially-designed liquid pH probe, but this probe was determined to be too fragile for use in CPC simulant experiments), 3) a gas supply line to provide purge gas throughout the experiment, 4) an off-gas leg to carry gas and steam from the kettle to the downstream off-gas train, 5) an Inconel-clad type-T thermocouple for continuous temperature monitoring, 6) a return

[b] Insoluble solids values are the result of a calculation using measured values for total solids and dissolved solids.

line for condensate produced downstream, 7) an acid addition line through which nitric and glycolic acids could be added subsurface, and 8) a glass sampler to allow for sampling throughout the experiment without the need to impact the vessel headspace or integrity. The ground glass fitting was used to introduce antifoam throughout the experiments, as well as to introduce any bulk chemical/material additions (DI H_2O for cannister blast simulations, frit, etc.). Mixing was provided via overhead motor through a magnetic coupling specially designed by SRNL researchers.

Upstream of the reaction vessel, purge gases comprised of compressed air and high purity krypton (blended at a 0.5% Kr concentration) were provided using MKS flow controllers. Additionally, a glass addition funnel was used to hold and deliver acid(s) to a Cole-Parmer reciprocating pump, which was used to meter acids into the reaction vessel at pre-determined rates.

Downstream of the reaction vessel, excess gases produced/introduced into the reaction vessel were transferred to a glass condenser (referred to as the SRAT or SME condenser) and cooled with 25 °C water. Steam and any other condensables were condensed here and allowed to drain to a glass vessel approximating the Mercury Water Wash Tank (MWWT) in DWPF. From the MWWT, condensate could be returned to the vessel or collected as a part of a dewater campaign. Non-condensables traveled from the SRAT/SME condenser to the ammonia scrubber, where a dilute nitric acid solution was recirculated with the use of a Cole-Parmer gear pump and allowed to coat glass Raschig rings in order to remove any ammonia from the process vapors.

After contacting nitric acid in the ammonia scrubber, remaining vapors were transferred to a second condenser (referred to as the Formic Acid Vent Condenser (FAVC)) and cooled with 4 °C water. Following the FAVC, process gases were passed through a Nafion membrane dryer for further H_2O removal before exiting the fume hood and proceeding to off-gas analysis equipment.

After exiting the hood, off-gas was carried first to an Inficon Fusion MicroGC where a small fraction of the total gas flow rate was pulled for GC analysis. The remainder of the off-gas was carried further downstream to an Extrel mass spectrometer (MS) and MKS Fourier Transform Infrared (FT-IR) spectrophotometer. Following analysis by MS and IR, the off-gas was carried to ACTL building ventilation and allowed to exhaust into the laboratory ventilation system.

A schematic of the experimental apparatus used in SB 10 simulant testing is given in Figure 2-2. A photograph of the equipment is given in Figure 2-3.

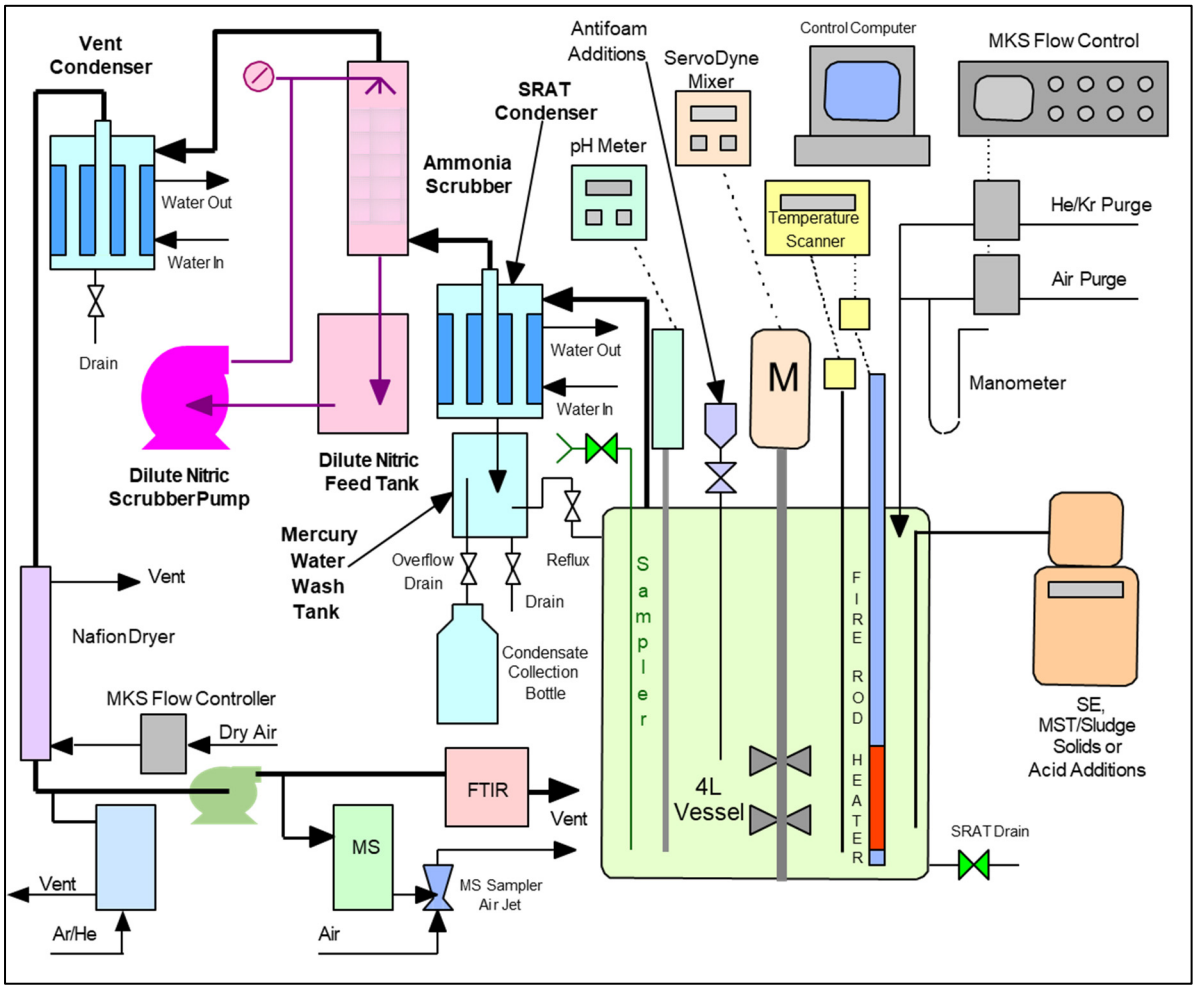

Figure 2-2. Diagram of 4L CPC Testing Apparatus.

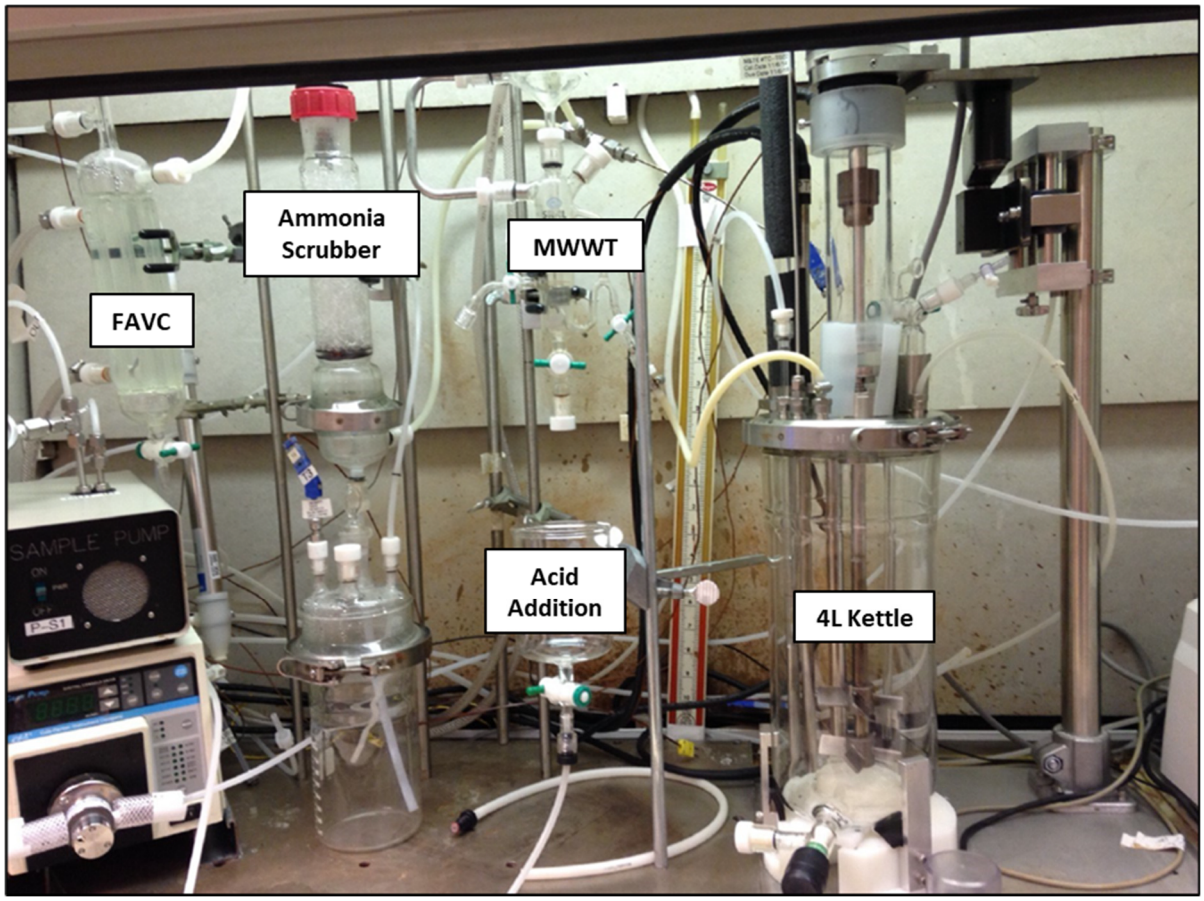

Figure 2-3. Photograph of 4L CPC Testing Apparatus at SRNL.

Purge gas flow rates, mixing speed, liquid addition rates, and fire rod power input were all controlled by LabVIEW™ software. This software also provided continuous monitoring of liquid temperature, pH, mixing torque, flow rates, and GC measurements.

2.3 Experimental Execution

Fourteen CPC simulations were performed to support SB 10 flowsheet development. These tests and the experimental parameters associated with them are given in Table 2-5.

Table 2-5. Experimental Parameters Used in SB 10 Testing.

Test Name	Sludge Used	Target Stoichiometry (% KMA)	Target REDOX ($Fe^{2+}/\Sigma Fe$)	Run Type	Flowsheet Used	Boilup Rate (lb h^{-1})	Test Objective
Tk51-1	Tk 51	70	0.1	SRAT-SME	Sludge-Only	5,000	Qualification Test Support
Tk51-2	Tk 51	110	0.1	SRAT-SME	Sludge-Only	5,000	
Tk51-3	Tk 51	100	0.1	SRAT-SME	Sludge-Only	5,000	
Tk51-4	Tk 51	100	0.1	SRAT-SME	Sludge-Only	5,000	
Tk40-1	Tk 40	100	0.1	SRAT-Only	Coupled	5,000	Flowsheet Variation Study
Tk40-2	Tk 40	120	0.1	SRAT-Only	Coupled	5,000	
Tk40-3	Tk 40	100	0.3	SRAT-Only	Coupled	5,000	
Tk40-4	Tk 40	120	0.3	SRAT-Only	Coupled	5,000	
Tk40-5	Tk 40	110	0.1	SRAT-Only	Coupled	5,000	Flowsheet Centroid
Tk40-6	Tk 40	90	0.1	SRAT-Only	Coupled	5,000	Flowsheet Acid Window Extension
Tk40-7	Tk 40	130	0.1	SRAT-Only	Coupled	5,000	
Tk40-8	Tk 40	100	0.1	SRAT-SME	Coupled	5,000	SRAT-SME Evaluation
Tk40-9	Tk 40	100	0.1	SRAT-SME	Coupled	3,000	Reduced Boil-up Rate
Tk40-10	Tk 40	100	0.1	SRAT-SME	Sludge-Only	5,000	Sludge-Only Flowsheet

Experiments with Tank 51 sludge were performed to support the SRNL Shielded Cells qualification test and were therefore performed as sludge-only experiments at the design basis boilup rate of 5,000 lb h^{-1}. The first experiment in this set (Tk51-1) was performed at a targeted stoichiometry of 70% and generated SRAT product too thick to carry forward into further testing. For this reason, this experiment was stopped early and not used for qualification recommendation discussion. A brief discussion of Tk51-1 results and observations are included in 1.1.1.1.1Appendix A.

Tk51-2 and Tk51-3 were performed to better understand the impact of stoichiometry at acid loadings that produced processable sludge. Tk51-3 exhibited signs of leaking and yielded anion measurements below expected values. For this reason, Tk51-4 was performed as a repeat of Tk51-3. These runs are discussed in more detail in the Shielded Cells Recommendation Memorandum.[12]

Tank 40 experiments were performed to support SB 10 implementation at the DWPF, and therefore explored more variations of experimental parameters. Tests Tk40-1 through Tk40-7 were performed as SRAT-only experiments to better understand the impacts of acid stoichiometry and REDOX target (which is expressed as a difference in the percentage of acid added as reducing acid, or PRA) on CPC processing. These tests were performed at acid stoichiometries (reported as a percentage of the Koopman Minimum Acid requirement) between 90% and 130%. Tk40-8 was performed to extend this knowledge to the SME

cycle. Tk40-9 was performed as a way to examine the impact of lower boilup rates often used in the DWPF. Tk40-10 was performed to quantify changes associated with the introduction of SWPF waste streams.

The CPC simulations described in this report were performed with the following steps:

SRAT Cycle (all runs)

1. Sludge simulant (Tank 40 or Tank 51) was added to the reaction vessel (approximately 3.5 L)
2. Trim metals (silver nitrate, palladium nitrate, rhodium nitrate, ruthenium chloride, mercury oxide) were added to the vessel. Ag, Pd, Rh, and Ru were added at 125% of the concentrations in SB 10 (as predicted by solids projections and Tank 51 sludge elemental analysis), while Hg was added at ~100% of the expected concentrations
3. SRE simulant was added to the vessel as a slurry (~130 g for Tank 40 sludge, ~165 g for Tank 51 sludge) – This completes the addition of receipt materials and is the basis for the 6,000 gallon scaling factor in SB 10 testing
4. (Coupled operation testing only)-15% MST was added to the vessel as a slurry (equivalent to MST added with 3,000 gallons (scaled) of MST/SS waste)
5. Reaction vessel was sealed, mixing and gas purge was initiated (94 SCFM, scaled)
6. Mixtures were mixed for ≥30 min and sampled (SRAT Receipt sample)
7. (Coupled operations only) – MST/SS Addition and Caustic Boiling
    a. Vessel was heated to boiling
    b. Once boiling was reached, soluble MST/SS simulant (~1300 g) was added continuously for ~5 hours (equivalent to soluble components of 3,000 gallon (scaled) volume of MST/SS waste)
    c. Condensate was collected from the MWWT
    d. At completion of MST/SS soluble stream addition and dewater collection, vessel was allowed to cool for sampling (Post MST/SS Sample)
8. Mixture was heated/cooled to 93 °C (± 2 °C allowance from calibration procedure)
9. Nitric acid (50%) was added to slurry at a scaled rate equivalent to approximately 4.6 gallons per minute
10. Glycolic acid (70%) was added to slurry at a scaled rate equivalent to approximately 4 gallons per minute
11. Mixture was heated to boiling
12. Slurry was concentrated to target solids loading by removing condensate from MWWT
13. (Coupled operations only) – SEFT Addition
    a. Strip effluent simulant was added to the reaction vessel while simultaneously removing condensate from MWWT at a scaled volume equivalent to 15,000 gallons
14. Reaction mixture was boiled while refluxing condensate to achieve desired time at boiling for Hg removal
15. Reaction mixture was cooled and sampled (SRAT Product sample)

SME Cycle (SRAT-SME runs only)

1. DI H_2O was added to reaction vessel to simulate a scaled 1,000 gallon cannister blast addition
2. Purge rate was reduced to SME target value (72 SCFM, scaled)
3. Vessel was heated to boiling. Added H_2O was evaporated and collected as condensate
4. Heating is stopped and vessel was allowed to cool below boiling
5. Steps 1 – 4 were repeated as many times as necessary to simulate multiple cannister blasts (total of 6 blast simulations performed in SB 10 testing)
6. Vessel was allowed to cool to 80 °C before frit addition
7. First half of frit was added with equivalent mass of DI H_2O
8. Vessel was reheated to boiling. Added H_2O was evaporated and collected as condensate
9. Vessel was cooled to 80 °C before second frit addition

10. Second half of frit was added with equivalent mass of DI H_2O
11. Vessel was reheated to boiling. Final dewater was performed to achieve desired solids target

Antifoam Y-17112 was added periodically throughout every experiment described in this report. Addition amounts and frequencies were consistent with the methodology outlined by Lambert.[10]

2.4 Off-gas Analysis

GC analysis was provided by an Inficon Fusion MicroGC equipped with a MolSieve 5A column (Ar carrier gas) and a PoraPlot Q column (He carrier gas). A 120 second isothermal method was used to adequately separate H_2, He, N_2, O_2, Kr, CH_4, CO_2, and N_2O. Sample volumes were increased relative to previous tests in order to better detect H_2 at lower levels (<10 ppm). GC sampling occurred approximately every four minutes during a given CPC experiment. The GC was calibrated before and after every experiment with a calibration gas composed of 50 ppm H_2, 101 ppm CH_4, 1.01% CO_2, 0.503% N_2O, 0.5% Kr, and Air.

MS analysis was provided by an Extrel Core MS. The fast sampling capability of the MS (approximately 7 seconds per reading) allowed the use of a spectrometer to obtain mass spectrometry data from multiple experiments simultaneously. H_2, He, Ar, N_2, O_2, NO, NO_2, and CO_2 responses were calibrated using separate calibration gases. Additionally, the MS employed a scanning feature, allowing the occasional collection of raw mass spectrometry data to investigate for unidentified gases.

IR analysis was provided by an MKS FT-IR Spectrophotometer. Only one FT-IR was available at the time of this testing, so IR analysis was not performed for every SB 10 simulant experiment (specifically, experiments Tk51-1, Tk40-7, and Tk40-9 were performed without IR support). The FT-IR was able to measure N_2O, NO, NO_2, CO_2 NH_3, and CH_4 using literature libraries of example spectra as a basis for calibration. The FT-IR was also able to match unknown observed peaks to library spectra in order to offer possible identities for new species.

Table 2-6 lists the species of gases observed in SB 10 testing and identifies the analytical techniques used to quantify each molecule.

Table 2-6. SB 10 Gas Species by Analytical Technique.

Gas	GC	MS	IR
H_2	x	x	
He	x	x	
Ar		x	
N_2	x	x	
O_2	x	x	
N_2O	x		x
NO		x	x
NO_2		x	x
CO_2	x	x	x
NH_3			x
CH_4	x		x

As discussed above, the MS and IR can be used to screen for new, unidentified compounds during CPC experiments. Any unidentified compounds detected are discussed in the relevant sections of this report.

2.5 Liquid and Slurry Analysis

Several types of liquid samples were drawn in the course of SB 10 CPC simulant testing. Sludge samples were drawn 1) from the 4L reaction vessel directly, using a glass sampler, or 2) as a subsample of agitated

sludge product at the conclusion of an experiment. Sludge supernatant samples were taken by first obtaining a sludge sample and centrifuging the slurry for 60 min at approximately 3000 rpm. Once centrifuged, supernatant was decanted from the sample and submitted as a filtrate. Condensate samples were drawn from bulk condensate collected during the experiment.

Liquid samples were submitted to the SRNL Process Science Analytical Laboratory (PSAL) or Sensing and Metrology (SAM) groups for quantitation. These samples were then prepared and analyzed using a variety of techniques. The list of preparations and analyses performed is given in Table 2-7.

Table 2-7. Preparations and Analyses Performed by PSAL and SAM.

Analysis	PSAL Technique	SAM (Method)
Sludge Samples		
% Solids	Drying Oven (110 °C for total solids, 1100 °C for calcined solids) / Balance	NM
Density	Anton Parr Density Meter	NM
Elemental Composition	Aqua Regia Digestion/Atomic Emission Spectroscopy (ICP-AES)	NONRAD ICP-AES
Anion Composition†	Weighted Dilution/Ion Chromatography (IC)	IC-ANIONS/IC-ANIONS GLYCOLATE
Free OH	NM	T BASE/FREE OH
Titration to pH 7	Titration	NM
CO_3^{2-}	NM	TIC/TOC
Organic Carbon	NM	TIC/TOC
NH_4^+	NM	IC-CATIONS
Volatile Organics	NM	VOA/SVOA
Supernatant Samples		
% Solids	Drying Oven / Balance	NM
Density	Anton Parr Density Meter	NM
Elemental Composition	ICP-AES	NONRAD ICP-AES
Anion Composition	IC	IC-ANIONS/IC-ANIONS GLYCOLATE
CO_3^{2-}	NM	TIC/TOC
Organic Carbon	NM	TIC/TOC
NH_4^+	NM	IC-CATIONS
Volatile Organics	NM	VOA/SVOA
Organic Hg††	NM	METHYLHG/VOA
Condensate Samples		
Density	Anton Parr Density Meter	NM
Elemental Composition	ICP-AES	NONRAD ICP-AES
Anion Composition	IC	IC-ANIONS/IC-ANIONS GLYCOLATE
CO_3^{2-}	NM	TIC/TOC
Organic Carbon	NM	TIC/TOC
NH_4^+	NM	IC-CATIONS
Volatile Organics	NM	VOA/SVOA
Organic Hg	NM	METHYLHG/VOA

†IC measurements of glycolate were performed by first treating the sludge sample with 50% NaOH, consistent with the caustic quench measurement methodology used in previous studies.
††Organic mercury samples were prepared by treating supernatant or condensate samples with high purity HCl then transferred to a polytetrafluoroethylene bottle with minimal headspace and stored in a chemical refrigerator until measurement was performed.

NM = Not Measured.

2.6 Quality Assurance

The functional identification of this work is considered Safety Class.[1-2] Specifically, elements of this study used to evaluate the DWPF Technical Safety Requirement (TSR) Safety Administrative Controls (SACs) 5.8.2.11, 5.8.2.23, and 5.8.2.25. These controls require knowledge of:

- Soluble, insoluble, and total solids concentration of sludge slurry
- Density measurements
- Hydrogen generation during SRAT and SME processing
- Ammonium concentrations in condensate generated from SRAT and SME processing
- Analysis of Antifoam Degradation Products (ADPs) resulting from antifoam use in CPC tests

Measurements of solids concentrations, densities, ammonium concentrations, and ADPs are governed by analytical procedures. Data generated from these procedures are sufficient for Safety Class use "as-is". Hydrogen generation rates during SRAT and SME processing are calculated using measurements of Kr and purge air flow rates as well as measurements of Kr and H_2 in the off-gas. These measurements are performed with the use of Measuring and Test Equipment (M&TE) flow controllers and Measurement Systems and Equipment (MS&E) gas chromatography columns. Calculations are subject to design verification to ensure compatibility with Safety Class designation.

The Data Acquisition and Control (DAC) software employed in this testing was used to control mass flow meters, overhead mixers, liquid addition pumps, and heating rod power input. This software was also used to continuously monitor and log data taken from thermocouples, pH meters, flow meters, and heating rod power supply meters. This software is classified as level D. The DAC software does not perform calculations that are used in this report. Monitored data was recorded manually every 30 minutes to supplement the files and logs generated by the DAC software.

Requirements for performing reviews of technical reports and the extent of review are established in manual E7 2.60.[13] SRNL documents the extent and type of review using the SRNL Technical Report Design Checklist contained in WSRC-IM-2002-00011, Rev. 2.[14] The data described in this report is recorded for permanent retention in the Electronic Laboratory Notebook (ELN)[15] within notebooks C8102-00274-19, C8102-00274-20, and L7748-00442-01. The use of any Measuring and Test equipment (M&TE) or Measurement Systems and Equipment (MS&E) is also recorded in this notebook.

3.0 Results and Discussion

3.1 SRAT Receipt Conditions

During SB 10 simulant testing, two sludge simulants were employed with and without coupled operations processing. This led to the production of four distinct SRAT Receipt compositions:

- Tk51 Receipt – Combination of Tank 51 sludge simulant, SRE simulant, and trim metals. This mixture is representative of Tank 51 material charged to the SRAT vessel before the addition of nitric acid (applicable to expected conditions and acid requirements in the SRNL Shielded Cells qualification experiment)
- Tk40 Receipt – Combination of Tank 40 sludge simulant, SRE simulant, and trim metals. This mixture is representative of Tank 40 material charged to the SRAT vessel before the addition of MST/SS or nitric acid (applicable to expected conditions and acid requirements in the DWPF when operating a sludge-only flowsheet)

- Tk40 Post MST/SS – Combination of Tank 40 sludge simulant, SRE simulant, trim metals, and 15% MST slurry, followed by caustic boiling and introduction of MST/SS soluble salt components. This mixture is representative of Tank 40 material following the conclusion of MST/SS addition and caustic boiling, before the addition of nitric acid (applicable to the expected conditions and acid requirements in the DWPF when operating a coupled flowsheet)
- Tk40 w/ MST – Combination of Tank 40 sludge simulant, SRE simulant, trim metals, and 15% MST slurry. This mixture is representative of Tank 40 material following the addition of 15% MST slurry, before the addition of MST/SS soluble salt solution and caustic boiling (not applicable to expected CPC processing, but useful for interpreting impacts of caustic boiling on chemical reactions)

The target noble metal concentrations for Tank 40 Sludge Receipt were 1.19×10^{-2}, 5.84×10^{-2}, 2.53×10^{-3}, and 9.86×10^{-3} percent of total dried solids for Rh, Ru, Pd, and Ag, respectively.[7] The target noble metal concentrations for Tank 51 Sludge Receipt were 16.1, 80.6, 3.5, and 12.5 mg kg^{-1} for Rh, Ru, Pd, and Ag, respectively.[8] These concentrations are consistent with 125% of the concentrations expected in SB 10 processing.

A calculational error was made while preparing for SB 10 testing, substituting the molecular weight of ruthenium monochloride (RuCl) for ruthenium trichloride ($RuCl_3$). This resulted in the addition of ~34% less ruthenium than was desired in Tank 40 and Tank 51 testing. This offset, coupled with the 125% increase in noble metal concentrations typically employed in CPC simulant tests indicates that actual ruthenium concentrations employed in the tests described here were approximately 82% of the concentrations expected in radioactive waste (3.85×10^{-2} % of total dried solids and 53.2 mg kg^{-1} for Tank 40 and Tank 51 simulants, respectively). This difference is not expected to have any significant impact on conclusions or processing recommendation made in this report.

The density and solids properties of these four SRAT receipt conditions are given in Table 3-1. “Tank 40 Receipt” was measured from the Tk40-10 SRAT receipt sample. Results for “Tk40 w/ MST” are the averages of five Tk40 SRAT receipt sample measurements. Results for “Tk40 Post MST/SS” are the averages of seven Tk40 post-MST/SS addition samples. Results for “Tk51 Receipt” are the averages of four Tk51 experiment SRAT receipt samples.

Table 3-1. Density and Solids Properties of Simulant Receipt Sludges.

Parameter	Tk40 Receipt	Tk40 w/ MST	Tk40 Post MST/SS	Tk51 Receipt
Slurry Density (g/mL)	1.112	1.116	1.138	1.116
Supernatant Density (g/mL)	1.045	1.042	1.059	1.045
Total Dried Solids (wt% of slurry)	13.9	14.2	16.2	14.1
Dissolved Solids (wt% of filtrate)	5.95	5.57	7.69	5.86
Insoluble Solids (wt% of slurry)	8.49	9.14	9.28	8.78
Soluble Solids (wt% of slurry)	5.44	5.06	6.97	5.35
Calcined Solids (wt% slurry)	10.0	10.5	12.1	10.5

From the data in Table 3-1, it is clear that the addition of MST to Tank 40 sludge simulant has a minor impact on total solids (increasing from 13.9% to 14.2%) and insoluble solids (increasing from 8.49% to 9.14%). The impact of MST/SS caustic boiling is also clear, dramatically increasing total dried solids to 16.2% and soluble solids to 6.97% (up from 5.06% before caustic boiling). No significant change is seen in insoluble solids from the caustic boiling step alone (increasing from 9.14% insoluble solids in Tk40 w/ MST to 9.28% insoluble solids in Tk40 Post MST/SS), which is consistent with the method of MST/SS addition described here. Calcined solids, however, do increase with caustic boiling, consistent with the addition of a sodium-rich supernatant phase. Most notably, Tank 40 and Tank 51 sludge simulants seem to

bear similar solids properties. This is expected, given that the majority of SB 10 Tank 40 is expected to be comprised of SB 10 Tank 51 material.

Compositions of the SRAT Receipt Slurries are given in Table 3-2 and Table 3-3. Table 3-2 reports the concentration of sludge components on a volume of slurry basis, while Table 3-3 reports the compositions of each supernatant phase on a volume of supernatant basis.

Table 3-2. Composition of Simulant Receipt Sludges.

Parameter	Tk40 Receipt	Tk40 w/ MST	Tk40 Post SS/MST	Tk51 Receipt
Ag (% of TS)	<0.07	<0.08	<0.08	<0.08
Al (% of TS)	12.08	12.82	12.53	13.92
B (% of TS)	<0.07	<0.07	<0.08	<0.07
Ba (% of TS)	<0.07	<0.07	<0.08	<0.07
Ca (% of TS)	0.67	0.75	0.69	0.76
Cr (% of TS)	0.23	0.24	0.22	0.31
Cu (% of TS)	<0.07	<0.07	<0.08	<0.07
Fe (% of TS)	11.31	11.91	10.94	11.29
Hg (% of TS)	3.8	3.29	2.46	2.37
K (% of TS)	<0.07	<0.07	<0.08	<0.07
Li (% of TS)	<0.07	<0.08	<0.08	<0.07
Mg (% of TS)	0.22	0.24	0.22	0.25
Mn (% of TS)	4.16	4.19	3.87	4.12
Na (% of TS)	14.16	12.9	15.09	12.78
Ni (% of TS)	0.43	0.46	0.43	0.32
P (% of TS)	<0.07	<0.07	<0.07	<0.07
Pd (% of TS)	<0.07	<0.07	<0.08	<0.07
Rh (% of TS)	<0.07	<0.07	<0.07	<0.07
Ru (% of TS)	<0.07	<0.07	<0.08	<0.07
S (% of TS)	0.23	0.23	0.24	0.24
Si (% of TS)	0.69	0.15	0.22	0.48
Sn (% of TS)	0.09	<0.07	<0.07	<0.07
Ti (% of TS)	<0.07	3.91	3.59	<0.08
Zn (% of TS)	<0.07	<0.07	<0.07	<0.07
Zr (% of TS)	0.14	0.16	0.14	0.19
HCO_2^- (M)	<2.47E-03	<2.48E-03	<2.53E-03	<2.48E-03
Cl^- (M)	<3.14E-03	<3.15E-03	<3.21E-03	<3.15E-03
NO_2^- (M)	2.20E-01	2.68E-01	3.31E-01	2.41E-01
NO_3^- (M)	1.32E-01	1.35E-01	1.82E-01	1.85E-01
PO_4^{3-} (M)	<1.17E-03	<1.17E-03	<1.20E-03	<1.17E-03
SO_4^{2-} (M)	1.47E-02	1.43E-02	1.65E-02	1.72E-02
$C_2O_4^{2-}$ (M)	8.11E-03	7.37E-03	7.95E-03	5.98E-03
$HOCH_2CO_2^-$ (M)	<1.48E-03	<1.49E-03	<1.52E-03	<1.49E-03
CO_3^{2-} (M)	7.73E-02	9.72E-02	1.31E-01	4.27E-02
OH^- (M)	1.60E-01	1.60E-01	3.08E-01	2.10E-01
Titration to pH 7 (M)	5.18E-01	4.86E-01	6.49E-01	5.50E-01

Table 3-3. Composition of Simulant Receipt Supernatants (mol/L Supernatant).

Parameter	Tk40 Receipt	Tk40 w/ MST	Tk40 Post SS/MST	Tk51 Receipt
Ag	<9.27E-06	<9.27E-06	<9.27E-06	<9.27E-06
Al	9.08E-02	9.09E-02	1.21E-01	1.49E-01
B	1.36E-03	1.33E-03	1.56E-03	1.18E-02
Ba	<7.28E-06	<7.28E-06	<7.28E-06	<7.28E-06
Ca	<2.50E-05	<2.50E-05	<2.50E-05	<2.50E-05
Cr	1.20E-03	8.83E-04	3.62E-03	1.17E-03
Cu	<1.57E-05	<1.57E-05	<1.57E-05	<1.57E-05
Fe	<1.79E-05	<1.79E-05	<1.79E-05	<1.79E-05
Hg	2.37E-04	2.63E-04	3.62E-04	6.05E-04
K	1.44E-03	1.54E-03	7.53E-03	1.71E-03
Li	<1.44E-04	<1.44E-04	<1.44E-04	<1.44E-04
Mg	<4.11E-05	<4.11E-05	<4.11E-05	<4.11E-05
Mn	<1.82E-05	<1.82E-05	<1.82E-05	<1.82E-05
Na	8.55E-01	8.31E-01	1.16E+00	8.65E-01
Ni	<1.70E-05	<1.70E-05	<1.70E-05	<1.70E-05
P	5.97E-05	7.42E-05	1.26E-04	9.00E-05
Pd	2.29E-05	1.66E-05	1.41E-05	1.51E-05
Rh	<9.72E-06	<9.72E-06	<9.72E-06	<9.72E-06
Ru	<9.89E-06	<9.89E-06	<9.89E-06	<9.89E-06
S[c]	1.51E-02	4.28E-05	7.65E-03	1.38E-02
Si	<3.56E-05	<3.56E-05	4.52E-05	<3.56E-05
Sn	2.12E-04	<8.42E-06	<8.42E-06	<8.42E-06
Ti	<2.09E-05	<2.09E-05	<2.09E-05	<2.09E-05
Zn	<1.53E-05	<1.53E-05	<1.53E-05	<1.53E-05
Zr	<1.10E-05	<1.10E-05	<1.10E-05	<1.10E-05
HCO_2^-	<2.22E-03	<2.22E-03	<2.22E-03	<2.22E-03
Cl^-	<2.82E-03	<2.82E-03	<2.82E-03	<2.82E-03
NO_2^-	2.41E-01	2.40E-01	2.91E-01	2.16E-01
NO_3^-	1.37E-01	1.21E-01	1.60E-01	1.66E-01
PO_4^{3-}	<1.05E-03	<1.05E-03	<1.05E-03	<1.05E-03
SO_4^{2-}	1.47E-02	1.28E-02	1.45E-02	1.54E-02
$C_2O_4^{2-}$	8.02E-03	6.61E-03	6.98E-03	5.36E-03
$HOCH_2CO_2^-$	<1.33E-03	<1.33E-03	<1.33E-03	<1.33E-03
CO_3^{2-}	9.41E-02	9.99E-02	1.34E-01	4.38E-02
OH^-	1.64E-01	1.64E-01	3.16E-01	2.16E-01

Generally speaking, the compositions shown in Table 3-2 and Table 3-3 agree well with the processing differences between each sample. Slurry concentrations of metals present in Tank 40 sludge simulant do not significantly change upon addition of MST slurry or performance of the caustic boiling step. However, soluble components (such as sodium) increase drastically upon performance of caustic boiling.

The sludge compositions discussed above provide enough information to determine an effective acid requirement. The acid stoichiometry metric used in SB 10 simulant testing is that recommended by Koopman, given in Equation [1].[16]

$$\left[n_{acid}\right] = \left[OH_{equiv}\right] + \left[Hg\right] + \left[CO_3\right]_{dissolved} + \left[NO_2\right] + 1.5\left\{\left[Ca\right] + \left[Mg\right] + \left[Mn\right]\right\} \quad [1]$$

[c] The sulfur measurement for Tk40 w/ MST is inconsistent with the measurement of SO_4^{2-} by IC. It is likely that the sulfur measurement is an outlier and should not be considered representative of actual sulfur concentrations.

Where,

$[n_{acid}]$ is the amount of acid needed in mol L^{-1},

$[OH_{equiv}]$ is the concentration of base equivalents (equal to the amount of acid required to bring the slurry to pH 7) in mol L^{-1},

$[Hg]$ is the concentration of mercury in mol L^{-1},

$[CO_3]_{dissolved}$ is the amount of soluble carbonate in mol L^{-1},

$[NO_2]$ is the concentration of nitrite in mol L^{-1},

$[Ca]$ is the concentration of calcium in mol L^{-1},

$[Mg]$ is the concentration of magnesium in mol L^{-1}, and

$[Mn]$ is the concentration of manganese in mol L^{-1}.

A separate methodology for calculating acid stoichiometry is given by Hsu and is currently employed at the DWPF. The equation for Hsu stoichiometry is given in Equation [2].

$$[n_{acid}] = [OH_{equiv}] + [Hg] + 2[CO_3] + 0.75[NO_2] + 1.2[Mn] \quad [2]$$

Each experiment performed in SB 10 simulant testing is listed in Table 3-4, along with the target and actual Koopman Minimum Acid (KMA) employed, the equivalent Hsu stoichiometry, and the percentage of acid added as glycolic (reducing acid), or PRA.

Table 3-4. Nominal Vs. Effective Acid Stoichiometries in SB 10 Testing.

Experiment	Target Acid (% KMA)	Percent Reducing Acid (%)	Actual Acid (% KMA)	Actual Acid (% Hsu)
Tk40-1	100	53.0	107.9	113.0
Tk40-2	120	52.6	127.1	133.2
Tk40-3	100	60.6	107.9	113.0
Tk40-4	120	59.2	128.6	134.7
Tk40-5	110	56.8	118.3	123.9
Tk40-6	90	56.3	92.3	96.6
Tk40-7	130	56.8	137.7	144.3
Tk40-8	100	57.0	105.7	110.7
Tk40-9	100	57.0	103.6	108.5
Tk40-10	100	58.2	106.2	113.9
Tk51-1	70	57.4	76.3	85.8
Tk51-2	110	54.3	116.6	131.2
Tk51-3	100	57.5	106.1	119.4
Tk51-4	100	54.2	107.3	120.8

The data in Table 3-4 show good general agreement between the target and actual % KMA employed in SB 10 testing, with differences falling between 2 and 8 percent. The stoichiometries shown in Table 3-4 are calculated from the receipt concentrations reported in Table 3-2 and Table 3-3. Based on the analyses given in these tables, it seems that the small discrepancy between target and actual stoichiometries is the result of a small difference between expected and received nitrite in sludge simulants (accounts for ~5

percentage points) and the differences between expected and taken sample sizes (accounts for ~ 2 percentage points). These differences are expected to be minor and have no significant impact on the conclusions from this testing.

There is a notable difference in the %KMA stoichiometric calculation and the Hsu stoichiometric calculation when comparing Tank 40 simulant and Tank 51 simulant. For Tank 40 experiments, the Hsu stoichiometry is approximately 5% lower than the Koopman Minimum Acid stoichiometry. However, for Tank 51 experiments, the stoichiometry difference is approximately 12%. This is due to differences in the relative concentrations of manganese, nitrite, and carbonate in the sludge simulant, as well as the addition of calcium and magnesium in the KMA calculation.

3.2 SRAT and SME Product Analyses

SRAT product solids characteristics and densities for each run performed in SB 10 simulant testing is given in Table 3-5.

Table 3-5. SRAT Product Slurry Solids and Density Analyses.

Run	Total Dried Solids (wt%)	Soluble Solids (wt%)	Insoluble Solids (wt%)	Calcined Solids (wt%)	Slurry Density (g/mL)	Supernatant Density (g/mL)
Tk40-1	28.5	19.0	9.6	15.1	1.1955	1.1472
Tk40-2	26.1	17.8	8.3	13.3	1.1945	1.1530
Tk40-3	28.1	17.2	10.9	14.7	1.1559	1.1262
Tk40-4	27.1	17.8	9.2	13.7	1.2013	1.1329
Tk40-5	26.6	18.2	8.3	13.6	1.1974	1.1384
Tk40-6	27.0	17.0	10.0	15.1	1.1948	1.1117
Tk40-7	25.5	19.7	5.8	13.0	1.1896	1.1442
Tk40-8	27.6	15.6	12.0	14.9	1.1413	1.1174
Tk40-9	28.4	15.8	12.5	15.3	1.1945	1.1211
Tk40-10	22.8	11.6	11.2	12.2	1.1666	1.0832
Tk51-2	25.3	15.3	10.0	13.0	1.1843	1.1020
Tk51-3	21.4	9.4	12.0	11.7	1.1554	1.0800
Tk51-4	25.9	13.6	12.3	13.9	1.1910	1.0840

With the exception of Tk51-3 and Tk40-10, all SB 10 experiments performed were able to achieve a SRAT total solids target of 25% or more. Tk51-3 was observed to exhibit heating rod fouling, presumably due to sludge thickness. This prompted the addition of DI H_2O for dilution before continuing the experiment. The change in insoluble solids concentrations during the SRAT cycle (beginning from a SRAT receipt IS concentration of 8.5 – 9.3% and changing by between -3.5 – 3.5%) seems to be comparable to the changes observed in SB 9 testing (beginning from a SRAT receipt IS concentration of 10.6% and changing by between -2.1 – 8.7%).

Similar properties for SME products from each experiment are given in Table 3-6.

Table 3-6. SME Product Slurry Solids and Density Analyses.

Run	Total Dried Solids (wt%)	Soluble Solids (wt%)	Insoluble Solids (wt%)	Calcined Solids (wt%)	Slurry Density (g/mL)	Supernatant Density (g/mL)
Tk40-8	44.6	12.7	31.8	34.0	1.3414	1.1255
Tk40-9	39.9	11.2	28.8	30.8	1.2636	1.1020
Tk40-10	45.8	10.3	35.5	36.1	1.3435	1.1019
Tk51-2	44.9	13.7	31.2	34.1	1.2811	1.1160
Tk51-3	40.0	10.6	29.4	30.6	1.3199	1.1030
Tk51-4	40.6	10.6	30.1	31.4	1.3127	1.0740

As can be seen in Table 3-6, half of the experiments were carried out to the targeted solids loading of approximately 45% total solids. The remainder of the experiment purposefully targeted lower solids loading in order to ensure that slurry liquid levels did not fall below the fire rods' heating zones. It is recommended that future SRNL SB testing investigate alternative methods of heating to allow further concentration of dilute sludge batches.

Table 3-7 and Table 3-8 give the elemental composition of SRAT products from SB 10 simulant testing for SRAT-only runs and SRAT-SME runs, respectively.

Table 3-7. SRAT Product Slurry Elemental Analyses (for SRAT-only Runs, in Percentage of Total Dried Solids).

Elements	Tk40-1	Tk40-2	Tk40-3	Tk40-4	Tk40-5	Tk40-6	Tk40-7
Ag	<0.06	<0.05	<0.06	<0.06	<0.05	<0.06	<0.05
Al	8.47	8.33	8.89	8.54	8.73	9.20	8.37
B	<0.05	<0.05	<0.05	<0.05	<0.05	<0.06	<0.05
Ba	<0.05	<0.05	<0.05	<0.05	<0.05	<0.06	<0.05
Ca	0.50	0.47	0.50	0.48	0.46	0.49	0.43
Cr	0.16	0.15	0.16	0.15	0.15	0.16	0.14
Cu	<0.05	<0.05	<0.05	<0.05	<0.05	<0.06	<0.05
Fe	7.72	7.56	7.81	7.51	7.19	7.76	6.92
Hg	0.04	0.05	0.05	0.03	0.03	0.04	0.05
K	0.29	<0.05	0.30	0.05	0.06	<0.06	<0.05
Li	<0.06	<0.05	<0.06	<0.06	<0.05	<0.06	<0.05
Mg	0.16	0.15	0.16	0.15	0.15	0.16	0.14
Mn	2.85	2.73	2.81	2.65	2.55	2.71	2.46
Na	10.86	10.40	10.76	10.24	10.54	11.47	9.85
Ni	0.31	0.27	0.30	0.28	0.29	0.30	0.27
P	<0.05	<0.05	<0.05	<0.05	<0.05	<0.06	<0.05
Pd	<0.05	<0.05	<0.05	<0.05	<0.05	<0.06	<0.05
Rh	<0.05	<0.05	<0.05	<0.05	<0.05	<0.06	<0.05
Ru	<0.05	<0.05	<0.05	<0.05	<0.05	<0.06	<0.05
S	0.18	0.16	0.18	0.17	0.19	0.20	0.16
Si	<0.05	<0.05	0.06	<0.05	<0.05	0.46	0.33
Sn	<0.05	<0.05	<0.05	<0.05	<0.05	<0.06	<0.05
Ti	2.63	2.77	2.07	2.75	1.82	2.18	2.76
Zn	<0.05	<0.05	<0.05	<0.05	<0.05	<0.06	<0.05
Zr	0.11	0.10	0.10	0.10	0.09	0.10	0.08

Table 3-8. SRAT Product Slurry Elemental Analyses (for SRAT-SME Runs, in Percentage of Dried Solids).

Elements	Tk40-8	Tk40-9	Tk40-10	Tk51-2	Tk51-3	Tk51-4
Ag	<0.05	<0.05	<0.05	<0.05	<0.06	<0.05
Al	8.17	8.11	9.09	9.55	9.58	9.88
B	<0.05	<0.05	<0.05	<0.05	NR	<0.05
Ba	<0.05	<0.05	<0.05	<0.05	<0.05	<0.05
Ca	0.54	0.53	0.52	0.60	0.47	0.50
Cr	0.15	0.15	0.18	0.19	0.23	0.23
Cu	<0.05	<0.05	<0.05	<0.05	<0.05	<0.05
Fe	6.93	6.91	8.36	7.51	8.31	8.07
Hg	0.04	0.04	0.03	0.98	0.39	0.66
K	<0.05	<0.05	<0.05	0.31	<0.05	<0.05
Li	<0.05	<0.05	<0.05	<0.05	<0.06	<0.05
Mg	0.14	0.14	0.16	0.16	0.19	0.19
Mn	2.58	2.57	3.08	2.71	3.02	2.92
Na	10.36	10.50	11.06	9.13	9.30	9.17
Ni	0.27	0.29	0.32	0.20	0.24	0.24
P	<0.05	<0.05	<0.05	<0.05	<0.05	<0.05
Pd	<0.05	<0.05	<0.05	<0.05	<0.05	<0.05
Rh	<0.05	<0.05	<0.05	<0.05	<0.05	0.60
Ru	<0.05	<0.05	<0.05	<0.05	<0.05	<0.05
S	0.18	0.18	0.20	0.19	0.21	0.22
Si	0.11	0.07	0.09	0.31	0.37	0.35
Sn	<0.05	0.06	0.07	<0.05	<0.05	<0.05
Ti	2.82	3.19	<0.05	<0.05	<0.06	<0.05
Zn	<0.05	<0.05	<0.05	<0.05	<0.05	<0.05
Zr	0.09	0.09	0.11	0.12	0.14	0.14

NR = Not Reported.

Hg is notably low in all Tank 40 SRAT products, with a maximum of 8.04×10^{-4} mol Hg per L slurry observed in Tk40-2 (equates to 0.05% of total solids). This is consistent with excellent Hg removal during SRAT processing. Higher values are seen in Tank 51 experiments, varying between 4.8×10^{-3} and 1.47×10^{-2} mol Hg per L slurry (0.39 – 0.98 % of total solids), suggesting less efficient Hg removal in Tank 51 material. Possible reasons for this are discussed later in this report.

SME product slurry elemental concentrations are given in Table 3-9.

Table 3-9. SME Product Slurry Elemental Analyses (for SRAT-SME Runs, in Percentage of Dried Solids).

Elements	Tk40-8	Tk40-9	Tk40-10	Tk51-2	Tk51-3	Tk51-4
Ag	<0.07	<0.07	<0.07	<0.08	<0.07	<0.07
Al	4.51	4.02	4.35	5.11	5.47	6.13
B	1.02	1.25	1.26	1.22	NR	1.16
Ba	<0.08	<0.08	<0.08	<0.08	<0.08	<0.08
Ca	0.33	0.24	0.26	0.35	0.27	0.28
Cr	0.08	<0.08	0.08	0.11	0.12	0.12
Cu	<0.08	<0.08	<0.08	<0.08	<0.08	<0.08
Fe	3.65	3.53	3.88	4.04	4.32	4.21
Hg	0.02	0.01	0.01	0.12	0.02	0.03
K	<0.08	<0.08	<0.08	0.31	<0.08	<0.08
Li	1.55	1.55	1.61	1.58	1.56	1.55
Mg	0.08	0.07	0.08	0.10	0.10	0.10
Mn	1.36	1.30	1.46	1.42	1.59	1.52
Na	7.45	8.48	8.18	7.23	7.14	7.29
Ni	0.15	0.13	0.14	0.11	0.18	0.12
P	<0.08	<0.08	<0.08	<0.08	<0.08	<0.08
Pd	<0.08	<0.08	<0.08	<0.08	<0.08	<0.08
Rh	<0.08	<0.08	<0.08	<0.08	<0.08	0.47
Ru	<0.08	<0.08	<0.08	<0.08	<0.08	<0.08
S	0.08	<0.08	<0.08	0.11	0.11	0.11
Si	17.51	18.38	19.44	17.77	17.77	18.29
Sn	<0.08	<0.08	<0.08	<0.08	<0.08	<0.08
Ti	1.53	1.46	<0.07	<0.08	<0.07	<0.07
Zn	<0.08	<0.08	<0.08	<0.08	<0.08	<0.08
Zr	<0.08	<0.08	<0.08	0.09	0.08	<0.08

NR = Not Reported.

Again, Hg is low in all SME products reported in Table 3-9, ranging from 1.52×10^{-4} to 3.32×10^{-3} mol L^{-1} (0.01 – 0.12 % of total solids). Increases in B and Si concentrations (relative to those reported in Table 3-8) are consistent with the addition of glass frit.

Supernatant elemental compositions of SRAT products are given in Table 3-10 and Table 3-11 for SRAT-only experiments and SRAT-SME experiments, respectively.

Table 3-10. SRAT Product Supernatant Elemental Analyses (for SRAT-only Runs, in moles per liter of supernatant).

Elements	Tk40-1	Tk40-2	Tk40-3	Tk40-4	Tk40-5	Tk40-6	Tk40-7
Ag	<9.27E-06	<9.27E-06	<9.27E-06	<9.27E-06	<9.27E-06	<9.27E-06	<9.27E-06
Al	5.32E-02	1.45E-01	3.56E-02	9.78E-02	9.60E-02	3.98E-03	9.45E-02
B	4.76E-02	4.21E-02	4.27E-02	3.72E-02	4.95E-02	3.23E-02	3.10E-02
Ba	3.12E-05	4.93E-05	2.63E-05	4.35E-05	5.75E-05	8.81E-06	6.90E-05
Ca	6.57E-02	5.07E-02	4.55E-02	4.35E-02	5.55E-02	3.87E-03	3.19E-02
Cr	1.59E-03	4.02E-03	2.16E-03	4.46E-03	4.98E-03	1.06E-04	4.29E-03
Cu	9.70E-04	1.23E-03	9.03E-04	1.06E-03	1.33E-03	5.52E-05	8.05E-04
Fe	3.92E-02	1.05E-01	2.68E-02	6.15E-02	6.48E-02	1.37E-03	8.33E-02
Hg	6.39E-05	1.72E-05	4.31E-05	2.98E-05	5.21E-05	<4.99E-06	5.31E-05
K	7.05E-02	6.84E-03	4.87E-02	5.11E-03	7.56E-03	5.45E-03	4.08E-03
Li	7.30E-03	8.15E-03	6.84E-03	6.54E-03	8.13E-03	6.34E-03	4.61E-03
Mg	8.26E-03	9.02E-03	7.56E-03	7.83E-03	1.01E-02	6.36E-03	7.34E-03
Mn	1.78E-01	1.77E-01	1.60E-01	1.43E-01	2.08E-01	9.24E-02	1.26E-01
Na	1.93E+00	1.87E+00	1.79E+00	1.55E+00	2.00E+00	1.80E+00	1.23E+00
Ni	7.17E-03	8.39E-03	7.96E-03	9.05E-03	1.16E-02	6.92E-04	8.47E-03
P	<3.23E-05	4.02E-05	<3.23E-05	<3.23E-05	<3.23E-05	<3.23E-05	4.25E-05
Pd	<9.40E-06	<9.40E-06	<9.40E-06	<9.40E-06	<9.40E-06	<9.40E-06	<9.40E-06
Rh	1.51E-04	2.18E-04	1.48E-04	2.11E-04	2.29E-04	3.58E-05	1.80E-04
Ru	2.64E-04	3.02E-04	2.23E-04	2.97E-04	3.80E-04	4.92E-05	2.64E-04
S	2.56E-04	4.58E-04	1.83E-04	3.33E-04	2.67E-02	2.48E-02	1.56E-02
Si	<3.56E-05	<3.56E-05	<3.56E-05	<3.56E-05	5.20E-04	8.42E-05	5.79E-04
Sn	4.82E-03	9.65E-03	6.13E-03	1.40E-02	<8.42E-06	<8.42E-06	6.22E-04
Ti	2.07E-02	4.36E-02	2.42E-02	5.72E-02	4.58E-02	3.99E-04	3.83E-02
Zn	<1.53E-05	5.63E-05	3.59E-05	4.60E-05	5.73E-05	<1.53E-05	4.10E-05
Zr	5.17E-04	1.98E-03	7.00E-04	1.73E-03	1.82E-03	2.64E-05	1.64E-03

Table 3-11. SRAT Product Supernatant Elemental Analyses (for SRAT-SME Runs, in moles per liter of supernatant).

Elements	Tk40-8	Tk40-9	Tk40-10	Tk51-2	Tk51-3	Tk51-4
Ag	<9.27E-06	<9.27E-06	<9.27E-06	<9.27E-05	<9.27E-06	<9.27E-06
Al	3.24E-02	3.20E-02	7.39E-03	4.50E-02	1.80E-02	1.81E-02
B	3.72E-02	3.91E-02	1.83E-03	1.58E-02	1.31E-02	1.64E-02
Ba	2.88E-05	2.79E-05	1.43E-05	<7.28E-05	1.25E-05	1.19E-05
Ca	2.45E-02	2.20E-02	8.52E-03	3.68E-02	1.56E-02	1.63E-02
Cr	1.04E-03	9.68E-04	2.86E-04	3.35E-03	5.46E-04	1.50E-03
Cu	5.00E-04	5.30E-04	2.94E-05	4.66E-04	1.70E-04	5.48E-04
Fe	1.58E-02	1.35E-02	4.90E-03	3.81E-02	8.79E-03	1.40E-02
Hg	<4.99E-06	5.71E-06	<4.99E-06	1.18E-05	5.44E-05	3.25E-05
K	5.20E-03	5.46E-03	2.02E-03	1.22E-02	3.13E-03	2.58E-03
Li	5.37E-03	6.12E-03	5.11E-03	4.53E-03	3.37E-03	4.10E-03
Mg	6.32E-03	6.91E-03	5.80E-03	1.21E-02	8.65E-03	1.00E-02
Mn	1.52E-01	1.58E-01	8.38E-02	1.59E-01	1.19E-01	1.46E-01
Na	1.58E+00	1.77E+00	1.21E+00	1.11E+00	9.95E-01	1.27E+00
Ni	6.63E-03	6.79E-03	2.80E-03	7.81E-03	2.92E-03	5.70E-03
P	<3.23E-05	<3.23E-05	<3.23E-05	<3.23E-04	<3.23E-05	4.08E-05
Pd	<9.40E-06	<9.40E-06	<9.40E-06	<9.40E-05	<9.40E-06	<9.40E-06
Rh	1.01E-04	1.03E-04	5.81E-05	<9.72E-05	4.99E-05	9.57E-05
Ru	1.89E-04	1.78E-04	1.39E-04	<9.89E-05	1.86E-04	3.36E-04
S	2.01E-02	2.10E-02	2.01E-02	1.41E-02	1.31E-02	2.25E-02
Si	3.06E-04	2.71E-04	2.98E-04	<3.56E-04	1.35E-03	2.57E-03
Sn	1.92E-04	1.83E-04	6.02E-05	<8.42E-05	<8.42E-06	2.72E-04
Ti	1.15E-02	1.03E-02	<2.09E-05	<2.09E-04	<2.09E-05	<2.09E-05
Zn	3.11E-05	3.10E-05	<1.53E-05	<1.53E-04	<1.53E-05	2.48E-05
Zr	3.12E-04	2.58E-04	1.49E-04	2.06E-03	4.37E-04	8.51E-04

Data in Table 3-10 and Table 3-11 indicate large-scale dissolution of Mn following SRAT processing. Mn concentrations in SRAT supernatant vary from 8.38×10^{-2} mol L^{-1} to 2.08×10^{-1} mol L^{-1}, consistent with 70 to 100% solubility of Mn, slightly higher than the 65% and 88% solubilities observed by Martino in SB 10/SRE solubility experiments at 100% and 140% acid addition, respectively.[17] Iron, calcium, and magnesium also exhibit partial solubility in the SRAT product supernatant phase, likely resulting from the dissolution of these metals by nitric and glycolic acid.

SME Product supernatant elemental compositions are given in Table 3-12.

Table 3-12. SME Product Supernatant Elemental Analyses (for SRAT-SME Runs, in moles per liter of supernatant).

Elements	Tk40-8	Tk40-9	Tk40-10	Tk51-2	Tk51-3	Tk51-4
Ag	<9.27E-06	<9.27E-06	<9.27E-06	<9.27E-05	<9.27E-05	<9.27E-06
Al	3.74E-02	2.14E-02	9.45E-03	6.41E-02	2.32E-02	1.93E-02
B	4.23E-02	3.45E-02	6.07E-03	2.39E-02	1.94E-02	2.04E-02
Ba	2.96E-05	2.05E-05	1.24E-05	<7.28E-05	<7.28E-05	1.15E-05
Ca	2.13E-02	1.70E-02	1.04E-02	2.48E-02	1.63E-02	1.95E-02
Cr	1.16E-03	8.30E-04	3.53E-04	4.56E-03	7.42E-04	1.44E-03
Cu	5.26E-04	3.71E-04	3.32E-05	5.82E-04	<1.57E-04	4.68E-04
Fe	1.25E-02	7.34E-03	6.54E-03	6.16E-02	1.04E-02	1.49E-02
Hg	<4.99E-06	<4.99E-06	<4.99E-06	9.63E-05	2.81E-05	2.79E-05
K	5.46E-03	4.07E-03	2.57E-03	1.89E-02	4.72E-03	2.66E-03
Li	2.42E-02	1.75E-02	2.37E-02	2.68E-02	1.93E-02	2.03E-02
Mg	6.79E-03	6.32E-03	7.16E-03	1.51E-02	1.10E-02	1.05E-02
Mn	1.58E-01	1.23E-01	7.63E-02	1.62E-01	1.20E-01	1.10E-01
Na	1.74E+00	1.35E+00	1.53E+00	1.41E+00	1.28E+00	1.34E+00
Ni	7.04E-03	5.76E-03	3.16E-03	9.53E-03	3.54E-03	5.65E-03
P	<3.23E-05	3.66E-05	<3.23E-05	<3.23E-04	<3.23E-04	<3.23E-05
Pd	<9.40E-06	<9.40E-06	<9.40E-06	<9.40E-05	<9.40E-05	<9.40E-06
Rh	1.13E-04	7.96E-05	7.09E-05	<9.72E-05	<9.72E-05	8.94E-05
Ru	2.01E-04	1.44E-04	1.82E-04	<9.89E-05	2.40E-04	3.33E-04
S	2.13E-02	1.76E-02	2.70E-02	1.77E-02	1.74E-02	2.30E-02
Si	8.53E-04	9.10E-04	8.79E-04	<3.56E-04	1.55E-03	2.73E-03
Sn	2.13E-04	1.58E-04	6.86E-05	<8.42E-05	<8.42E-05	2.57E-04
Ti	1.13E-02	6.28E-03	<2.09E-05	<2.09E-04	<2.09E-04	<2.09E-05
Zn	5.67E-05	2.56E-05	<1.53E-05	<1.53E-04	<1.53E-04	2.49E-05
Zr	3.24E-04	1.47E-04	1.96E-04	2.00E-03	5.59E-04	7.83E-04

Data in Table 3-12 indicate continued solubility of Mn, Fe, Ca, and Mg, suggesting that these metals are not significantly reoxidized in the course of SME processing. Note also the low concentrations of Si ($<3.56\times10^{-4}$ to 8.53×10^{-4} mol L^{-1}), suggesting that most Si present is insoluble glass frit.

The data reported above may be used to calculate the percentage of each element that is soluble in each SRAT and SME product. These soluble percentages are given in Table 3-13 through Table 3-15. The value of "ND" is assigned to elements that exhibit a "Not Determinable" solubility due to slurry concentrations below detection limits.

Table 3-13. Percent Solubilities of Elements in SRAT Products (SRAT-Only Experiments, molar basis).

Elements	Tk40-1	Tk40-2	Tk40-3	Tk40-4	Tk40-5	Tk40-6	Tk40-7
Ag	ND	ND	ND	ND	ND	ND	ND
Al	4.7	14.3	3	9.1	9	0.3	9.8
B	ND	ND	ND	ND	ND	ND	ND
Ba	ND	ND	ND	ND	ND	ND	ND
Ca	100	100	100	100	100	9.6	96.4
Cr	14	42.7	20	45	51.1	1	50.4
Cu	ND	ND	ND	ND	ND	ND	ND
Fe	7.8	23.6	5.4	13.5	15.2	0.3	21.7
Hg	8.8	2	5	6.4	9.5	<0.7	7
K	100	ND	100	100	100	ND	ND
Li	ND	ND	ND	ND	ND	ND	ND
Mg	34.7	45.8	33.1	37.5	49.5	29	41.8
Mn	94.7	100	88.1	87.7	100	56.2	90.7
Na	100	100	100	100	100	100	92.7
Ni	37.3	54.6	44.4	55.1	71.3	4.1	59.7
P	ND	ND	ND	ND	ND	ND	ND
Pd	ND	ND	ND	ND	ND	ND	ND
Rh	ND	ND	ND	ND	ND	ND	ND
Ru	ND	ND	ND	ND	ND	ND	ND
S	1.3	2.7	0.9	1.9	100	100	100
Si	ND	ND	<0.5	ND	ND	0.2	1.6
Sn	ND	ND	ND	ND	ND	ND	ND
Ti	12.0	26.3	18.1	33.8	41.9	0.3	24.6
Zn	ND	ND	ND	ND	ND	ND	ND
Zr	12.3	56.7	17.3	47.1	54.5	0.7	57

ND = Not Determinable

Table 3-14. Percent Solubilities of Elements in SRAT Products (SRAT-SME Experiments, molar basis).

Elements	Tk40-8	Tk40-9	Tk40-10	Tk51-2	Tk51-3	Tk51-4
Ag	ND	ND	ND	ND	ND	ND
Al	3.1	2.9	0.8	4.1	1.9	1.5
B	ND	ND	ND	ND	ND	ND
Ba	ND	ND	ND	ND	ND	ND
Ca	52.1	46.1	23.7	79.4	51.2	40.7
Cr	10.6	9.2	3	29.2	4.7	10.6
Cu	ND	ND	ND	ND	ND	ND
Fe	3.6	3	1.2	9.1	2.2	3
Hg	<0.7	0.7	<1.2	0.1	1.1	0.3
K	ND	ND	ND	49.6	ND	ND
Li	ND	ND	ND	ND	ND	ND
Mg	31.6	33	30.8	59.7	42.6	40.8
Mn	92.3	92.6	53.8	100	82.4	85.8
Na	100	100	90.4	90.2	93.7	99.5
Ni	41.7	37.5	18.5	74.8	27.2	44.3
P	ND	ND	ND	ND	ND	ND
Pd	ND	ND	ND	ND	ND	ND
Rh	ND	ND	ND	ND	ND	0.5
Ru	ND	ND	ND	ND	ND	ND
S	100	100	100	75.8	74.7	100
Si	2.3	2.9	3.3	<1	3.9	6.4
Sn	ND	10.6	3.6	ND	ND	ND
Ti	6.4	4.9	ND	ND	ND	ND
Zn	ND	ND	ND	ND	ND	ND
Zr	9.4	7.4	4.6	50.1	11	17.9

ND = Not Determinable

Table 3-15. Percent Solubilities of Elements in SME Products (molar basis).

Elements	Tk40-8	Tk40-9	Tk40-10	Tk51-2	Tk51-3	Tk51-4
Ag	ND	ND	ND	ND	ND	ND
Al	3	2.3	0.7	4.6	1.8	1.4
B	6.1	4.8	0.7	2.9	ND	3
Ba	ND	ND	ND	ND	ND	ND
Ca	35.3	46	20.3	39.5	39	45.1
Cr	10.5	ND	2.9	30	5.2	10.3
Cu	ND	ND	ND	ND	ND	ND
Fe	2.6	1.9	1.2	11.7	2.2	3.2
Hg	<0.8	<2.7	<2.3	2.3	4.5	3.3
K	ND	ND	ND	32.7	ND	ND
Li	1.5	1.3	1.3	1.6	1.4	1.5
Mg	28.4	34.2	26.9	48.9	41.1	40.4
Mn	86.8	84.4	36.8	85.9	66.3	63.9
Na	72.9	59.3	54.9	61.5	65.9	67.7
Ni	38.7	43.1	17.1	69.1	18.8	43.5
P	ND	ND	ND	ND	ND	ND
Pd	ND	ND	ND	ND	ND	ND
Rh	ND	ND	ND	ND	ND	0.3
Ru	ND	ND	ND	ND	ND	ND
S	100	ND	ND	72.8	81.7	100
Si	0.02	0.02	0.02	<0.01	0.04	0.07
Sn	ND	ND	ND	ND	ND	ND
Ti	5.5	3.8	ND	ND	ND	ND
Zn	ND	ND	ND	ND	ND	ND
Zr	ND	ND	ND	27.4	10.3	ND

ND = Not Determinable

The solubilities reported in Table 3-13 through Table 3-15 indicate partial solubility of several metals (e.g., Mn, Ca, Mg, Ni), suggesting possible reduction through the addition of acid. Generally, iron tends to be only marginally soluble, reaching only ~24% in the highest cases.

SRAT product slurry ion concentrations are given in Table 3-16 and Table 3-17 for SRAT-only experiments and SRAT-SME experiments, respectively.

Table 3-16. SRAT Product Slurry Ion Analyses (for SRAT-only Runs, in moles per liter of slurry).

Ions	Tk40-1	Tk40-2	Tk40-3	Tk40-4	Tk40-5	Tk40-6	Tk40-7
HCO_2^-	2.86E-02	6.03E-02	4.04E-02	3.15E-02	1.97E-02	3.15E-02	3.92E-03
Cl^-	5.27E-02	5.67E-03	5.14E-02	7.87E-03	5.75E-03	5.61E-03	5.95E-03
NO_2^-	<2.17E-03	<2.17E-03	<2.17E-03	<2.17E-03	<2.17E-03	<2.17E-03	<2.17E-03
NO_3^-	1.37E+00	1.36E+00	1.20E+00	1.27E+00	1.20E+00	1.06E+00	1.09E+00
PO_4^{-3}	<1.05E-03	<1.05E-03	<1.05E-03	<1.05E-03	<1.05E-03	<1.05E-03	<1.05E-03
SO_4^{-2}	1.77E-02	1.39E-02	1.76E-02	1.61E-02	1.60E-02	1.85E-02	1.42E-02
$C_2O_4^{-2}$	3.14E-02	3.52E-02	3.14E-02	5.23E-02	4.19E-02	1.82E-02	3.50E-02
$HOCH_2CO_2^-$	9.07E-01	9.54E-01	1.07E+00	1.16E+00	1.04E+00	8.43E-01	9.30E-01
CO_3^{-2}	1.40E-02	1.33E-02	1.93E-02	1.73E-02	1.12E-02	2.26E-02	<6.66E-03
NH_4^+	<2.77E-04	<2.77E-04	<2.77E-04	<2.77E-04	<2.77E-04	<2.77E-04	<2.77E-03

Table 3-17. SRAT Product Slurry Ion Analyses (for SRAT-SME Runs, in moles per liter of slurry).

Ions	Tk40-8	Tk40-9	Tk40-10	Tk51-2	Tk51-3	Tk51-4
HCO_2^-	1.71E-02	2.05E-02	2.77E-02	4.27E-03	2.05E-02	4.56E-03
Cl^-	3.70E-03	3.99E-03	4.02E-03	4.11E-02	5.05E-03	4.88E-03
NO_2^-	<2.48E-03	<2.60E-03	<2.54E-03	<2.57E-03	<2.17E-03	<2.17E-03
NO_3^-	1.07E+00	1.05E+00	8.01E-01	1.02E+00	7.89E-01	9.34E-01
PO_4^{-3}	<1.20E-03	<1.26E-03	<1.23E-03	<1.25E-03	<1.05E-03	<1.05E-03
SO_4^{-2}	1.75E-02	1.91E-02	1.80E-02	1.80E-02	1.65E-02	2.02E-02
$C_2O_4^{-2}$	2.53E-02	2.93E-02	2.41E-02	3.31E-02	1.91E-02	2.65E-02
$HOCH_2CO_2^-$	9.06E-01	9.65E-01	6.23E-01	6.86E-01	6.10E-01	6.36E-01
CO_3^{-2}	<6.66E-03	2.66E-02	<6.66E-03	<6.66E-03	<6.66E-03	<6.66E-03
NH_4^+	<2.77E-03	<2.77E-03	<2.77E-03	<2.77E-03	<2.77E-03	<2.77E-03

At first review of the data in Table 3-16 and Table 3-17, it is clear that all SRAT cycles performed in SB 10 simulant experiments were capable of destroying nitrite to levels below detection limit. It is also apparent that chloride concentrations are greater in SRAT product slurries than originally present in SRAT receipt samples. While some of this concentration increase can be attributed to the removal of water during SRAT processing or the failure of liquid pH probes, it is likely that chloride concentrations are increased to unrealistic levels (relative to SB 10 targeted concentrations) due to the use of ruthenium chloride as a source for ruthenium metal. Marginal increases in formate and oxalate concentrations are also observed in SRAT products. These increases are consistent with small conversion fractions of added glycolate to formate and oxalate as reaction side products. Anion conversions for each experiment are discussed in detail in Section 3.6.

Most notably, there is no sign of detectable ammonium in SRAT products obtained from SB 10 testing. This is consistent with previous observations that the nitric-glycolic flowsheet drastically decreases the potential for ammonium formation.[5]

SME product ion concentrations are reported in Table 3-18.

Table 3-18. SME Product Slurry Ion Analyses (for SRAT-SME Runs, in moles per liter of slurry).

Ions	Tk40-8	Tk40-9	Tk40-10	Tk51-2	Tk51-3	Tk51-4
HCO_2^-	2.14E-02	3.06E-02	3.69E-02	6.05E-03	9.23E-03	1.01E-02
Cl^-	<3.78E-03	3.58E-03	4.29E-03	4.10E-02	4.32E-03	4.20E-03
NO_2^-	<2.92E-03	<2.75E-03	<2.92E-03	<2.78E-03	<2.87E-03	<2.17E-03
NO_3^-	9.53E-01	8.03E-01	8.42E-01	1.03E+00	8.04E-01	7.50E-01
PO_4^{-3}	<1.41E-03	<1.33E-03	<1.41E-03	<1.35E-03	<1.39E-03	<1.05E-03
SO_4^{-2}	1.68E-02	1.36E-02	1.94E-02	1.87E-02	1.87E-02	1.81E-02
$C_2O_4^{-2}$	3.06E-02	2.35E-02	3.77E-02	5.09E-02	2.20E-02	3.17E-02
$HOCH_2CO_2^-$	8.63E-01	6.04E-01	6.33E-01	6.55E-01	6.63E-01	5.49E-01
CO_3^{-2}	2.51E-02	<6.66E-03	<6.66E-03	7.49E-03	1.33E-03	<6.66E-03
NH_4^+	<2.77E-03	<2.77E-03	<2.77E-03	<2.77E-03	<2.77E-03	<2.77E-03

Data in Table 3-18 suggest that the SME cycle is largely inert with respect to anion conversion chemistry. Similar concentrations of formate, nitrate, oxalate and glycolate are observed in both SRAT and SME product with minimal variation. SME cycle anion conversions are discussed in Section 3.6. SME products also failed to produce measurable ammonium, indicating continued efficiency of the nitric-glycolic flowsheet to minimize flammable byproducts.

Supernatant phase ion concentrations for SRAT products (from both SRAT-only and SRAT-SME experiments) and SME products are given in Table 3-19, Table 3-20, and Table 3-21, respectively. Concentrations of ammonium and carbonate are calculated from slurry concentrations reported earlier and converted to a supernatant basis to provide a conservative value.

Table 3-19. SRAT Product Supernatant Ion Analyses (for SRAT-only Runs, in moles per liter of supernatant).

Ions	Tk40-1	Tk40-2	Tk40-3	Tk40-4	Tk40-5	Tk40-6	Tk40-7
HCO_2^-	7.62E-03	1.16E-02	7.49E-03	9.59E-03	3.53E-02	2.60E-02	9.88E-03
Cl^-	5.19E-02	<2.82E-03	4.51E-02	<2.82E-03	5.62E-03	<2.82E-03	4.15E-03
NO_2^-	<2.17E-03	<2.17E-03	<2.17E-03	<2.17E-03	<2.17E-03	<2.17E-03	<2.17E-03
NO_3^-	1.44E+00	1.54E+00	1.02E+00	1.09E+00	1.52E+00	9.99E-01	1.26E+00
PO_4^{-3}	<1.05E-03	<1.05E-03	<1.05E-03	<1.05E-03	<1.05E-03	<1.05E-03	<1.05E-03
SO_4^{-2}	2.03E-02	1.75E-02	1.73E-02	1.46E-02	2.15E-02	1.92E-02	1.42E-02
$C_2O_4^{-2}$	2.40E-02	2.93E-02	2.03E-02	3.04E-02	3.28E-02	1.35E-02	3.69E-02
$HOCH_2CO_2^-$	9.23E-01	9.99E-01	9.66E-01	9.56E-01	1.07E+00	7.24E-01	9.66E-01
$CO_3^{-2\dagger}$	1.48E-02	1.40E-02	2.11E-02	1.80E-02	1.16E-02	2.34E-02	<6.80E-03
$NH_4^{+\dagger}$	<2.94E-04	<2.92E-04	<3.03E-04	<2.88E-04	<2.87E-04	<2.87E-04	<2.83E-03

†Supernatant carbonate and ammonium values are calculated from the slurry measurements and converted to a supernatant basis to provide a conservative value.

Table 3-20. SRAT Product Supernatant Ion Analyses (for SRAT-SME Runs, in moles per liter of supernatant).

Ions	Tk40-8	Tk40-9	Tk40-10	Tk51-2	Tk51-3	Tk51-4
HCO_2^-	1.86E-02	2.16E-02	1.86E-02	3.91E-03	3.45E-03	9.14E-03
Cl^-	2.99E-03	3.03E-03	3.06E-03	4.39E-02	<2.82E-03	<2.82E-03
NO_2^-	<2.13E-03	<2.17E-03	<2.17E-03	<2.17E-03	<2.17E-03	<2.17E-03
NO_3^-	1.11E+00	1.15E+00	8.53E-01	1.13E+00	7.60E-01	1.06E+00
PO_4^{-3}	<1.03E-03	<1.05E-03	<1.05E-03	<1.05E-03	<1.05E-03	<1.05E-03
SO_4^{-2}	1.77E-02	1.87E-02	5.56E-03	1.76E-02	1.53E-02	1.83E-02
$C_2O_4^{-2}$	2.16E-02	2.34E-02	5.82E-03	2.82E-02	1.28E-02	8.99E-03
$HOCH_2CO_2^-$	8.28E-01	8.71E-01	5.79E-01	7.06E-01	5.04E-01	5.50E-01
$CO_3^{-2\dagger}$	<7.41E-03	2.86E-02	<6.96E-03	<6.89E-03	<7.07E-03	<6.91E-03
$NH_4^{+\dagger}$	<3.08E-03	<2.97E-03	<2.90E-03	<2.87E-03	<2.94E-03	<2.88E-03

†Supernatant carbonate and ammonium values are calculated from the slurry measurements and converted to a supernatant basis to provide a conservative value.

Table 3-21. SME Product Supernatant Ion Analyses (for SRAT-SME Runs, in moles per liter of supernatant).

Ions	Tk40-8	Tk40-9	Tk40-10	Tk51-2	Tk51-3	Tk51-4
HCO_2^-	1.97E-02	2.24E-02	2.62E-02	7.74E-03	1.06E-02	1.78E-02
Cl^-	2.65E-03	2.83E-03	3.95E-03	5.60E-02	3.81E-03	<2.82E-03
NO_2^-	<1.82E-03	<2.17E-03	<2.17E-03	<2.17E-03	<2.17E-03	<2.17E-03
NO_3^-	9.78E-01	1.01E+00	1.09E+00	1.46E+00	9.68E-01	1.09E+00
PO_4^{-3}	<8.83E-04	<1.05E-03	<1.05E-03	<1.05E-03	<1.05E-03	<1.05E-03
SO_4^{-2}	1.58E-02	1.61E-02	4.07E-03	2.42E-02	2.03E-02	1.95E-02
$C_2O_4^{-2}$	2.21E-02	2.39E-02	4.23E-03	6.61E-02	7.68E-03	7.28E-03
$HOCH_2CO_2^-$	7.26E-01	7.32E-01	6.82E-01	7.93E-01	6.00E-01	5.14E-01
$CO_3^{-2\dagger}$	3.09E-02	<8.16E-03	<8.47E-03	9.49E-03	1.58E-03	<7.80E-03
$NH_4^{+\dagger}$	<3.41E-03	<3.40E-03	<3.52E-03	<3.51E-03	<3.28E-03	<3.24E-03

†Supernatant carbonate and ammonium values are calculated from the slurry measurements and converted to a supernatant basis to provide a conservative value.

SRAT and SME supernatant ion concentrations are largely unremarkable. Nitrite concentrations remain undetectable, while nitrate, formate, glycolate and oxalate exist at concentrations consistent with those reported in the bulk slurries.

Additional SRAT and SME product analyses for total organic carbon, volatile and semivolatile organic concentrations, and product pH measurements are given in Table 3-22 and Table 3-23, respectively. Full pH profiles during SRAT and SME processing are given in 1.1.1.1.1Appendix B.

Table 3-22. Other SRAT Product Analyses.

Run	TOC[d] (mg/L slurry)	VOA (mg/L slurry)	SVOA (mg/L slurry)	pH
Tk40-1	20,000	<0.2	<1	4.62
Tk40-2	25,300	<0.2	<1	3.58
Tk40-3	25,300	<0.25	<1	4.77
Tk40-4	29,100	<0.25	<1	3.82
Tk40-5	25,800	<0.2	<1	4.03
Tk40-6	24,200	<0.2	<1	7.07
Tk40-7	26,400	<0.2	<1	3.37
Tk40-8	1,760	<0.2	<1	4.96
Tk40-9	17,020	<0.2	<1	4.94
Tk40-10	17,200	<0.2	<1	6.29
Tk51-2	20,700	<0.2	<1	4.57
Tk51-3	512	<0.2	<1	6.01
Tk51-4	18,100	<0.2	<1	5.13

[d] TOC measurements for Tk40-8 and Tk51-3 are abnormally low and inconsistent with IC measurements for glycolate and formate. These TOC concentrations are therefore suspect and should not be considered quantitative.

Table 3-23. Other SME Product Analyses.

Run	TOC[e] (mg/L slurry)	VOA (mg/L slurry)	SVOA (mg/L slurry)	pH
Tk40-8	13,400	<0.2	<1	4.99
Tk40-9	14,200	<0.2	<1	5.12
Tk40-10	15,400	<0.2	<1	6.47
Tk51-2	14,700	<0.2	<1	4.39
Tk51-3	496	<0.2	<1	6.14
Tk51-4	15,200	<0.2	<1	5.21

As the data in Table 3-22 and Table 3-23 show, no detectable volatile or semivolatile organic compounds were identified in the SB 10 SRAT or SME product sludges. This is consistent with previous observations made by Lambert.[10] With the exception of experiments Tk40-8 and Tk51-3, SRAT product total organic carbon (TOC) measurements fall between 17,020 and 29,100 mg/L, while SME product TOC measurements fall between 13,400 and 15,400 mg/L. The outlier concentrations reported for Tk40-8 and Tk51-3 products are not consistent with organic compound concentrations measured by IC, suggesting that these TOC measurements are likely the result of analytical error and should not be considered representative of expected TOC concentrations.

Generally speaking, SRAT and SME products remain acidic following the conclusion of testing. This is consistent with previous observations that the nitric-glycolic flowsheet produces sludge products that exhibit stable pHs throughout testing.[5] SRAT product pH values seem to be inversely proportional to acid stoichiometry. The SRAT product pH values for Tank 40 and Tank 51 sludges are plotted against KMA stoichiometry in Figure 3-1. A plot of acid stoichiometry (as Hsu equivalent stoichiometry) vs pH can be reproduced (not shown here) with similar results).

[e] The TOC measurement for Tk51-3 is abnormally low and inconsistent with IC measurements for glycolate and formate. This TOC concentration is therefore suspect and should not be considered quantitative.

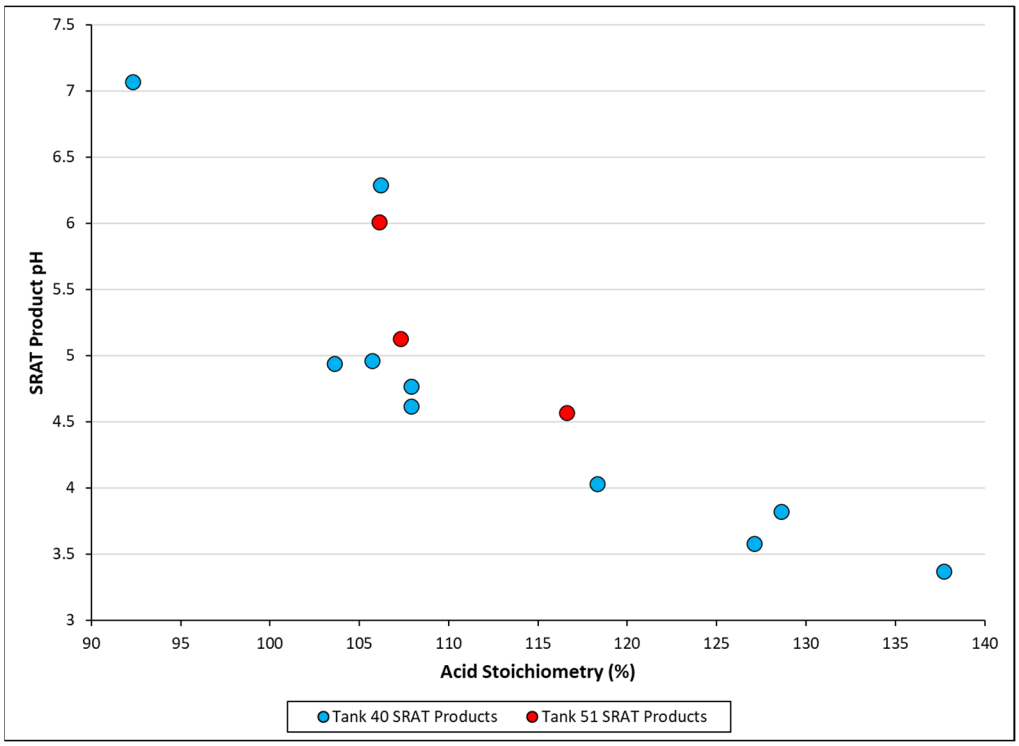

Figure 3-1. SB 10 SRAT Product pHs.

Generally, Tank 40 SRAT pH values fall along a similar trend, increasing with decreasing acid stoichiometry. An exception to this seems to be the SRAT product from Tk40-10 (stoichiometry = 106.2%, pH = 6.29). This experiment was a sludge-only test, whereas the remaining Tk40 experiments were coupled. This small delta in final pH vs. acid stoichiometry response may be an indicator of the impact of coupled processing on acid demand. Tank 51 SRAT products appear to fall slightly higher than Tank 40 SRAT products at corresponding acid stoichiometries. If the delta in pH observed in Tk40-10 can be attributed to differences in coupled operations, then it is possible the slight increase in pHs observed in Tank 51 compared to Tank 40 could also be due to performing all Tank 51 tests as sludge-only experiments.

The data reported in Table 3-23 indicate minimal change in pH following the SME cycle. This reinforces the concept that the SME cycle is largely inert during CPC processing.

3.3 Rheology

SRS sludge is most often approximated rheologically as a Bingham plastic. A Bingham plastic is characterized by viscous flow at shear stress that exceed the yield stress of the material. These parameters (yield stress and viscosity) are determined by measuring a shear rate-shear stress curve and fitting linear variables associated with the flow curve generated, according to Equation [3].

$$\tau = \tau_{YS} + \mu\dot{\gamma} \qquad [3]$$

Where,

τ is the shear stress in Pa,

τ_{YS} is the yield stress in Pa,

μ is the viscosity in daP, and

$\dot{\gamma}$ is the shear rate in s^{-1}.

Note that the ~34% decrease in ruthenium mentioned earlier represents a decrease of less than 0.1% in insoluble solids (< 1 milligram of insoluble solids decreased per gram of insoluble solids) and is therefore not expected to have any impact on rheological measurements provided in this report.

Table 3-24 gives the measured rheological parameters of the various SRAT receipt materials used in SB 10 simulant testing.

Table 3-24. SRAT Receipt and Pre-Acid Rheological Measurements.

Run	Total Dried Solids (wt%)	Insoluble Solids (wt%)	Sludge Density (g/mL)	Supernatant Density (g/mL)	Yield Stress (Pa)	Viscosity (cP)
Tk40 Receipt	13.9	8.49	1.112	1.045	0.9	5.2
Tk40 Receipt + MST	14.2	9.14	1.116	1.042	1.0	5.4
Tk40 Post PRFT Addition	16.2	9.28	1.138	1.059	1.6	6.9
Tk51 Receipt	14.1	8.78	1.116	1.045	3.6	9.9

As can be seen in Table 3-24, introduction of 15% MST slurry does not seem to have a significant impact on the rheology of Tank 40 sludge simulant. Tank 40 receipt exhibits a modest viscosity of 5.2 cP and a yield stress of 0.9 Pa, whereas the addition of MST increases these measurements to 5.4 cP and 1.0 Pa, respectively. Caustic boiling and introduction of soluble salts do appear to significantly impact both the viscosity and yield stress, increasing to 6.9 cP and 1.6 Pa, respectively. This is likely due to the increased solids content, the increase in supernatant density, and other parameters associated with the introduction of MST/SS waste. It is interesting to note that Tank 51 receipt appears to be thicker than any corresponding Tank 40 material, with viscosity as high as 9.9 cP and a yield stress of 3.6 Pa.

Rheological measurements of SRAT products produced in SB 10 testing are given in Table 3-25.

Table 3-25. SRAT Product Rheological Measurements.

Run	Total Dried Solids (wt%)	Insoluble Solids (wt%)	Sludge Density (g/mL)	Supernatant Density (g/mL)	Yield Stress (Pa)	Viscosity (cP)
Tk40-1	28.5	9.6	1.1955	1.1472	3.3	7.8
Tk40-2	26.1	8.3	1.1945	1.1530	0.1	3.2
Tk40-3	28.1	10.9	1.1559	1.1262	2.1	7.3
Tk40-4	27.1	9.2	1.2013	1.1329	0.4	3.9
Tk40-5	26.6	8.3	1.1974	1.1384	0.4	3.8
Tk40-6	27.0	10.0	1.1948	1.1117	10.8	11
Tk40-7	25.5	5.8	1.1896	1.1442	0.1	3.2
Tk40-8	27.6	12.0	1.1413	1.1174	2.4	7.5
Tk40-9	28.4	12.5	1.1945	1.1211	2.7	8.0
Tk40-10	22.8	11.2	1.1666	1.0832	0.3	3.5
Tk51-2	25.3	10.0	1.1843	1.1020	0.9	8.6
Tk51-3	21.4	12.0	1.1554	1.0800	0.8	5.3
Tk51-4	25.9	12.3	1.191	1.0840	4.6	9.4
			Design Basis	**Min**	**1.5**	**5.0**
				Max	**5.0**	**12.0**

The data in Table 3-25 are reproduced graphically in Figure 3-2 and Figure 3-3 for ease of interpretation.

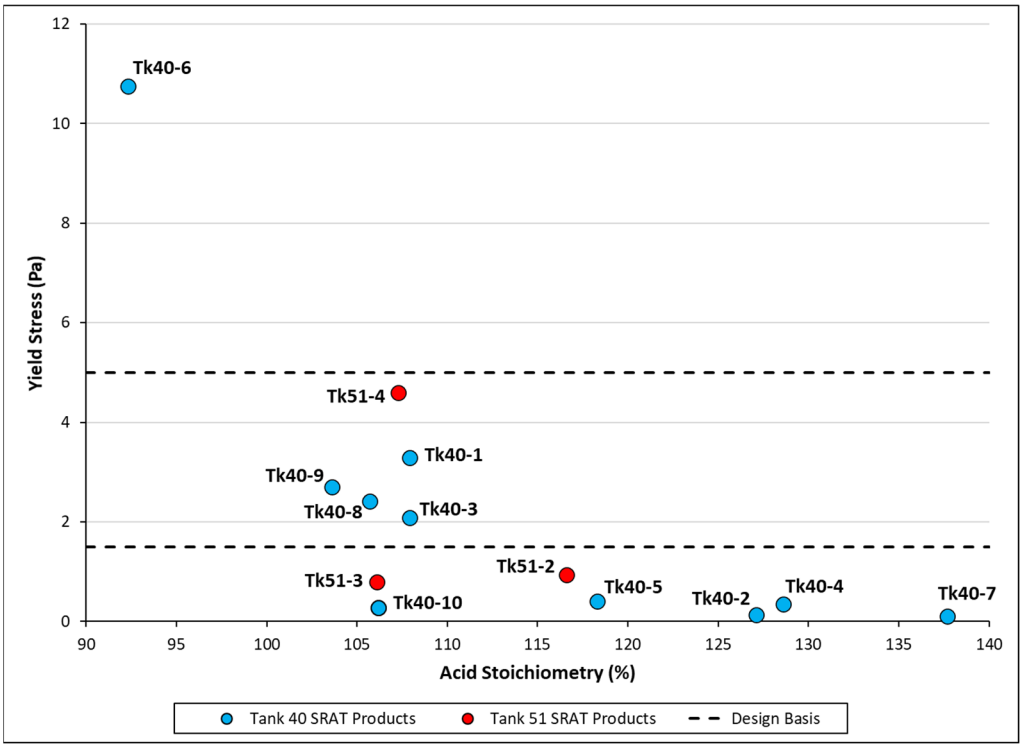

Figure 3-2. SRAT Product Yield Stress as a Function of Acid Stoichiometry.

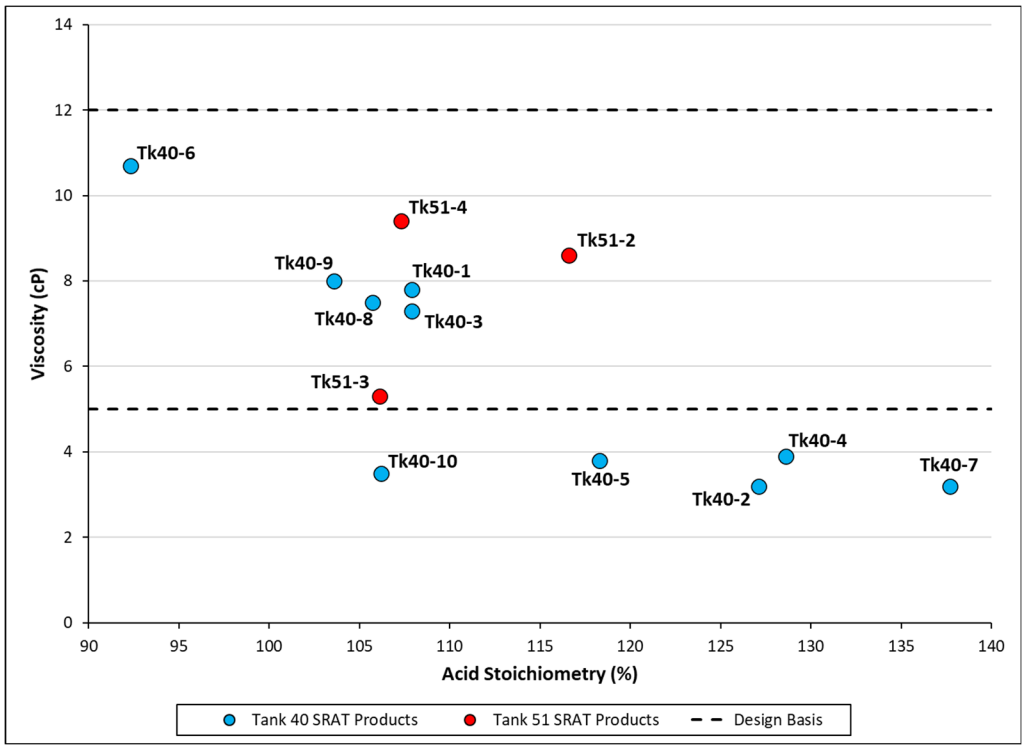

Figure 3-3. SRAT Product Viscosity as a Function of Acid Stoichiometry.

The yield stress data plotted in Figure 3-2 indicates that stoichiometries higher than 110% tend to produce SRAT products with yield stresses lower than the DWPF design basis lower limit of 1.5 Pa. Alternatively, the single experiment performed at a stoichiometry lower than 100% produced a SRAT product with a yield stress well above the DWPF design basis upper limit of 5 Pa. This suggests that an optimum stoichiometry exists between approximately 100 and 110% of the Koopman minimum acid where ideal yield stress could be achieved from Tank 40 material.

A similar trend can be observed in viscosity data plotted in Figure 3-3. At stoichiometries higher than 110%, viscosities fall below the DWPF design basis lower limit of 5 cP. No SRAT product with viscosity exceeding the DWPF design basis upper limit of 12 cP was produced in SB 10 testing.

Note that results from experiment Tk40-10 (sludge-only experiment) fall short of equivalent stoichiometric experiments conducted under the coupled operations flowsheet. At this time, it is unclear if this departure is due to the absence of coupled operations processing, or if it is due to the lower solids loadings observed in Tk40-10 SRAT product. It is recommended that further rheological testing be performed to better understand and decouple the impacts of acid stoichiometry and solids concentration on rheological parameters.

SME product rheological measurements are given in Table 3-26.

Table 3-26. SME Product Rheological Measurements.

Run	Total Dried Solids (wt%)	Insoluble Solids (wt%)	Sludge Density (g/mL)	Supernatant Density (g/mL)	Yield Stress (Pa)	Viscosity (cP)
Tk40-8	44.6	31.8	1.3414	1.1255	9.2	24.8
Tk40-9	39.9	28.8	1.2636	1.1020	2.9	13.3
Tk40-10	45.8	35.5	1.3435	1.1019	2.4	13.1
Tk51-2	44.9	31.2	1.2811	1.1160	6.5	39.7
Tk51-3	40.0	29.4	1.3199	1.1030	7.9	26.0
Tk51-4	40.6	30.1	1.3127	1.0740	11.3	34.1
			Design Basis	**Min**	**2.5**	**10.0**
				Max	**15.0**	**40.0**

Generally speaking, the yield stress and viscosities of SME products generated in SB 10 testing fall within the DWPF design basis windows of 2.5 – 15.0 Pa and 10.0 – 40.0 cP, respectively. Marginal exceptions are Tk40-10 (exhibited a yield stress ~0.1 Pa lower than the design basis window) and Tk51-2 (exhibited a viscosity within 0.3 cP of the design basis window). Given that these experiments are so similar in solids concentration (39.9 – 45.8%) and acid stoichiometry (103.6 – 116.6%), it is difficult to ascertain the reason behind the large variation of viscosity (13.1 – 39.7 cP) and yield stress (2.4 – 11.3 Pa). For this reason, it is recommended to perform additional rheological testing to better decouple the impacts of these parameters on yield stress and viscosity. Nevertheless, the results in Table 3-26 suggest that a SME product produced at a stoichiometry between 100 and 110% of the Koopman minimum acid has a high likelihood of exhibiting acceptable rheological characteristics.

3.4 SRAT and SME Condensate Analyses

3.4.1 Bulk Condensate Compositions

Table 3-27 and Table 3-28 give the reported compositions of SRAT dewater streams collected during SB 10 testing for SRAT-only experiments and SRAT-SME experiments, respectively.

Table 3-27. Composition of SRAT Dewater Streams (SRAT-only Experiments, in milligrams per liter of condensate).

Analyte†	Tk40-1	Tk40-2	Tk40-3	Tk40-4	Tk40-5	Tk40-6	Tk40-7
F^-	13.8	12.5	<10	<10	<10	<10	<10
HCO_2^-	30.8	18	34	<10	<10	<10	19
NO_2^-	<10	<10	<10	<10	14.7	154	<10
NO_3^-	7790	4910	6530	6030	5290	14000	6180
PO_4^{3-}	<10	<10	<10	<10	<10	<10	<10
SO_4^{2-}	<10	<10	<10	<10	<10	<10	<10
$C_2O_4^{2-}$	<10	<10	<10	<10	<10	<10	<10
$HOCH_2CO_2^-$	53.3	64.3	47.4	71.8	52.8	24.5	90.5
NH_4^+	<5	<5	<5	<5	<5	<5	<5
TIC	<80	<80	<80	<80	<80	<80	<20
TOC	168	<80	275	198	666	198	160
VOA	<0.2	<0.2	<0.25	<0.25	<0.2	<0.2	<0.2
SVOA	<1	<1	<1	<1	<1	<1	<1
Total Hg	82.8	63.8	384	466	537.3	617	169
Ca	<0.108	<0.108	<0.108	<0.108	<0.108	<0.108	0.18
Cr	0.025	<0.01	<0.01	<0.01	<0.066	<0.066	<0.058
Fe	0.155	<0.021	<0.021	<0.021	0.117	<0.05	<0.249
Mg	0.015	0.017	<0.006	<0.006	0.019	0.016	0.032
Mn	0.488	0.464	0.123	0.438	0.527	0.271	0.852
Na	<3.45	<1.3	<0.271	<1.25	1.62	1.35	<2.71
Ni	<0.054	1.14	<0.018	0.867	<0.069	0.669	1.04
Si	<1.17	<1.17	<0.69	1.58	<1.61	<1.61	2.29

†The elements Ag, Al, B, Ba, Be, Br, Cd, Ce, Cl, Co, Cu, K, La, Li, Mo, P, Pb, S, Sb, Sn, Sr, Th, Ti, U, V, Zn, Zr were found to be below detection limits in these tests. After this determination, subsequent condensates were submitted for limited elemental analysis to eliminate sample needs and waste generation.

Table 3-28. Composition of SRAT Dewater Streams (SRAT-SME Experiments, in milligrams per liter of condensate).

Analyte	Tk40-8	Tk40-9	Tk40-10	Tk51-2	Tk51-3	Tk51-4
HCO_2^-	95.8	76.6	30.5	12	15	<10
NO_2^-	<10.0	15.7	37.0	<10.0	19.5	24
NO_3^-	9970	8675	7860	5190	7505	7950
PO_4^{3-}	<10	<10	<10	<10	<10	<10
SO_4^{2-}	<10	<10	<10	<10	<10	<10
$C_2O_4^{2-}$	<10	<10	<10	<10	<10	<10
$HOCH_2CO_2^-$	47.0	50.6	21.7	33.6	20.1	<10
NH_4^+	<5	<5	<5	<10	<1	<5
TIC	<20	<20	<20	<20	<40	<80
TOC	91.4	96.7	33.8	174	120	<80
VOA	<0.2	<0.2	<0.2	<0.2	<0.2	<0.2
SVOA	<1	<1	<1	<1	<1	<1
Hg	488	658	502	166	565	194
Na	2.6	8.1	1.3	NR	NR	<2.7
Si	1.5	2.9	2.1	1.1	1.2	0.8

NR = Not Reported.

Generally, SRAT dewater compositions match well with what has been seen in previous studies.[5] The most dominant species in any particular condensate is nitrate, which comes from the selective scrubbing of gaseous NO_2 produced from the SRAT kettle. This reaction is known to produce nitrous acid as well as nitric acid, which accounts for the small amounts of nitrite observed in some condensates (Tk40-5, Tk40-6, Tk40-10, and Tk51-3). Note that the amounts of nitrite and nitrate observed in condensates are not equimolar (as is expected by the scrubbing reaction). This is likely due to continued destruction of nitrite in these condensate mixtures.

Organic acids are also observed in these SRAT condensates as a result of CPC processing. Formate (12 – 34 mg/L) and glycolate (20 – 90 mg/L) are seen in SRAT dewaters. It should be noted that the ratios of formate and glycolate observed in SRAT dewaters are likely driven by relative concentrations in the SRAT vessel as well as equilibrium vapor pressures, which may account for the relative abundance of glycolate. No detectable oxalate was noted in SRAT dewaters during SB 10 testing.

Species that represent flammability hazards (e.g., ammonium, volatile organics, semivolatile organics) are also absent from testing. These absences are consistent with earlier findings that the nitric-glycolic flowsheet tends to produce less ammonium and that operation with antifoam Y-17112 produces less volatile organics.[10]

Measured compositions of dewater collected during caustic boiling and MST/SS addition are given in Table 3-29.

Table 3-29. Composition of Dewater During MST/SS Addition (in milligrams per liter of condensate).

Component	Tk40-1	Tk40-2	Tk40-3	Tk40-4	Tk40-5	Tk40-6	Tk40-7
HCO_2^-	<10	<10	<10	<10	<10	<10	<10
NO_2^-	<10	<10	<10	<10	<10	<10	<10
NO_3^-	<10	<10	<10	43	<10	58.7	83.3
PO_4^{3-}	<10	<10	<10	<10	<10	<10	<10
SO_4^{2-}	<10	<10	<10	<10	<10	<10	<10
$C_2O_4^{2-}$	<10	<10	<10	<10	<10	<10	<10
$HOCH_2CO_2^-$	<10	<10	<10	<10	<10	<10	<10
SVOA	<1	<1	<1	<1	<1	<1	<1
VOA	<0.2	<0.2	<0.25	<0.25	<0.2	<0.2	<0.2
Hg (total)	4.61	67	4.32	5.57	4	15.9	19.0

At first glance, caustic boiling condensate (collected before acid addition) compositions seem unremarkable. Some samples yield small amounts of nitrate and mercury. Given that mercury is added as a nonvolatile oxide, the concurrent evidence of Hg and nitrate suggests the possibility of a mercury reduction involving nitrite, as proposed in Equation [4].

$$HgO + 2NO_2^- + H_2O \rightarrow Hg^0 + 2NO_2 + 2OH^- \quad [4]$$

As was seen with SRAT dewater, no detectable volatile organics were observed in caustic boiling dewater. No glycolate was observed, which is consistent with the timing of caustic boiling in SRNL experiments (before the addition of glycolic acid). It should be noted, however, that this is not an indication that the DWPF CPC would not experience glycolate carryover during caustic boiling. The DWPF CPC operates with a heel of SRAT product present in every SRAT reaction. This heel would be expected to carry some

appreciable concentration of glycolate, which may be volatilized during caustic boiling. The observations of glycolate carryover into condensates are discussed further in Section 3.4.3.

The compositions of condensates collected during SEFT addition are given in Table 3-30.

Table 3-30. Composition of Dewater During SEFT Addition (in milligrams per liter of condensate).

Analyte	Tk40-1	Tk40-2	Tk40-3	Tk40-4	Tk40-5	Tk40-6	Tk40-7
F^-	<10	<10	<10	<10	<10	<10	<10
HCO_2^-	13	14.6	<10	<10	<10	<10	13.6
Cl^-	<10	<10	<10	<10	<10	<10	<10
NO_2^-	<10	<10	<10	<10	10.7	<10	<10
NO_3^-	<10	605	535	16.5	200	489	29.7
PO_4^{3-}	<10	<10	<10	<10	<10	<10	<10
SO_4^{2-}	<10	<10	<10	<10	<10	<10	<10
$C_2O_4^{2-}$	<10	<10	<10	<10	<10	<10	<10
Br^-	<50	<50	<50	<10	<50	<50	<50
$HOCH_2CO_2^-$	<10	28.7	11.5	17.9	10.1	<10	25.1
SVOA	<1	<1	<1	<1	<1	<1	<1
VOA	<0.2	<0.2	<0.25	<0.2	<0.2	<0.2	<0.2
Total Hg	7.8	132	38.5	45.8	40.8	110	5.4

Given that SEFT addition occurs after SRAT dewater in SRNL CPC experiments, it is unsurprising that SEFT condensate compositions resemble SRAT dewater compositions at reduced concentrations. SEFT condensates are again dominated by nitrate, but at notably lower levels than those seen in SRAT dewaters (<10 – 605 mg/L in SEFT vs. 4910 – 14000 mg/L in SRAT dewaters). This is likely due to the fact that off-gas production (including the generation of NO_2) has largely decreased by the time of SEFT addition. Small concentrations of Hg (5.4 – 132 mg/L) are observed, as are glycolate (<10 – 28.7 mg/L) and formate (<10 – 14.6 mg/L). Beyond these few analytes, SEFT condensate compositions are unremarkable.

Table 3-31 and Table 3-32 give the compositions of the ammonia scrubber solution at the conclusion of the SRAT cycle for SRAT-only experiments and SRAT-SME experiments, respectively.

Table 3-31. Composition of Ammonia Scrubber Solution Following SRAT Cycle (SRAT-only Experiments, in milligrams per liter of solution).

Analyte	Tk40-1	Tk40-2	Tk40-3	Tk40-4	Tk40-5	Tk40-6	Tk40-7
NO_2^-	<10	<10	<10	<10	<10	<10	<10
NO_3^-	13500	11100	15100	11000	11600	17700	10600
PO_4^{3-}	<10	<10	<10	<10	<10	<10	<10
SO_4^{2-}	<10	<10	<10	<10	<10	<10	<10
$C_2O_4^{2-}$	<10	<10	<10	<10	<10	<10	<10
$HOCH_2CO_2^-$	<10	<10	<10	<10	<10	<10	<10
NH_4^+	<5	<5	<5	<5	<5	<5	<5
TIC	<80	<80	<80	<80	<80	<80	<20
TOC	<80	<20	<80	<80	<80	<80	<20
VOA	<0.2	<0.2	<0.25	<0.25	<0.2	<0.2	<0.2
SVOA	<1	<1	<1	<1	<1	<1	<1
Total Hg	44.3	10.5	27.2	45.3	16.9	56.1	94.4
Cr	0.103	0.104	0.034	0.051	<0.066	<0.066	<0.058
Fe	0.37	0.455	0.059	0.143	0.146	0.239	<0.249
Mn	0.275	0.101	0.063	0.096	0.123	0.105	0.097
Si	<1.17	<1.17	<0.69	0.937	<1.61	<1.61	1.22

Table 3-32. Composition of Ammonia Scrubber Solution Following SRAT Cycle (SRAT-SME Experiments, in milligrams per liter of solution).

Analyte	Tk40-8	Tk40-9	Tk40-10	Tk51-2	Tk51-3	Tk51-4
F^-	<100	<100	<100	<10.0	<10.0	<10
Cl^-	<100	<100	<100	<10.0	<10.0	<10
NO_2^-	<100	<100	<100	<10.0	<10.0	<10
NO_3^-	12800	13800	16200	12700	14000	21500
PO_4^{3-}	<100	<100	<100	<10.0	<10.0	<10
SO_4^{2-}	<100	<100	<100	<10.0	<10.0	<10
$C_2O_4^{2-}$	<100	<100	<100	<10.0	<10.0	<10
$HOCH_2CO_2^-$	<100	<100	<100	<10.0	<10.0	<10
NH_4^+	<5	<5	<5	<10	<1	<5
TIC	<20	<20	<80	<20	<40	<20
TOC	<20	<20	<80	53	56	<20
VOA	<0.2	<0.2	<0.2	<0.2	<0.2	<0.2
SVOA	<1	<1	<1	<1	<1	<1
Total Hg	56	68	70	41	123	76
Fe	<1.00	<1.00	<1.00	NR	NR	0.666
Si	<1.00	<1.00	2	2.2	1.4	1.4

The drastic increase in nitrate concentrations in the ammonia scrubber relative to what was seen in other condensate streams is of particular interest here. The high concentrations (11,000 – 21,500 mg/L) of nitrate are likely due to the recirculating nature of the ammonia scrubber system as well as the use of the scrubber itself; as a scrubber for vapor-phase emissions, it is likely to be more efficient at removing soluble gases from the process vapor. It should be noted here that the setup and use of an ammonia scrubber in SRNL testing is not necessarily representative of ammonia scrubber use at the DWPF. SRNL experiments use a single reservoir of dilute nitric acid to serve as the scrubber solution, whereas the DWPF CPC ammonia scrubber uses condensate returned from the SRAT and SME reaction vessels during boiling. These streams obviously differ in initial composition and may therefore exhibit different performance in the removal of gas molecules. Furthermore, trace elements observed in the ammonia scrubber solution are likely due to

corrosion of glass and metal used in the ammonia scrubber unit and are not necessarily representative of expected DWPF conditions.

No detectable glycolate was seen in the ammonia scrubber following a SRAT cycle. This suggests that the glycolate carryover mechanism is only active as far as the SRAT condenser and does not impact downstream condensates significantly. Mercury was detected in varying amounts (10.5 – 123 mg/L).

Compositions of SME cycle condensates collected during SB 10 simulant experiments are given in Table 3-33.

Table 3-33. Composition of SME Dewater Streams (in milligrams per liter of condensate).

Analyte	Tk40-8	Tk40-9	Tk40-10	Tk51-2	Tk51-3	Tk51-4
HCO_2^-	<10	<10	<10	<10	<10	<10
Cl^-	<10	<10	<10	<10	<10	<10
NO_2^-	<10	<10	<10	<10	<10	<10
NO_3^-	<10	16	18	36	14	<10
PO_4^{3-}	<10	<10	<10	<10	<10	<10
SO_4^{2-}	<10	<10	<10	<10	<10	<10
$C_2O_4^{2-}$	<10	<10	<10	<10	<10	<10
$HOCH_2CO_2^-$	<10	<10	<10	<10	<10	<10
NH_4^+	<5	<5	<5	<10	<1	<5
TIC	<20	<20	<20	<20	<40	<20
TOC	<20	<20	<20	<20	<40	<20
VOA	<0.2	<0.2	<0.2	<0.2	<0.2	<0.2
SVOA	<1	<1	<1	<1	<1	<1
Total Hg	1.745	3.55	2.82	15.521	2.168	0.664
B	<1.00	<1.00	<1.00	NR	<1.00	<0.526
Fe	<1.00	<1.00	<1.00	NR	NR	<0.249
Na	<1.00	2.885	1.675	NR	NR	<2.71
Si	<1.00	1.475	1.145	1.5175	<1.00	<0.253

With no detectable glycolate, ammonium, or volatile organics and only small amounts of nitrate, SME condensates are also relatively unremarkable. This is consistent with previous observations that the SME cycle is relatively inert compared to the SRAT cycle. Small concentrations of mercury (≤15.5 mg/L) were observed, indicating the continued (but diminished) removal of Hg from SME cycle sludges.

3.4.2 Antifoam Performance and Degradation Compounds

SRNL was requested to assess the efficacy of antifoam Y-17112 and determine the presence of antifoam degradation compounds in condensates and collection points throughout processing. Throughout SB 10 testing, the antifoam addition strategy developed by Lambert was employed:[10]

- 50 mg kg^{-1} of undiluted antifoam added prior to caustic boiling (not performed during sludge-only processing)
- 25 mg kg^{-1} of undiluted antifoam added prior to glycolic acid addition
- 50 mg kg^{-1} of undiluted antifoam added prior to SRAT dewater
- 25 mg kg^{-1} of undiluted antifoam added every 12 hours during boiling
- 25 mg kg^{-1} of undiluted antifoam added prior to first canister decontamination blast addition
- 25 mg kg^{-1} of undiluted antifoam added prior to the first frit addition
- 25 mg kg^{-1} of undiluted antifoam added as needed to control foaming throughout experiment (not necessary during SB 10 simulant testing)

Antifoam Y-17112 prevented foaming in all SB 10 simulant experiments. No additional antifoam was necessary to mitigate foaming or foamovers during processing. Therefore, it is recommended that DWPF employ the strategy developed by Lambert for SB 10 processing.

Specific guidance for ADP determination was given to reproduce sampling frequency and points documented in an earlier study.[18] To accomplish this goal, multiple samples were drawn from the ammonia scrubber throughout several Tank 40 experiments in addition to samples from collected condensate. These samples were submitted for ADP analysis. The results of these experiments are given in Table 3-34.

Table 3-34. Volatile and Semivolatile Organic Analyses of SRAT Cycle Condensates (in milligrams per liter of solution).

Sample Description	Analysis	Tk40-1	Tk40-2	Tk40-3	Tk40-4
Ammonia Scrubber (Post Caustic Boiling)	VOA	<0.2	<0.2	<0.25	<0.25
	SVOA	<1	<1	<1	<1
Collected Condensate (Post Caustic Boiling)	VOA	<0.2	<0.2	<0.25	<0.25
	SVOA	<1	<1	<1	<1
Ammonia Scrubber (Post Nitric Acid)	VOA	<0.2	<0.2	<0.25	<0.25
	SVOA	<1	<1	<1	<1
Ammonia Scrubber (Post Glycolic Acid)	VOA	<0.2	<0.2	<0.25	<0.25
	SVOA	<1	<1	<1	<1
Ammonia Scrubber (Post SRAT Dewater)	VOA	<0.2	<0.2	<0.25	<0.25
	SVOA	<1	<1	<1	<1
Collected Condensate (SRAT Dewater)	VOA	<0.2	<0.2	<0.25	<0.25
	SVOA	<1	<1	<1	<1
Ammonia Scrubber (Post SEFT Addition)	VOA	<0.2	<0.2	<0.25	<0.25
	SVOA	<1	<1	<1	<1
Collected Condensate (SEFT Dewater)	VOA	<0.2	<0.2	<0.25	<0.2
	SVOA	<1	<1	<1	<1
Sludge (SRAT Product)	VOA	<0.2	<0.2	<0.25	<0.25
	SVOA	<1	<1	<1	<1

Results in Table 3-34 indicate a complete absence of known ADPs in SB 10 simulant testing. Previous campaigns performed with Antifoam 747 have yielded significant amounts of trimethylsilanol (TMS, 1-140 mg/L in SB 9 condensate samples) and hexamethyldisiloxane (HMDSO, nearly 1,000 ppm in off-gas during peak production in SB 9 testing),[6, 19] whereas these samples (all performed with Y-17112) yield less than detectable amounts of any volatile or semivolatile organic compound. This indicates that Y-17112 is not a significant generator of volatile organic compounds in CPC processing. Upon discovering this from the first four Tank 40 experiments, it was decided to forgo the analyses of the condensate samples from the remaining experiments.

Similar measurements are reported for SME cycle materials in Table 3-35.

Table 3-35. Volatile and Semivolatile Organic Analyses of SME Cycle Condensates.

Sample Description	Analysis	Tk40-8	Tk40-9	Tk40-10
Collected Condensate (SME Dewater)	VOA (mg/L)	<0.2	<0.2	<0.2
	SVOA (mg/L)	<1	<1	<1
Sludge (SME Product)	VOA (mg/L)	<0.2	<0.2	<0.2
	SVOA (mg/L)	<1	<1	<1

Similar results were observed in the SME cycle condensates, where no detectable volatile or semivolatile organics were discovered. This further validates the use of Y-17112 as an antifoam agent with little to no impact on volatile organic production.

3.4.3 Glycolate Carryover and Entrainment

Table 3-36 gives the measured concentrations of glycolate in the various process condensates produced during SB 10 simulant testing.

Table 3-36. Glycolate Measurements in SRAT and SME Cycle Condensates (in milligrams per liter of condensate).

Experiment	Caustic Boiling Dewater	SRAT Dewater	SEFT Dewater	SME Dewater
Tk40-1	<10	53.3	<10	N/A
Tk40-2	<10	64.3	28.7	N/A
Tk40-3	<10	47.4	11.5	N/A
Tk40-4	<10	71.8	17.9	N/A
Tk40-5	<10	52.8	10.1	N/A
Tk40-6	<10	24.5	<10	N/A
Tk40-7	<10	90.5	25.1	N/A
Tk40-8	<10	47.0	<10	<10
Tk40-9	<10	50.6	<10	<10
Tk40-10	N/A	21.7	N/A	<10

N/A = Not Applicable. Tk40-1 through Tk40-7 were SRAT-only experiments and therefore produced no SME-cycle dewater. Tk40-10 was a sludge-only experiment and therefore did not undergo caustic boiling or SEFT addition.

Across all Tank 40 experiments, no glycolate could be detected in dewater collected during the MST/SS caustic boiling and dewater periods. This is not surprising, given that glycolic acid had not yet been added when caustic boiling was performed. This result is not necessarily an indication of lack of glycolate carryover during caustic boiling. Rather, it is the basis for recommendation that future SB testing incorporate glycolate as a minor component of SRAT receipt materials to better understand the potential volatility of glycolate during caustic boiling.

Glycolate was detected in both SRAT and SEFT condensates, with apparent diminishing returns as a given experiment progresses. SRAT dewater glycolate concentrations were found to vary between 24.5 and 90.5 mg/L, whereas SEFT concentrations were found to vary between <10 to 28.7 mg/L. Given that SEFT condensate masses are expected to vastly exceed SRAT dewater masses (~10x), it is safe to assume that glycolate concentrations in condensate being routed to the Recycle Collection Tank (RCT) will likely be less than 50 mg/L.

3.5 Off-gas Generation

Table 3-37 and Table 3-38 give the observed peak gas generation rates for the SRAT cycle of each experiment. Table 3-37 gives the rates seen in SRAT-only tests, whereas Table 3-38 gives the rates seen in SRAT-SME experiments.

Table 3-37. Peak SRAT Cycle Off-gas Generation Concentrations and Rates (SRAT-Only Experiments).

Gas	Unit	Tk40-1	Tk40-2	Tk40-3	Tk40-4	Tk40-5	Tk40-6	Tk40-7
H_2	ppm_v	6.8	7.7	7.5	8.1	12.1	10.5	7.5
	lb h^{-1}	1.71E-04	1.63E-04	1.87E-04	1.86E-04	3.03E-04	2.42E-04	1.69E-04
N_2O	vol %	1.3	1.0	1.5	1.1	1.1	0.8	0.9
	lb h^{-1}	5.71E+00	6.26E+00	9.73E+00	1.01E+01	1.03E+01	4.05E+00	6.14E+00
NO	vol %	18.3	9.1	17.3	13.0	11.6	20.3	12.8
	lb h^{-1}	8.35E+01	3.09E+01	7.56E+01	7.91E+01	6.46E+01	7.71E+01	3.06E+01
NO_2	vol %	5.6	1.4	5.2	1.5	1.6	4.3	1.8
	lb h^{-1}	2.77E+01	7.70E+00	2.83E+01	8.79E+00	1.04E+01	1.31E+01	5.47E+00
CO_2	vol %	51.1	52.4	51.0	52.0	52.0	53.1	50.5
	lb h^{-1}	1.60E+02	1.73E+02	2.43E+02	2.22E+02	2.30E+02	2.19E+02	2.05E+02
CH_4[f]	ppm_v	<33	<33	<33	18.1	11.1	<33	13.4

Table 3-38. Peak SRAT Cycle Off-gas Generation Concentrations and Rates (SRAT-SME Experiments).

Gas	Unit	Tk40-8	Tk40-9	Tk40-10	Tk51-2	Tk51-3	Tk51-4
H_2	ppm_v	6.8	5.8	11.0	4.5	12.1	9.2
	lb h^{-1}	2.23E-04	1.83E-04	3.59E-04	1.49E-04	3.90E-04	2.97E-04
N_2O	vol %	1.5	1.6	0.6	0.7	0.6	0.7
	lb h^{-1}	1.04E+01	1.12E+01	4.35E+00	2.04E+00	4.99E+00	8.31E+00
NO	vol %	16.3	19.3	10.3	9.9	1.8	18.6
	lb h^{-1}	6.97E+01	4.70E+01	5.02E+01	4.71E+01	3.96E+00	9.91E+01
NO_2	vol %	2.9	2.6	2.2	1.9	3.2	2.1
	lb h^{-1}	1.66E+01	8.26E+00	1.24E+01	1.27E+01	1.10E+01	1.47E+01
CO_2	vol %	50.4	52.2	50.3	29.3	34.4	33.9
	lb h^{-1}	2.54E+02	1.88E+02	2.01E+02	2.05E+02	2.75E+02	2.87E+02
CH_4[f]	ppm_v	<33	14.6	30.9	20.3	38.9	86.7

Generally speaking, hydrogen flammability is a non-issue in the nitric-glycolic flowsheet. This is demonstrated further by the data given in Table 3-37 and Table 3-38. In every case, SRAT cycle hydrogen concentrations were observed below 13 ppm, well below the acknowledged lower flammability limit of 40,000 ppm. The highest observed hydrogen production rate was 3.90×10^{-4} lb h^{-1} (DWPF basis), observed in experiment Tk51-3. This value is significantly lower than the 2.4×10^{-2} lb h^{-1} limit currently proposed for the nitric glycolic flowsheet. The ~34% difference in ruthenium concentration would not be reasonably expected to challenge this conclusion.

Other observed gases agree with what has been seen previously in nitric glycolic testing. N_2O concentrations are kept to below 2% in all tests. CO_2 achieves concentrations over 50% during peak off-gas production, which is concurrent with the acidification of carbonate and the destruction of glycolate. NO

[f] The GC limits of detection and quantitation for CH_4 are approximately 13 and 33 ppm, respectively. A lower approximate measurement by FTIR is achievable but is heavily dependent on gas composition. Values lower than 33 ppm should be viewed as semiquantitative.

achieves concentrations as high as 20% during peak off-gas production. As has been seen previously, this high concentration of NO is observed during a <1 hour period of anoxic (O_2 concentration near zero) behavior, during which the oxygen added as purge gas is consumed by NO to make NO_2, according to Equation [5].

$$2NO+O_2 \rightarrow 2NO_2 \quad [5]$$

NO_2 concentrations are seemingly limited to less than 6% throughout testing, despite the prevalence of NO and the consumption of O_2 described above. This is due to the ability of NO_2 to be absorbed by aqueous solution and hydrolyzed to make nitrous and nitric acids, according to Equation [6].

$$2NO_2+H_2O \rightarrow HNO_2+HNO_3 \quad [6]$$

This reaction is the basis for downstream collection of nitric acid from the SRAT vessel.

Peak off-gas generation rates and concentrations for the SME cycles performed in SB 10 simulant testing are given in Table 3-39.

Table 3-39. Peak SME Cycle Off-gas Generation Concentrations and Rates (SRAT-SME Experiments).

Gas	Unit	Tk40-8	Tk40-9	Tk40-10	Tk51-2	Tk51-3	Tk51-4
H_2	ppm	14.8	15.6	24.5	8.1	15.5	19.2
	lb h^{-1}	3.66E-04	3.78E-04	6.04E-04	2.67E-04	3.82E-04	4.76E-04
N_2O[g]	%	<0.02	<0.02	0.004	<0.02	0.006	0.01
	lb h^{-1}	ND	ND	2.14E-02	ND	ND	5.18E-02
NO	%	0.04	0.07	0.05	0.03	0.02	0.03
	lb h^{-1}	9.74E-02	1.34E-01	1.09E-01	2.52E-01	3.14E-02	7.33E-02
NO_2	%	0.10	0.05	0.08	0.03	0.02	0.09
	lb h^{-1}	2.83E-01	1.51E-01	2.89E-01	2.31E-01	8.37E-02	2.84E-01
CO_2	%	0.9	1.0	0.8	0.5	1.0	1.0
	lb h^{-1}	5.23E+00	6.09E+00	5.47E+00	2.87E+00	4.81E+00	6.43E+00
CH_4	ppm	<33	<33	6.9	<33	3.4	2.5

ND = Not Determinable

Data in Table 3-39 show an expected trend in hydrogen generation during SME cycles. Generally, H_2 concentrations during SME processing (between 8.1 and 24.5 ppm_v) exceed those seen during SRAT processing (between 4.5 and 12.1 ppm_v). This behavior is consistent with observations made during previous SB campaigns. Despite these higher hydrogen values, the peak rates of hydrogen formation (ranging between 2.67×10^{-4} and 6.04×10^{-4} lb h^{-1}) still fall far below the limit for SME processing in DWPF (2.4×10^{-2} lb h^{-1}). This is further indication that hydrogen flammability is not expected to be problematic during SB 10 processing under the nitric glycolic flowsheet. The ~34% difference in ruthenium concentration would not be reasonably expected to challenge this conclusion.

Note that some experiments exhibited periods of higher hydrogen generation rates than those reported above. These increased rates are believed to be the results of heating rod fouling and temperature excursions.

[g] The GC limits of detection and quantitation for N_2O are approximately 0.006% and 0.02%, respectively. A lower approximate measurement by FTIR is achievable but is heavily dependent on gas composition. Values lower than 0.02% should be viewed as semiquantitative.

Because these phenomena are unique to SRNL testing, these regions were omitted when considering periods of maximum hydrogen generation applicable to CPC processing. Full profiles of hydrogen generations rates (including data from temperature excursions) are given in 1.1.1.1.1Appendix D.

Other gases exhibit universally lower concentrations during SME processing than in SRAT processing. CO_2 peaks at ~1.0% during SME processing, whereas NO and NO_2 both peak at less than 0.1%. The relatively low amount of nitrate collected in SME condensates combined with the near-quantitative measurement of atmospheric oxygen in the off-gas suggest that minimal NO/NO_2 is being formed in general (as opposed to the possibility that significant NO/NO_2 is being formed and absorbed by condensate as nitrous and nitric acids). N_2O peaks at less than 0.01% and is often undetectable in SME processing.

Methane (CH_4) was observed in both SRAT and SME segments of testing. The presence of this gas was first detected by GC (see Figure 3-4) and confirmed by IR analysis (see Figure 3-5). SB 10 is the first occasion in which CH_4 has been observed in SB testing at SRNL. This is likely due to the fact that SB 10 is the first sludge batch to benefit from improvements in GC measurement capabilities developed during hydrogen generation rate testing.[20] Concentrations of CH_4 are frequently too low to detect or quantify during much of the SRAT and SME processing in SB 10 tests. The highest observed concentration of CH_4 in a SRAT cycle was ~87 ppm_v, whereas the highest observed concentration during a SME cycle was ~7 ppm_v (via FTIR).

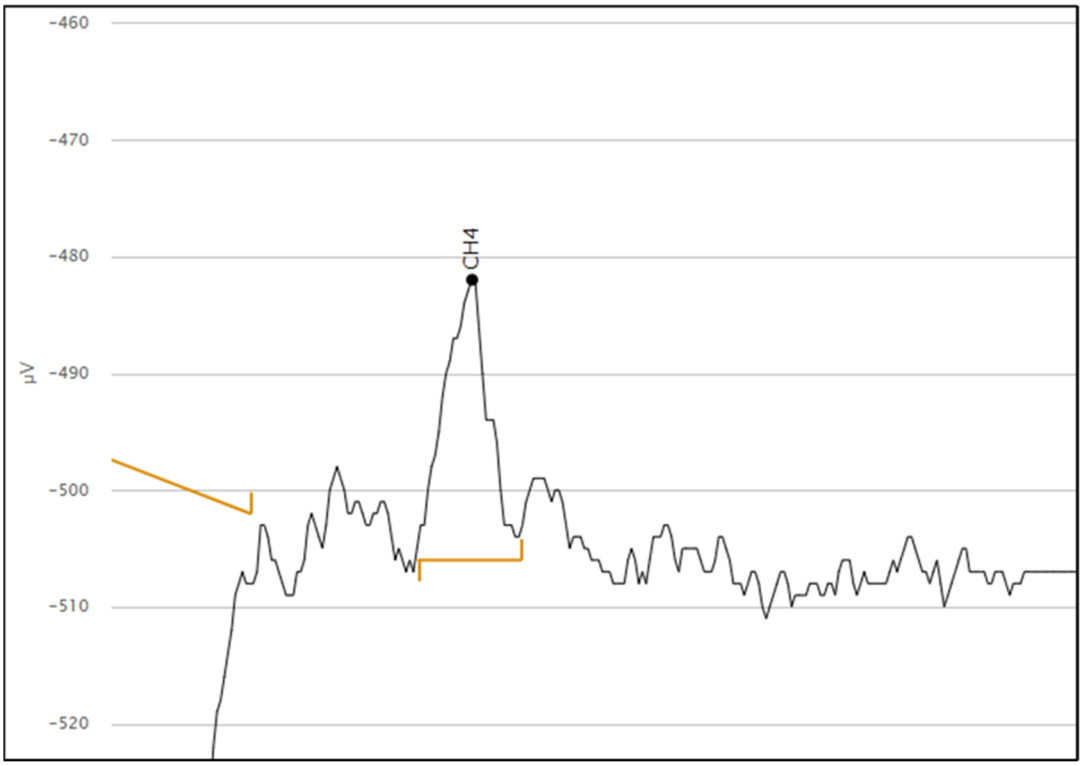

Figure 3-4. GC Chromatograph of CH_4 Observed During Tk51-2 SRAT Cycle.

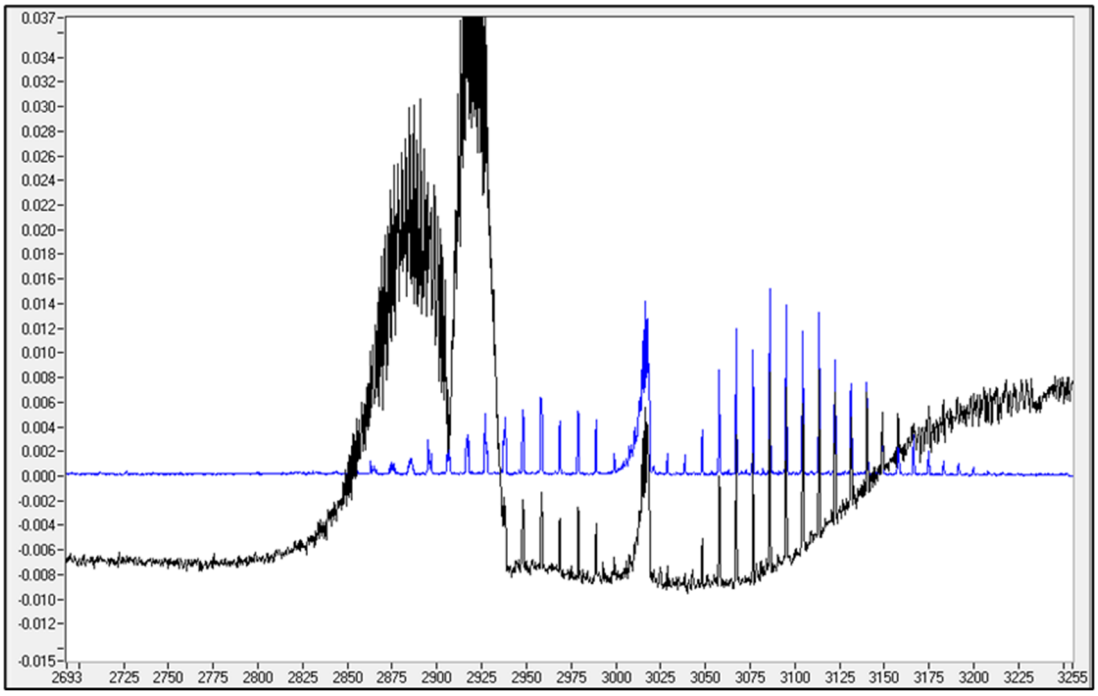

Figure 3-5. IR Spectrum of CH_4 Observed During Tk51-4. Black line is the IR spectrum taken of Tk51-4 off-gas, and blue line is a reference spectrum of CH_4.

While most tests yielded sporadic measurements of CH_4 at concentrations near the limit of detection, a single experiment (TK51-4) yielded measurable CH_4 at levels high enough to quantify for a distinct period of time during the SRAT dewater phase (following acid addition). The CH_4 profile from Tk51-4 is given in Figure 3-6.

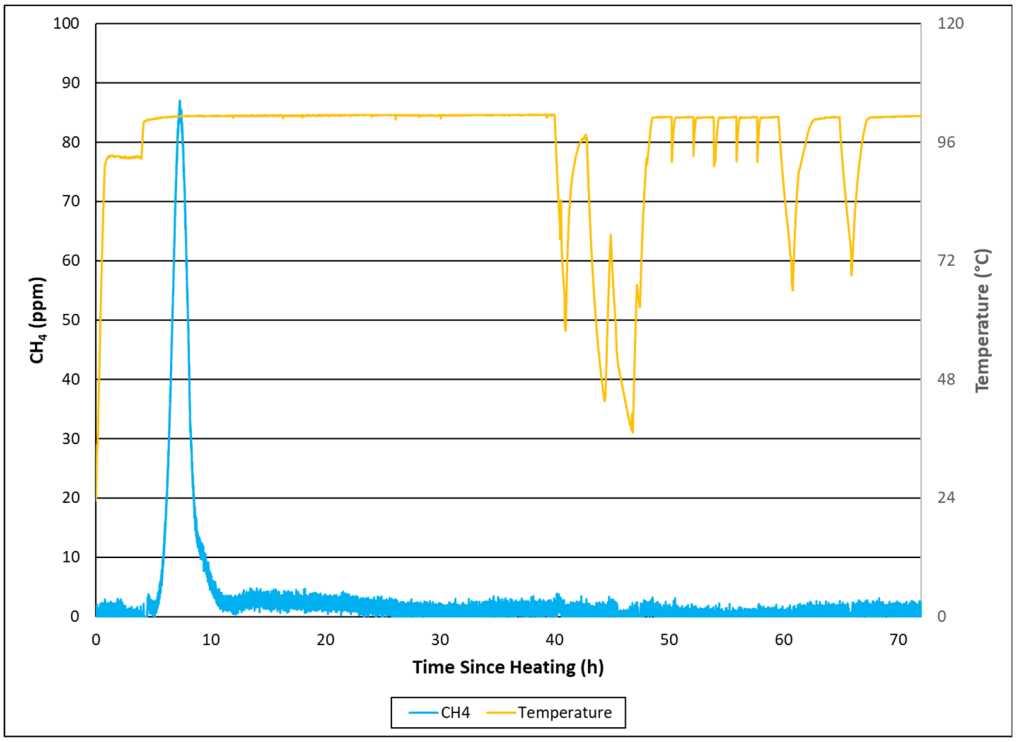

Figure 3-6. Methane Concentrations Observed during Tk51-4 as a Function of Time.

At this time, it is uncertain if the trend observed in Tk51-4 (peak CH_4 production aligning with the end of SRAT dewater) is consistent in other CPC simulations. However, this stage of processing exhibits a high degree of reactivity (NO_X formation), so the possibility of a correlation between SRAT dewater and CH_4 should not be ruled out.

It should be noted that, although CH_4 is a flammable gas and was detected during SB 10 testing, it has not been determined if the CH_4 is representative of expected processing in DWPF or if it is a due to circumstances unique to testing at SRNL and differences during CPC simulation (i.e., use of organosilicon lubricants to prevent leaking, greased ball bearings to allow overhead mixing, etc.). Furthermore, the highest concentrations observed (<100 ppm during SRAT testing) is still far less than the lower flammability limit for CH_4. This suggests that, even if the CH_4 can be determined to be representative of DWPF processing, it is not expected to represent a flammability concern during CPC operations.

A small portion of the SB 10 flowsheet experiments exhibited periods where an unknown gas was detected by IR. Qualitatively, this gas appears to be a hydrocarbon species, possibly including an alcohol functional group and bearing spectral resemblance to long (>10 carbon atoms) chain species. At this time, the gas cannot be positively identified due to interaction with CO_2 and NO_2 spectra. Because an identification cannot be made, no attempt at quantification can be performed. It should be noted that the observation of an apparent hydrocarbon species in SRNL SB 10 simulant testing does not necessarily indicate that hydrocarbons could be expected in the DWPF. As of yet, no evidence exists to indicate that this phenomenon is not unique to SRNL testing.

Full profiles of off-gas concentrations for each experiment are included in 1.1.1.1.1Appendix D for reference.

3.6 Anion Conversions

SRAT Cycle anion conversions for each experiment performed in SB 10 testing are given in Table 3-40.

Table 3-40. SRAT Cycle Anion Conversions.

Run	Glycolate Destruction (%)	Glycolate-to-Formate Conversion (%)	Glycolate-to-Oxalate Conversion (%)	Nitrite Destruction (%)	Nitrite-to-Nitrate Conversion (%)
Tk40-1	12.2	2.5	1.7	>99.4	58.9
Tk40-2	10.7	5.40	2.12	>99.4	94.4
Tk40-3	6.73	>3.29	1.58	>99.5	60.7
Tk40-4	6.73	2.30	3.15	>99.4	60.9
Tk40-5	6.79	2.80	2.58	>99.3	49.0
Tk40-6	11.1	2.95	0.35	>99.4	32.0
Tk40-7	21.4	>0.78	2.17	>99.4	33.4
Tk40-8	12.1	1.37	1.19	>99.5	23.5
Tk40-9	11.1	1.59	1.41	>99.5	8.27
Tk40-10	27.2	>2.91	1.60	>99.3	9.49
Tk51-2	26.1	>0.15	2.57	>99.2	39.6
Tk51-3	20.5	>2.35	1.07	>99.1	8.12
Tk51-4	28.7	>0.95	1.87	>99.4	5.61

At first glance, SRAT cycle anion conversions in SB 10 testing are unremarkable. It is easily seen that effectively all nitrite is destroyed as a result of SRAT processing, with greater than 99% nitrite destruction observed across the board. Glycolate-to-formate and glycolate-to-oxalate conversions are also within the range expected based on previous SB campaigns,[5] ranging from 0.1% to 5.4% and 0.3% to 3.1%, respectively.

Glycolate destruction values are slightly atypical compared to previous SB testing. The majority of Tank 40 experiments exhibit glycolate destruction percentages less than 13% (Tk40-7 and Tk40-10 being obvious exceptions). These values are marginally lower than values seen in SB 9 nitric-glycolic testing (16.5 – 30.5%), reported by Lambert.[5] Notably, glycolate destruction from Tk40-10 agrees well with the range of values observed in Tank 51 testing. Given that the point of similarity between Tk40-10 and all Tank 51 experiments is the performance of a sludge-only test, this may suggest an impact of coupled operations on glycolate destruction. It is therefore recommended that a starting stoichiometry of 105.7% be employed for SB 10 processing; this stoichiometry is expected to exhibit an 11.8% glycolate destruction factor (average of Tk40-1, Tk40-8, and Tk40-9) under a coupled operations flowsheet and a 27.2% glycolate destruction factor (Tk40-10) under a sludge-only operations flowsheet.

Nitrite-to-nitrate conversion values observed in SB 10 testing are largely without pattern. Reported values range from as low as 5% to as high as 94% (compared to 44.1 – 75.2% observed in SB 9 testing). The reason for this variation is unclear, but it's possible that uncertainty in analytical measurements is responsible for the large degree of variation. Nitrite-to-nitrate conversion is calculated according to Equation [7].

$$C_{NO_2-NO_3} = \frac{n_{NO_3}^{SRAT} - n_{NO_3}^{added}}{n_{NO_2}} \times 100 \qquad [7]$$

Where,

$C_{NO_2-NO_3}$ is the nitrite-to-nitrate conversion,

$n_{NO_3}^{SRAT}$ is the amount of nitrate present at the end of the SRAT cycle,

$n_{NO_3}^{added}$ is the amount of nitrate added as nitrate (either as SRAT receipt or nitric acid), and

n_{NO_2} is the amount of nitrite added as SRAT receipt.

The amount of nitrite added as a part of the sludge simulant is relatively small compared to the amount of nitrate added as nitric acid. For this reason, the amount of receipt nitrite is also relatively small compared to the amount of nitrate present at the end of the SRAT cycle. Because of these two facts, the nitrite-to-nitrate ratio is effectively the ratio of the difference of two large numbers to a single small number. Given that ~10% uncertainty is expected in IC measurements, there is a high probability that the large variation observed in nitrite-to-nitrate conversion factors is a result of analytical uncertainty on nitrate measurements.

Table 3-41 gives the anion conversions observed in SB 10 SME cycles. The anion conversions shown are calculated using the highest measured values for each anion species without regard to slurry or supernatant measurement (i.e., supernatant and slurry concentrations were determined and converted to a uniform slurry basis, then downselected to report the highest concentrations). The use of highest concentrations is justified in carbon and nitrogen mass balances, discussed later in this report.

Table 3-41. SME Cycle Anion Conversions.

Run	Glycolate Destruction (%)	Glycolate-to-Formate Conversion (%)	Glycolate-to-Oxalate Conversion (%)	Nitrate Conversion (%)
Tk40-8	0.85	0.57	0.72	-7.29
Tk40-9	18.6	2.00	0.13	0.04
Tk40-10	12.9	0.63	1.32	-9.87
Tk51-2	5.35	0.26	2.72	4.61
Tk51-3	0.33	-1.97	0.18	-4.89
Tk51-4	4.03	1.27	1.37	1.39

Anion conversions observed during SME processing suggest that for the most part, the SME is largely inert. Glycolate-to-formate conversion, glycolate-to-oxalate conversion, and nitrate conversion all fall within 10% of zero, suggesting that initial and final anion concentrations are sufficiently close as to be practically indistinguishable. The exception to this is glycolate destruction, which was observed to be greater than 10% in both Tk40-9 (18.65%) and Tk40-10 (12.89%). Given the low destruction values observed in Tank 51 testing, it is unlikely that the high destruction value from Tk40-10 is the result of sludge-only processing. It is possible that the high value in Tk40-9 is the result of the reduced boilup rates employed during the experiment, leading to increased time at temperature.

3.7 Mercury

Mercury concentrations in SB 10 simulant SRAT and SME products are given in Table 3-42.

Table 3-42. SRAT and SME Product Mercury Concentrations (dried solids basis).

Run	SRAT Product Hg (% of TS)	SME Product Hg† (% of TS)
Tk40-1	0.04	-
Tk40-2	0.05	-
Tk40-3	0.05	-
Tk40-4	0.03	-
Tk40-5	0.03	-
Tk40-6	0.04	-
Tk40-7	0.05	-
Tk40-8	0.04	0.02
Tk40-9	0.04	0.01
Tk40-10	0.03	0.01
Tk51-2	0.98	0.12
Tk51-3	0.39	0.02
Tk51-4	0.66	0.03

†SME Cycles were not performed for Tk40-1 through Tk40-7.

At first glance, it is obvious that Hg was easily removed from Tank 40 simulant during CPC processing. SRAT product Hg concentrations in Tank 40 SRAT products vary between 0.03 and 0.05 percent of total solids, significantly lower than the SRAT product target value of 0.8% of TS. This suggests that the assumed 750 g H_2O(steam) per g Hg stripping factor is adequate for Hg removal.

Tank 51 Hg removal seems to be more challenging. SRAT product from Tk51-2 exhibited a Hg concentration of 0.98 % of TS, higher than the 0.8% target. Further Tank 51 tests (Tk51-3 and Tk51-4) were able to surpass the Hg removal target (0.39 and 0.66 % of TS, respectively), but not to the same extent as Tank 40 tests. However, it should be noted that all SME products (including Tank 51 materials) achieved Hg concentrations well below the 0.45% of TS target, indicating that SRAT and SME processing is sufficient to remove Hg before the SME is transferred to the melter feed tank.

The observed difference in Hg removal efficiency between Tank 51 and Tank 40 sludge simulants may be related to the rheology of each sludge. As was shown in Section 3.2, Tank 51 SRAT products seem to be rheologically thicker than Tank 40 SRAT products. The increased viscosity may provide a hindrance to Hg removal during CPC operations. Nevertheless, the data from SB 10 testing reveal that the assumed 750 g H_2O (steam) per g Hg stripping factor is adequate for both SRAT and SME processing.

An alternative explanation for the low Hg concentrations reported in Table 3-42 might have been poor sampling habits (i.e., failure to collect Hg as a part of sampling). However, two facts can be used to rule out this alternative explanation. First, the Hg concentrations measured in SRAT Receipt samples (Table 3-2) agree well with the values expected based on HgO addition (2 – 4 % of TS). This observation suggests that sampling and measurement practices employed in SB 10 testing were sufficient to observe the majority of Hg present in the experiment slurries.

Second, good visual indication for Hg stripping was obtained via the collection of several small, time-dependent samples during SB 10. These samples were centrifuged to allow for measurement of the supernatant phase composition as a function of reaction progression. A photograph of these samples is given in Figure 3-7.

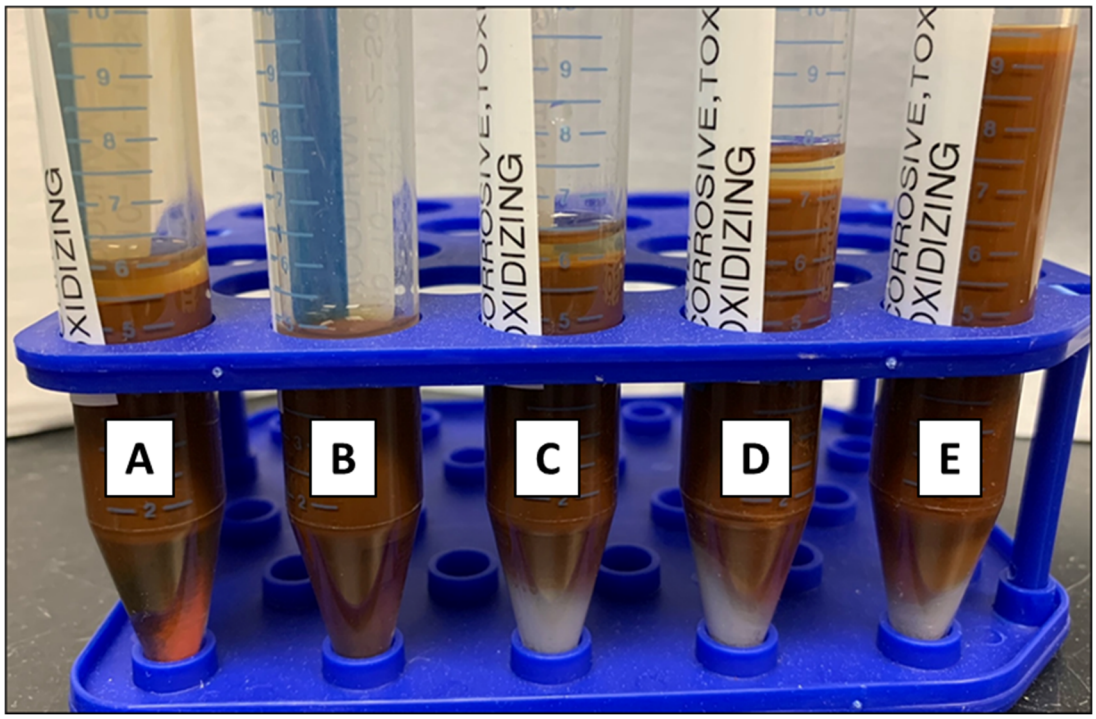

Figure 3-7. Photograph of Time-Dependent Samples Taken During Tk40-10.

From left to right, the samples photographed in Figure 3-7 are A) sludge after the addition of nitric acid, B) sludge after the addition of glycolic acid, C) sludge after the SRAT dewater stage, D) sludge after four hours of reflux boiling, and E) sludge after eight hours of reflux boiling. The samples shown were all centrifuged before being decanted. In the photograph, an obvious silver layer (corresponding to elemental mercury) seems to evolve some time during the SRAT dewater stage and persists through the first hours of reflux. This observation suggests a few details about the reduction kinetics of Hg in CPC processing. First, it suggests that Hg reduction is not an immediate process following the addition of glycolic acid. Rather, it seems to be slow, possibly limited by the production of formate from the action of glycolate on other metal oxides (as proposed by Zamecnik and Woodham).[21] Second, given the similar level of elemental Hg present in samples C, D, and E, it seems that only a trivial amount of Hg is stripped during the first few hours of CPC processing. This is important because in SRNL testing, the first few hours of Hg stripping are executed as SRAT dewater, whereas the vast majority of the remainder of Tk40-10 stripping time is reflux boiling. This suggests that only a small amount of Hg could be lost by acid redissolution in the MWWT (i.e., in sludge-only processing, the majority of stripping time is performed under reflux, which would be expected to return dissolved Hg to the SRAT kettle.

Sample C is compared to a centrifuged SRAT product sample taken from Tk40-10 in the photograph given in Figure 3-8.

Figure 3-8. Sample C (left) and SRAT Product (right) Taken from Tk40-10.

The absence of a silver layer in the SRAT product drawn from Tk40-10 is obvious in Figure 3-8. This agrees well with the low measurements of Hg concentration in SRAT products and reinforces the notion that low Hg concentration measurements are accurate and not a result of sampling or analytical error.

Methylmercury was also observed in SB 10 testing. Table 3-43 gives the organomercury concentrations observed in SB 10 simulant sludge supernatant and condensate materials.

Table 3-43. Liquid Phase Concentrations of Methylmercury (in mg L^{-1}).

Test	SRAT Dewater	SRAT Product†	Ammonia Scrubber	SME Dewater
Tk51-2	15.3	1.56	3.57	1.78
Tk40-1	6.71	<1	4.69	N/A
Tk40-2	25	<1	6.42	N/A

†Measurements of methylmercury in sludge are on a mg/L of sludge supernatant basis.

The data in Table 3-43 indicate that methylmercury is observed in SB 10 simulant testing. Note that the samples shown above represent only a portion of tests performed in SB 10 testing. Methylmercury samples were prepared for all SB 10 experiments; however, instrument failures were noted between February 2021 and August 2021, potentially impacting the majority of sample measurements. SRNL has issued a

temporary moratorium on the use of the data collected in this window and is in the process of ascertaining the applicability of results attained.[22] Values given in Table 3-43 are not a part of the moratorium and are therefore expected to be accurate.

Values in SRAT dewater streams tend to vary between 6 and 25 mg L^{-1}. Concentrations in SRAT product supernatant seem to be lower, near 1 mg L^{-1}. Ammonia scrubber methylmercury measurements appear to be moderate, yielding between 3.6 and 6.4 mg L^{-1}. The SME dewater concentration of methylmercury reported for Tk51-2 is 1.8 mg L^{-1}, notably lower than concentrations observed in SRAT dewater.

The observation that SRAT dewater concentrations of methylmercury are greater than those measured in the ammonia scrubber support the notion that methylmercury is 1) generated either in the SRAT kettle or SRAT condenser to a greater extent that in the ammonia scrubber, and 2) not sufficiently volatile in the off gas train to migrate downstream in large quantities. This difference is mostly academic, as the ammonia scrubber in DWPF is fed using condensate from the SRAT dewater cycle.

The fact that methylmercury is present in higher concentrations in the SRAT dewater than was observed in the SME dewater (for Tk51-2) suggests that the methylmercury formation mechanism present in SB 10 simulant testing diminishes as time increases. This is consistent with the decrease in available Hg in the SME kettle (compared to Hg in the SRAT kettle). This observation may indicate that methylmercury formation occurs in the kettle as well as condensates streams. This hypothesis may be proven with additional methylmercury samples from other Tank 40 SRAT products.

At this time, it is uncertain if the observation of methylmercury is due to expected CPC processing conditions (e.g., transmetallation of the methyl groups present in organosilicon antifoamer agents) or if the methylmercury observed in SB 10 experiments is due to conditions unique to SRNL simulant testing (e.g., the use of lubricants and greases in the 4-L SRAT apparatus). It is recommended that radioactive SB 10 testing collect sufficient sample for analyses necessary to evaluate the formation of organomercury in radioactive conditions.

The conclusions made above are drawn from a small collection of methylmercury samples. It is unlikely that additional sample analysis would appreciably alter any processing strategy or safety-relevant assumption related to SB 10 processing. However, the observation of methylmercury presence or absence in additional SB 10 streams and samples may provide further insight into generation mechanisms. For this reason, it is recommended that additional SB 10 samples be submitted for methylmercury analysis as needed to support an academic understanding of methylmercury presence in the CPC.

3.8 REDOX

The concentrations of anions in melter feed, REDOX measurements, and REDOX predictions made by the Jantzen equation.[23] for each SB 10 CPC experiment are given in Table 3-44. Note that for tests Tk40-1 through Tk40-7, SME testing wasn't performed. For these experiments, frit was added to SRAT product to achieve a desired waste loading of 36% and the anion concentrations and solids concentrations were corrected to account for frit addition. Measured SRAT and SME product compositions were used to calculate the necessary amount of lithium metaborate to add to adjust the glass viscosity before melting.[24]

Table 3-44. REDOX Predictions and Measurements.

Run†	Formate (mol/kg)	Glycolate (mol/kg)	Oxalate (mol/kg)	Nitrate (mol/kg)	Mn (mol/kg)	Total Solids (%)	Pred. REDOX	Meas. REDOX
Tk40-1	0.019	0.598	0.021	0.904	0.117	43.6	0.069	0.222
								0.077
								0.163
Tk40-2	0.041	0.646	0.024	0.990	0.105	40.2	0.035	<0.04
								0.036
								0.288
Tk40-3	0.028	0.733	0.022	0.823	0.114	43.0	0.326	NR
Tk40-4	0.021	0.776	0.035	0.850	0.105	41.4	0.364	0.52
								0.515
								0.47
Tk40-5	0.023	0.699	0.028	0.807	0.099	40.9	0.306	0.491
								0.417
Tk40-6	0.021	0.556	0.012	0.699	0.105	42.4	0.221	0.227
								0.257
								0.29
Tk40-7	0.007	0.646	0.025	0.842	0.093	39.5	0.185	0.549
								0.487
								0.529
Tk40-8	0.016	0.643	0.023	0.710	0.110	44.6	0.326	0.441
								0.419
								0.378
Tk40-9	0.024	0.478	0.019	0.653	0.094	39.9	0.179	0.397
								0.462
								0.418
Tk40-10	0.027	0.471	0.028	0.638	0.121	45.8	0.187	0.388
								0.453
								0.401
Tk51-2	0.005	0.511	0.041	0.900	0.116	44.9	-0.053	<0.04
								<0.03
								<0.04
Tk51-3	0.007	0.502	0.017	0.620	0.116	40	0.234	0.38
								0.261
								0.402
								0.281
								0.402
								0.277
Tk51-4	0.012	0.418	0.024	0.710	0.112	40.6	0.032	<0.03
								0.069
								0.065

†Experiments Tk40-1 through Tk40-7 were SRAT-only experiments. REDOX measurements were performed by adding frit to SRAT product at a specified waste loading of 36%. REDOX predictions were estimated by calculating the dilution of REDOX-active constituents by frit addition and correcting for total solids. All tests were performed by targeting a final REDOX of 0.1 (with the exception of Tk40-3 and Tk40-4, which targeted REDOX values of 0.3).
NR = Not reported. Attempts at melting Tk40-3 material failed to yield an intact crucible.

As mentioned, the column “Pred. REDOX” in Table 3-44 is a calculated value using the Jantzen equation to predict REDOX from measured anion concentrations and solids loadings. This equation (truncated for

applicability to this work) is given in Equation [8]. Note that no empirical term has been determined for carbon from Y-17112 antifoam, so this component is ignored (the impact of this is expected to be negligible due to low antifoam addition amounts used in SB 10 and the chemical similarity of Y-17112 to Antifoam 747).

$$\frac{Fe^{2+}}{\sum Fe} = 0.2358 + 0.1999\frac{0.45}{f_{TS}}\{2[F]+2[O]+6[G]-5[N]\} \quad [8]$$

Where,

$\frac{Fe^{2+}}{\sum Fe}$ is the REDOX value, or the ratio of iron(II) to total iron present in the glass,

f_{TS} is the fraction of total solids in the melter feed,

$[F]$ is the concentration of formate in the melter feed in mol kg^{-1},

$[O]$ is the concentration of oxalate in the melter feed in mol kg^{-1},

$[G]$ is the concentration of glycolate in the melter feed in mol kg^{-1}, and

$[N]$ is the combined concentration of nitrite and nitrate in the melter feed in mol kg^{-1}.

A fit of REDOX measurements to the predictions made by the Jantzen equation is given in Figure 3-9.

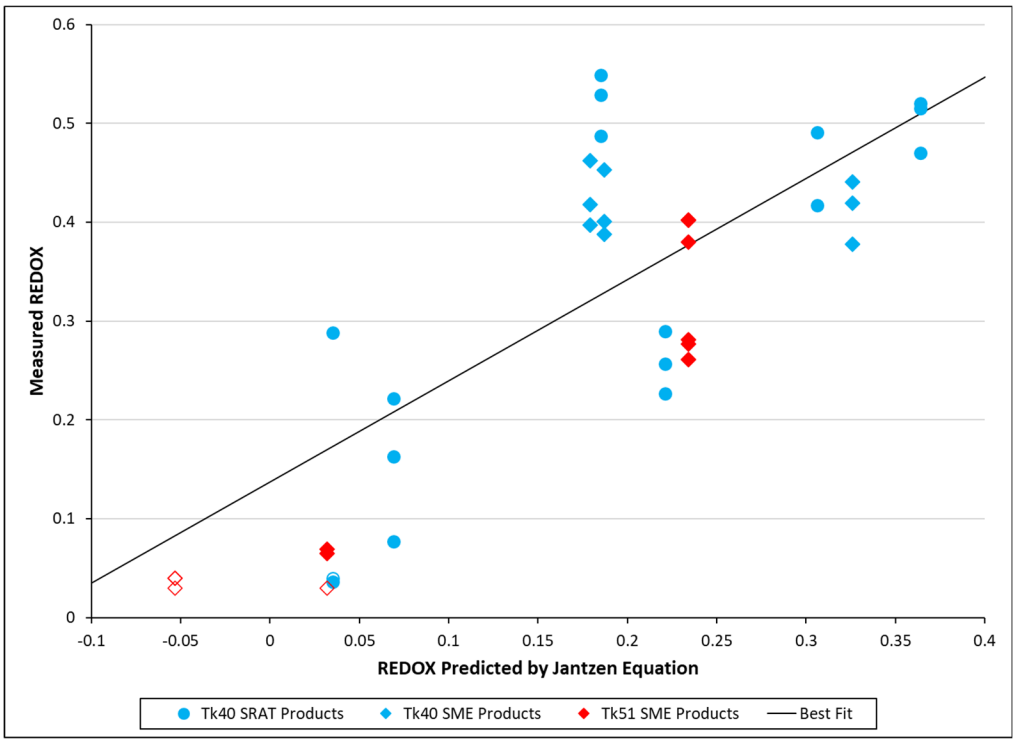

Figure 3-9. Plot of REDOX Predicted by the Jantzen Equation vs. Measured REDOX. Open symbols represent measurement at the limit of detection.

The intercept of the fit depicted in Figure 3-9 is approximately 0.12, suggesting that the Jantzen equation universally underpredicts the REDOX of SB 10 simulant sludges by approximately 0.137. Furthermore, the slope associated with this fit is approximately 1.02, indicating that the underestimating effect is slightly compounded in higher REDOX materials. These two observations suggest that SB 10 sludge is marginally more reducing than previous testing used to generate the Jantzen equation. The cause of this reducing bias is uncertain at this time. It is recommended that SB 10 results be evaluated against previous data in a separate memorandum to determine if a change to REDOX prediction is merited.

Fit parameters aside, the REDOX data plotted in Figure 3-9 seem to correlate linearly with the projections made by the Jantzen equation, suggesting that the method is qualitatively valid, and suggests that better control on anion conversion chemistry may result in better control on REDOX values.

3.9 Mass Balances

Mass balances for Tank 40 flowsheet SRAT experiments for carbon, nitrogen, and mercury are given in Table 3-45, Table 3-46, and Table 3-47, respectively.

Table 3-45. Carbon Mass Balance From SB-10 Flowsheet SRAT Experiments.

Amount (mol)	Tk40-1	Tk40-2	Tk40-3	Tk40-4	Tk40-5	Tk40-6	Tk40-7
Formate Before Acid	6.87E-03	6.29E-03	0.00E+00	7.09E-03	6.64E-03	7.88E-03	0.00E+00
Oxalate Before Acid	3.06E-02	3.12E-02	2.95E-02	3.17E-02	3.10E-02	3.34E-02	2.59E-02
TIC Before Acid	3.34E-01	3.68E-01	3.54E-01	3.59E-01	3.60E-01	4.16E-01	3.97E-01
Glycolate Added	2.23E+00	2.66E+00	2.55E+00	2.99E+00	2.63E+00	2.13E+00	3.11E+00
Carbon Before Acid	**4.86E+00**	**5.75E+00**	**5.51E+00**	**6.41E+00**	**5.68E+00**	**4.76E+00**	**6.66E+00**
Carbon in SRAT Prod.	4.11E+00	5.07E+00	4.99E+00	5.90E+00	5.17E+00	3.95E+00	5.09E+00
Carbon in Off-gas	2.60E-01	2.46E-01	2.72E-01	2.75E-01	2.41E-01	2.88E-01	2.72E-01
Carbon After Acid	**4.37E+00**	**5.31E+00**	**5.26E+00**	**6.18E+00**	**5.41E+00**	**4.23E+00**	**5.36E+00**
Mass Balance (%)	**89.9**	**92.4**	**95.4**	**96.4**	**95.3**	**89.0**	**80.5**

As shown in Table 3-45, the largest source of carbon in CPC experiments is glycolate added as glycolic acid. This source is approximately 10x greater than the next highest source of carbon (carbonate present in the sludge simulant) and approximately 100x greater than the third highest source (oxalate present in sludge simulant). Similarly, carbon in the SRAT product (calculated as the sum of glycolate, oxalate, and formate in the SRAT product) is approximately 20x greater than carbon lost as carbon dioxide. Carbon in the SRAT product and cumulative release of carbon dioxide accounts for between 80.5% and 96.4% of the carbon added during a SRAT experiment, indicating a reasonable mass balance of carbon during CPC processing.

Table 3-46. Nitrogen Mass Balance From SB-10 Flowsheet SRAT Experiments.

Amount (mol)	Tk40-1	Tk40-2	Tk40-3	Tk40-4	Tk40-5	Tk40-6	Tk40-7
Nitrite Before Acid	8.33E-01	7.95E-01	8.36E-01	8.20E-01	7.31E-01	7.76E-01	8.85E-01
Nitrate Before Acid	4.84E-01	4.93E-01	5.04E-01	4.96E-01	4.69E-01	4.83E-01	5.25E-01
Nitrate Added	1.98E+00	2.39E+00	1.66E+00	2.06E+00	2.00E+00	1.65E+00	2.36E+00
Nitrogen Before Acid	**3.30E+00**	**3.68E+00**	**3.00E+00**	**3.37E+00**	**3.20E+00**	**2.91E+00**	**3.77E+00**
NO_3 in SRAT Product	2.95E+00	3.64E+00	2.67E+00	3.05E+00	2.83E+00	2.38E+00	3.18E+00
NO_3 in SRAT Dewater	1.19E-01	6.33E-02	9.49E-02	7.72E-02	6.63E-02	2.11E-01	5.93E-02
NO_3 in SEFT Dewater	0.00E+00	7.28E-02	6.61E-02	NR	2.47E-02	6.03E-02	3.68E-03
NO_3 in Am. Scrubber	1.63E-01	1.35E-01	1.83E-01	1.33E-01	1.40E-01	2.14E-01	1.28E-01
Nitrogen in Off-gas	1.13E-01	7.48E-02	1.19E-01	1.01E-01	7.88E-02	1.06E-01	5.90E-02
Nitrogen After Expt.	**3.35E+00**	**3.98E+00**	**3.13E+00**	**3.36E+00**	**3.14E+00**	**2.98E+00**	**3.43E+00**
Mass Balance (%)	**101.6**	**108.2**	**104.5**	**99.7**	**98.0**	**102.2**	**91.0**

As was the case for carbon, acid addition comprises the majority of nitrogen added to a CPC experiment, as is shown in Table 3-46. Nitrogen added as nitric acid is more than double the amount of nitrogen added as nitrite. Similarly, nitrate in the SRAT product is the dominant source of nitrogen exiting the SRAT cycle. Masses of nitrate removed in condensate streams and off-gas are significantly smaller due to small concentrations. Nitrogen appears to be relatively well reconciled in Tank 40 testing, with mass balance closures of between 91.0% and 108.2% exhibited.

Table 3-47. Mercury Mass Balance From SB-10 Flowsheet SRAT Experiments.

Amount (mol)	Tk40-1	Tk40-2	Tk40-3	Tk40-4	Tk40-5	Tk40-6	Tk40-7
Hg Added	**9.82E-02**	**9.82E-02**	**9.82E-02**	**9.80E-02**	**9.83E-02**	**9.82E-02**	**1.08E-01**
Hg in Samples	1.34E-02	1.29E-02	1.42E-02	1.45E-02	1.45E-02	1.31E-02	1.38E-02
Hg in SRAT Product	1.48E-03	2.00E-03	1.75E-03	1.08E-03	1.25E-03	1.55E-03	1.91E-03
Hg in PRFT Dewater	3.58E-05	5.21E-04	3.35E-05	4.33E-05	3.12E-05	1.24E-04	1.49E-04
Hg in SRAT Dewater	3.90E-04	2.54E-04	1.73E-03	1.84E-03	2.08E-03	2.88E-03	5.01E-04
Hg in SEFT Dewater	2.93E-04	4.91E-03	1.47E-03	1.75E-03	1.56E-03	4.20E-03	2.05E-04
Hg in Am. Scrubber	1.66E-04	3.93E-05	1.02E-04	1.69E-04	6.32E-05	2.10E-04	3.53E-04
Hg from MWWT	7.41E-03	3.39E-02	4.39E-02	5.44E-02	5.75E-02	6.33E-02	6.07E-02
Hg After Experiment	**2.32E-02**	**5.45E-02**	**6.32E-02**	**7.38E-02**	**7.70E-02**	**8.53E-02**	**7.76E-02**
Mass Balance (%)	**23.6**	**55.5**	**64.3**	**75.3**	**78.4**	**86.9**	**72.2**

The data in Table 3-47 indicate generally poor mercury mass balances in SB 10 testing. Some experiments (notably Tk40-5 and Tk40-6) seem reasonable (78.4% and 86.9%, respectively). However, many data points fall below 50% mass balance closure, which is consistent with mass balance results from previous testing. It is interesting to note that the most dominant sources of Hg after an experiment are the Hg collected from the MWWT and samples taken (i.e., SRAT receipt and Product samples) during an experiment. This is consistent with the amount of sample needed to characterize SRAT receipt conditions relative to the total amount of slurry in the reaction vessel. This suggests that the Hg mass balance is generally acceptable until the addition of acid. Furthermore, because the amounts of Hg in SRAT receipt samples are consistent with the amount of Hg added to each experiment, it is safe to conclude that slurry sampling is likely not responsible for the poor Hg mass balance. Instead, transfer of the Hg into downstream vessels via a change in speciation is a more likely candidate. It is possible that some Hg is lost to off-gas and carried through the

ammonia scrubber and into the off-gas analysis train. It is recommended that SRNL investigate methods to determine mercury loss in off-gas during future CPC testing.

4.0 Conclusions

Fourteen CPC simulations were performed with nonradioactive sludge simulants at ACTL. Four of these experiments were performed with Tank 51 sludge simulant. The remaining ten were performed with Tank 40 sludge simulant. The purpose of these experiments was to elucidate the chemistry and characteristics of Sludge Batch 10 as anticipated in the DWPF. Experiments were performed at acid stoichiometries between 76% and 138% of the Koopman Minimum Acid requirement (85% - 144% of the Hsu acid requirement) and at REDOX targets between 0.1 and 0.3. Testing examined the impact of coupled operations and sludge-only operations during SRAT and SME processing at both design basis and nominal boilup rates.

The following conclusions are made as a result of this testing. Conclusions applicable to only one sludge type (Tank 40 or Tank 51) are indicated as needed.

- Acid stoichiometries as low as 76 % KMA (86% Hsu) are too low to effectively process SB 10 sludge. This stoichiometry leads to rheologically thick SRAT products that are prone to fouling, poor heat transfer, and poor mixing (Tank 51 sludge).
- The concentration of glycolate in condensates being sent to the Slurry Mix Evaporator Condensate Tank (SMECT) is expected to be <50 mg/L.
- Peak hydrogen generation rates observed in SB 10 testing are 3.90×10^{-4} lb h^{-1} and 6.04×10^{-4} lb h^{-1} during SRAT and SME processing, respectively. These values are well below the proposed SRAT and SME DWPF limits of 2.4×10^{-2} lb h^{-1}.
- CH_4 was observed during SB 10 simulant testing. Peak CH_4 production was shown in one experiment to coincide with the SRAT dewater stage of CPC processing. The appearance of CH_4 was confirmed by GC and FTIR. The presence of CH_4 has not been shown to be representative of expected CPC processing at the DWPF. Furthermore, observed concentrations of CH_4 (<100 ppm) do not indicate flammability hazard.
- Coupled operations processing may be responsible for a departure from previously observed glycolate destruction factors from SRAT processing, yielding a melter feed that is more glycolate-rich than would be expected in sludge-only processing (Tank 40 sludge).
- An assumed steam stripping factor of 750 g H_2O per g Hg appears to be adequate to achieve Hg concentration targets of 0.8 and 0.45% of total solids in SRAT and SME products, respectively.
- Methylmercury was observed during the SRAT and SME cycles. Evidence suggests that this reaction occurs in the reaction vessel itself, not exclusively downstream in condensate collection vessels. Furthermore, concentrations in condensates appear to be related to Hg concentrations in sludge.
- REDOX predictions made by the Jantzen equation correlate linearly with REDOX measurements in SB 10, indicating qualitative validity.
- No NH_4^+ was noted in the performance of SB 10 simulant experiments, indicating a lack of ammonia production during CPC processing.
- Acid stoichiometries greater than 100% and less than 110% (104% - 115% Hsu) are expected to yield an optimal yield stress during SRAT processing (Tank 40 sludge).
- Acid stoichiometries less than 110% (115% Hsu) are expected to yield an optimal viscosity during SRAT processing (Tank 40 sludge).
- Antifoam Y-17112 mitigated foaming in all SB 10 simulant experiments with no detectable evolution of antifoam degradation products.

5.0 Recommendations

The following recommendations are made as a result of this testing.

- SRNL may benefit by investigating alternative methods of heating to allow for maximum concentration of dilute sludge batches in future SB studies.
    - The SRNL Shielded Cells qualification experiment is expected to target lower solids during SRAT and SME processing, so over-concentration is not anticipated.
- Testing in the SRNL Shielded Cells should include capabilities to quantify methylmercury in liquid samples and methane in gas samples. Laboratory personnel should take sufficient sample to ensure adequate organomercury analyses and handle organomercury samples according to best practices.
    - Upon completion, organomercury results from the Shielded Cells qualification experiment should be compared to results obtained from simulant testing to determine similarities.
- SRNL should add glycolate at the beginning of future SRAT experiments (either as a trim chemical or as part of simulant development) to allow for an understanding of glycolate volatility during caustic boiling (recommended for Tank 40 sludge).
- Future CPC tests should include additional methylmercury analysis to assist in the understanding and closure of organomercury mass balances and amounts.
- SB 10 REDOX measurements should be compared against previous SB data sets to determine if changes to REDOX prediction methodology are merited.
- SRNL should investigate methods to determine Hg concentration and speciation in off-gas leaving the CPC condenser train.
- An acid stoichiometry of 105% is recommended for initial SB10 processing with Tank 40 material in the DWPF. At this stoichiometry, the glycolate destruction factor for coupled operations and sludge-only operations are expected to be 11.8% and 27.2%, respectively. At this stoichiometry, nitrite-to-nitrate conversions are expected to be between 8% and 94% (recommended for Tank 40 sludge).
- If future operational changes are made to increase the sludge solids output from SWPF, a separate investigation into the impacts of this increased sludge solids concentration on CPC chemistry should be performed.
- Additional rheology data gathered during SB 10 simulant testing should be documented and compared with rheological measurements that will be performed in the SRNL Shielded Cells (recommended for Tank 40 sludge).
- Additional SB 10 simulant samples should be submitted for methylmercury analysis to better elucidate the mechanism of methylmercury formation.
- SB 10 processing should be conducted with the antifoam addition strategy developed by Lambert.

6.0 References

1. Russell, K. J. "Sludge Batch 10 Simulant Testing"; X-TTR-S-00076, Rev. 2; Savannah River Remediation: **2021**.

2. Russell, K. J. "Sludge Batch 10 Simulant Testing with Addition of SRE Material"; X-TTR-S-00078, Rev. 1; Savannah River Remediation: **2021**.

3. Woodham, W. H.; Howe, A. M.; Siegfried, M. J. "Task Technical and Quality Assurance Plan for Sludge Batch 10 Simulant Flowsheet Studies"; SRNL-RP-2019-00744, Rev. 1; Savannah River National Laboratory: **2021**.

4. Smith, T. E.; Newell, J. D.; Woodham, W. H. "Defense Waste Processing Facility Simulant Chemical Processing Cell Studies for Sludge Batch 9"; SRNL-STI-2016-00281, Rev. 0; Savannah River National Laboratory: **2016**.

5. Lambert, D. P.; Williams, M. S.; Brandenburg, C. H.; Luther, M. C.; Newell, J. D.; Woodham, W. H. "Sludge Batch 9 Simulant Runs Using the Nitric-Glycolic Acid Flowsheet"; SRNL-STI-2016-00319, Rev. 0; Savannah River National Laboratory: **2016**.

6. Smith, T. E. "Antifoam Degradation Products in Off Gas and Condensate of Sludge Batch 9 Simulant Nitric-Formic Flowsheet Testing for the Defense Waste Processing Facility"; SRNL-STI-2016-00110; Savannah River National Laboratory: **2016**.

7. Woodham, W. H. "Run Plan for Simulant Testing to Support Sludge Batch 10 Tank 40 Flowsheet Qualification"; SRNL-L3100-2020-00050, Rev. 0; Savannah River National Laboratory: **2020**.

8. Woodham, W. H. "Run Plan for Simulant Testing of Sludge Batch 10 Tank 51 Flowsheet Evaluation in Support of Savannah River National Laboratory Shielded Cells Testing"; SRNL-L3100-2020-00040, Rev. 0; Savannah River National Laboratory: **2020**.

9. Shah, H., Email Communication - RE: SB10 Planning's projections needed. Woodham, W.; Johnson, F.; Fellinger, T.; Samadi-Dezfouli, A.; McNew, R.; Pennebaker, F.; Ray, J., Eds. Aiken, SC, 2020.

10. Lambert, D. P.; Howe, A. M.; Woodham, W. H.; Williams, M. S. "Antifoam Development for Eliminating Flammability Hazards and Decreasing Cycle Time in the Defense Waste Processing Facility"; SRNL-STI-2019-00677, Rev. 4; Savannah River National Laboratory: **2021**.

11. Smith, T. E.; Scherman, C.; Martin, D.; Suggs, P. "Next Generation Solvent Performance in the Modular Caustic Side Solvent Extraction Process"; SRR-LWE-2014-00118, Rev. 0; Savannah River Remediation: **2015**.

12. Woodham, W. H. "Recommendation for Sludge Batch 10 Qualification Processing in the Savannah River National Laboratory Shielded Cells"; SRNL-L3100-2021-00010, Rev. 0; Savannah River National Laboratory: **2021**.

13. "Technical Reviews"; Manual E7, 2.60, Rev. 19; **2021**.

14. "Technical Report Design Checklist"; WSRC-IM-2002-00011, Rev. 2; **2021**.

15. Woodham, W. H. "SB 10 Simulant Testing - Electronic Laboratory Notebook"; SRNL-L7748-00442-01; Savannah River National Laboratory: **2020**.

16. Koopman, D. C.; Best, D. R.; Pickenheim, B. R. "SRAT Chemistry and Acid Consumption During Simulated DWPF Melter Feed Preparation"; WSRC-STI-2008-00131, Rev. 0; Savannah River National Laboratory: **2008**.

17. Martino, C. J.; Coleman, C. J. "Solubility Testing to Support the Addition of Sodium Reactor Experiment Material to Sludge Batch 10"; SRNL-STI-2020-00294, Rev. 0; Savannah River National Laboratory: **2020**.

18. Fellinger, T. L.; Clark, M. C. "Sampling Plan for Determining Mercury and Antifoam Degradation Products for Batch 736 in Defense Waste Processing Facility (DWPF)"; SRR-WSE-2015-00042, Rev. 1; Savannah River Remediation: **2015**.

19. Lambert, D. P.; Zamecnik, J. R.; Newell, J. D.; Williams, M. S. "Antifoam Degradation Testing"; SRNL-STI-2015-00352, Rev. 0; Savannah River National Laboratory: **2015**.

20. Woodham, W. H.; Martino, C. J. "Evaluation of Thermolytic Production of Hydrogen from Glycolate and Common Tank Farm Organics in Simulated Waste"; SRNL-STI-2019-00605, Rev. 1; Savannah River National Laboratory: **2020**.

21. Woodham, W. H.; Zamecnik, J. R. "Evaluation of Simple Chemical Interactions in the Defense Waste Processing Facility (DWPF) Chemical Process Cell (CPC) Under the Glycolic Acid Flowsheet"; SRNL-STI-2017-00318, Rev. 0; Savannah River National Laboratory: **2018**.

22. Boggess, A. J.; White, T. L. "System Malfunction Leading to Incorrect Mercury Speciation Data Being Released to LIMS System"; SRNL-RP-2021-04720, Rev. 0; Savannah River National Laboratory: **2021**.

23. Jantzen, C. M.; Williams, M. S.; Edwards, T. B.; Trivelpiece, C. L.; Ramsey, W. G. "Nitric-Glycolic Flowsheet Reduction/Oxidation (REDOX) Model for the Defense Waste Processing Facility (DWPF)"; SRNL-STI-2017-00005, Rev. 0; Savannah River National Laboratory: **2017**.

24. L33 Manual. "Heat Treatment of Waste Slurries for Redox and Corrosion Analyses"; L33-0052, Rev. 1; Savannah River National Laboratory: **2021**.

Appendix A. Experiment Tk51-1 (Terminated Early Due to Sludge Thickening)

On October 26, 2020, SRNL personnel initiated experiment Tk51-1. Based on the successful use of 78% Koopman stoichiometry during SB 9 testing, it was decided that Tk51-1 would target a stoichiometry of 70% to further evaluate the effects of low acid additions on CPC processing.

At approximately 2:58 AM on October 27, 2020 (approximately 6.8 hours after heating began), abnormally high hydrogen concentrations (in excess of 100 ppm, equating to ~0.004 lb H_2 h^{-1} on a DWPF scale) were observed via GC. It was noted that around the time of the hydrogen peak, power input into the heating rods became irregular. Figure A-1 shows this trend along with relevant temperature data. Figure A-2 shows hydrogen generation and slurry temperature trends.

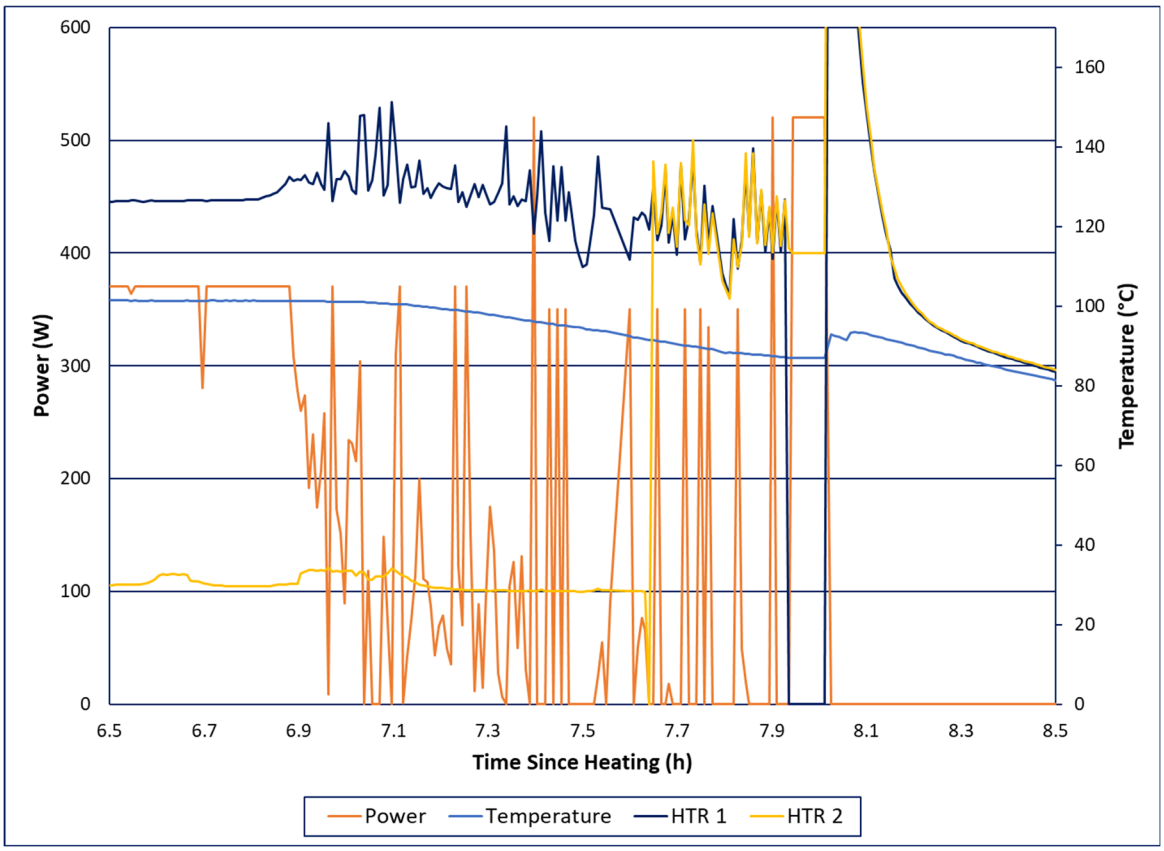

Figure A-1. Power Input and Temperature Trends Around the Time of Excursion During Tk51-1.

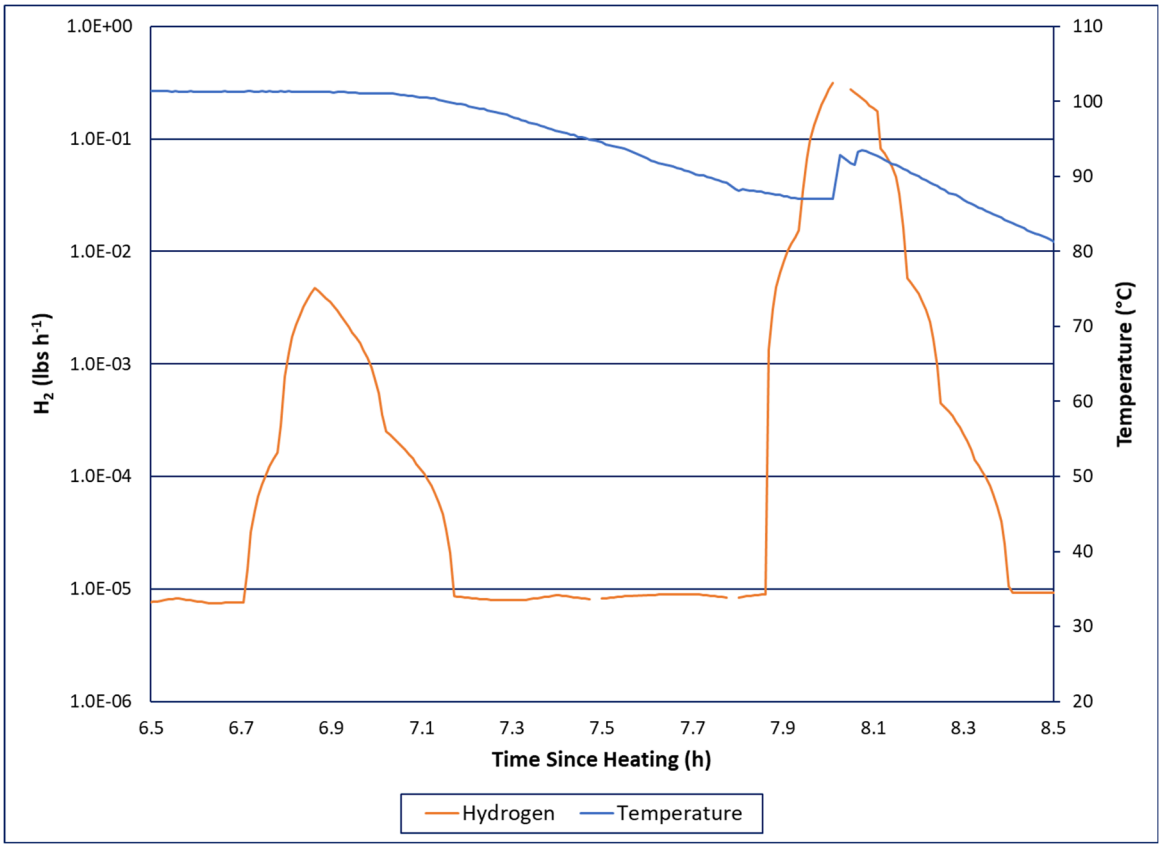

Figure A-2. Hydrogen and Slurry Temperature Trends Around the Time of Excursion During Tk51-1.

The power input data given in Figure A-1 indicate that the LabVIEW™ control software became unable to supply a constant power input due to the control constraints implemented into the software (e.g., no heating rod is able to be more than 30 °C hotter than the bulk liquid temperature. The slight increase in HTR 1 temperature at 6.8 hours is consistent with rod fouling, leading to a poor heat transfer coefficient and an inability to input the heat necessary to sustain desired boilup rates without triggering the 30 °C overtemperature control mechanism. This rod fouling then quickly provided a mechanism for excess hydrogen generation, shown in Figure A-2. Once the heating rod fouling had occurred, it became more difficult to transfer heat into the sludge slurry, as can be seen in the power input trend and the decreasing slurry temperature trend. This decrease in heating continued for approximately 1 hour, allowing the sludge slurry to fall below 90 °C. At this time, the principal investigator initiated bulk temp heating mode with the intent of providing a slow heat-up rate to return to boiling temperatures.

At approximately 4:05 AM, the temperature scanner employed in the testing exhibited a malfunction wherein the temperature scanner simultaneously failed to transmit the correct temperatures of heating rods 1 and 2 while also failing to update any temperature being recorded by the LabVIEW™ software. The conditions reported to the control PC for each relevant temperature between 4:05 AM and 4:09 AM were: 87 °C for slurry temperature, 0 °C for heating rod 1, and 113.2 °C for heating rod 2. The failure to update temperatures for ~ 4 minutes while under Bulk Temp heating mode allowed the control software to provide maximum heat to the rod for the duration of four minutes. This heat, combined with previous signs of rod fouling, lead to a significant hydrogen excursion at approximately 8 hours since heating began (0.27 lb H_2 h^{-1}, corresponding to approximately 12,000 ppm). The principal investigator reacted to this high hydrogen

production by initiating a “time-out”. At this time, accurate temperature monitoring was restored, indicating that the heating rods had reached temperatures over 400 °C.

Over the next ~15 hours, researchers worked to 1) replace fouled heating rods, and 2) determine the impact of the previous temperature excursion on remaining experiment plans. The solids concentration of the slurry was measured at 25% total solids despite having stopped the experiment prior to the completion of the SRAT dewater stage. This suggests that a leak may have formed during the course of the experiment. After the leak had been repaired and heating rods had been replaced, the experiment was resumed, proceeding directly into the reflux boiling stage of the SRAT cycle. Power and temperature trends for this period of testing are given in Figure A-3 and the hydrogen profile is given in Figure A-4.

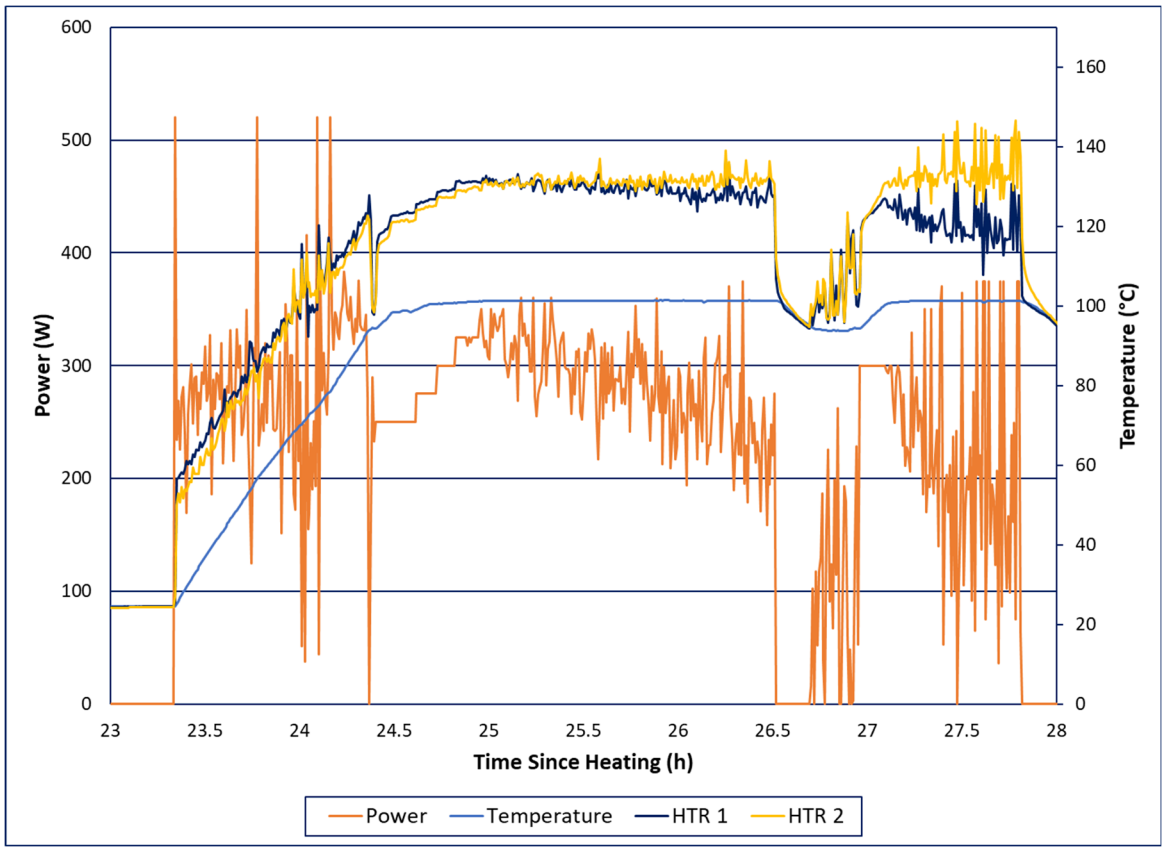

Figure A-3. Power Input and Temperature Trends for Tk51-1 Restart Period.

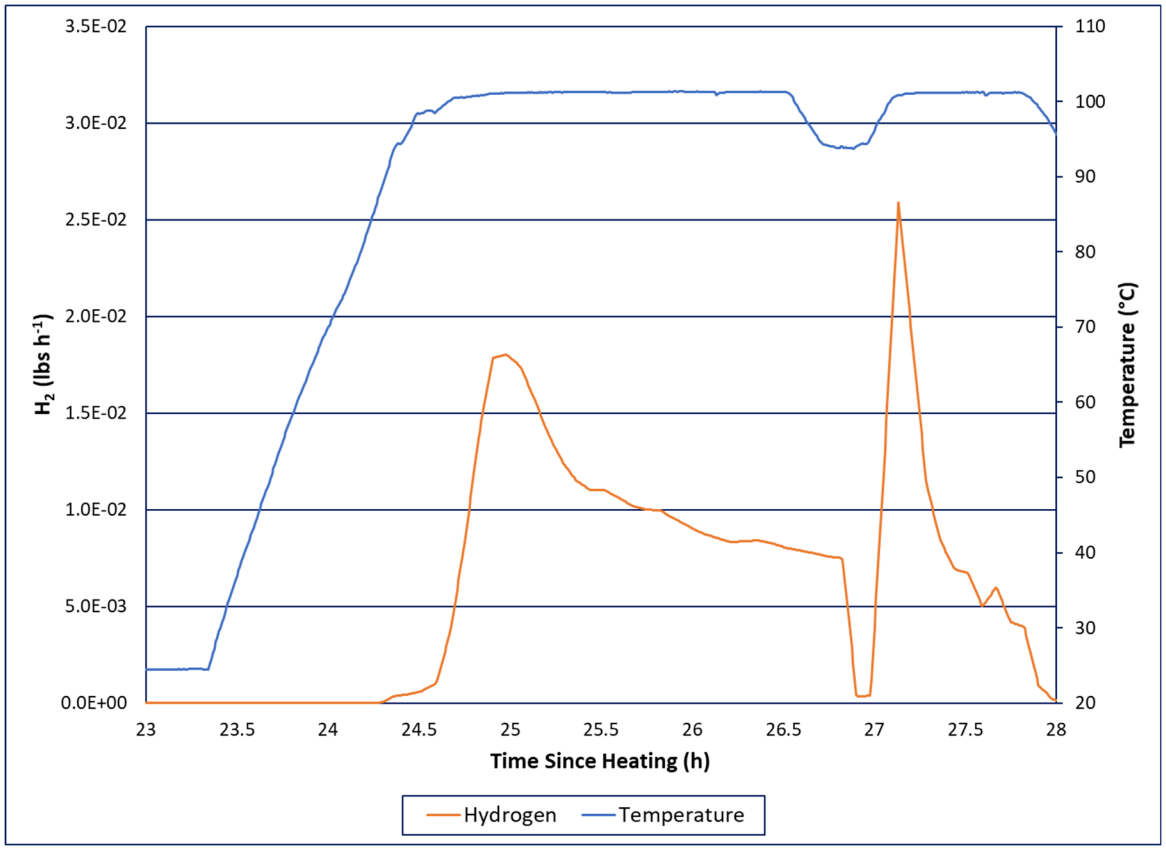

Figure A-4. Hydrogen and Slurry Temperature Trends for Tk51-1 Restart Period.

The temperature and power input profiles shown in Figure A-3 indicate continued noise in power input and gradually diverging heater rod temperatures, both of which are consistent with continued heater rod fouling. The evolution of H_2 gas in the same timeframe (up to ~0.018 lb h^{-1}, shown in Figure A-4) agrees well with the fouling conclusion. The principal investigator added DI H_2O to the vessel (at ~27 hours) in an attempt to dilute solids and prevent fouling, but subsequent heating and hydrogen profiles indicate continued rod fouling, abnormally high hydrogen production, and an inability to hit desired boil-up targets. A second "time-out" was called and heating was stopped.

During the second "time-out", a slurry sample was drawn to allow for rheological and solids measurements. These analyses determined a total solids concentration of 20%. Yield stress was observed to be 30.2 Pa (significantly higher than the SRAT design basis upper limit of 5 Pa) and consistency was observed to be 17.4 cP (notably higher than the SRAT design basis upper limit of 12 cP.

Based on the observations of continued rod fouling, unrealistically high hydrogen production, and unprocessable rheology, the decision was made to stop experiment Tk51-1. The discrepancies in this experiment preclude the use of data generated from Tk51-1 for assisting in the development of the SB 10 flowsheet. The sole conclusion taken from the experiment is that 70% stoichiometry is likely far too low for Tank 51 SB 10 sludge.

Appendix B. pH Profiles of SB 10 Simulant Experiments

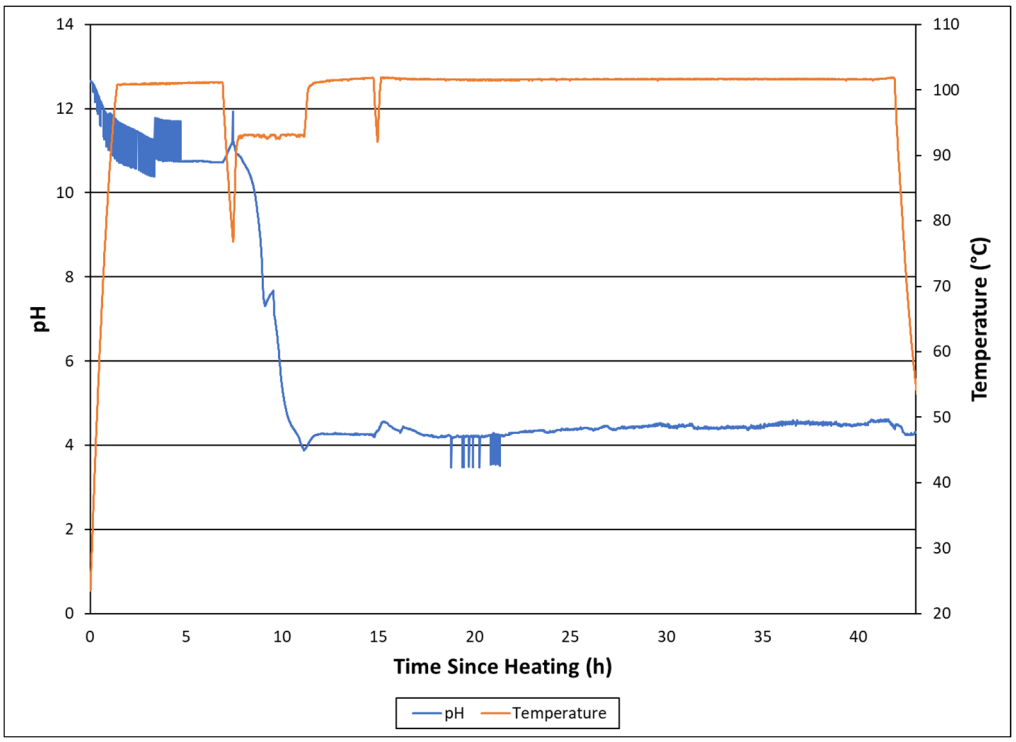

Figure B-1. Tk40-1 pH and Temperature Profiles.

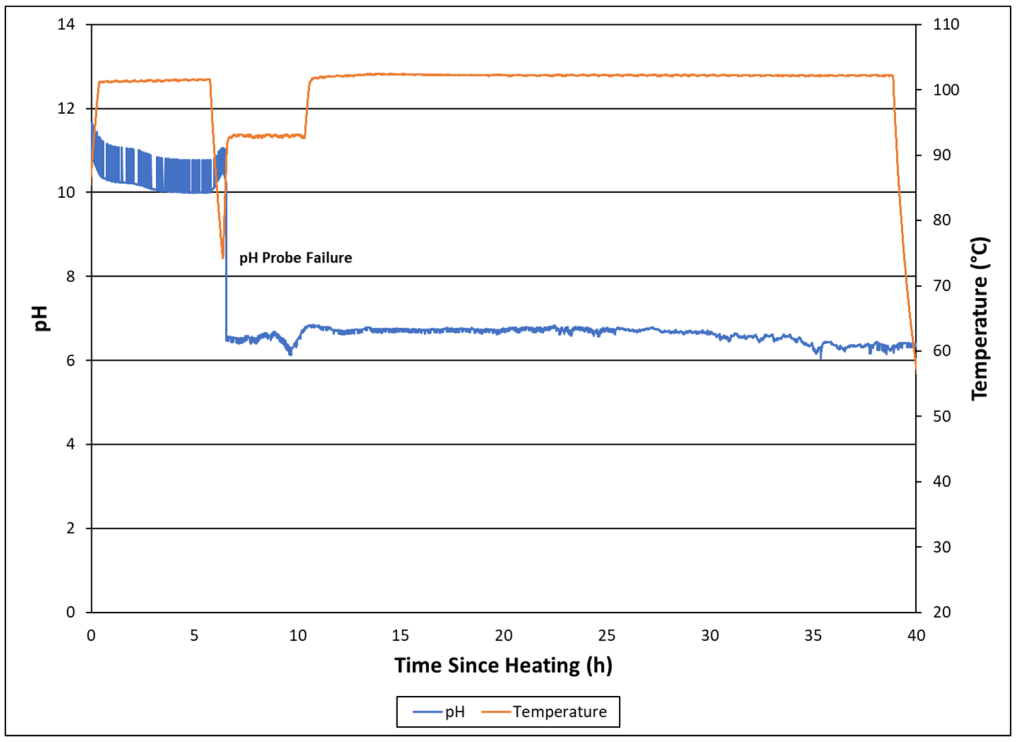

Figure B-2. Tk40-2 pH and Temperature Profiles.

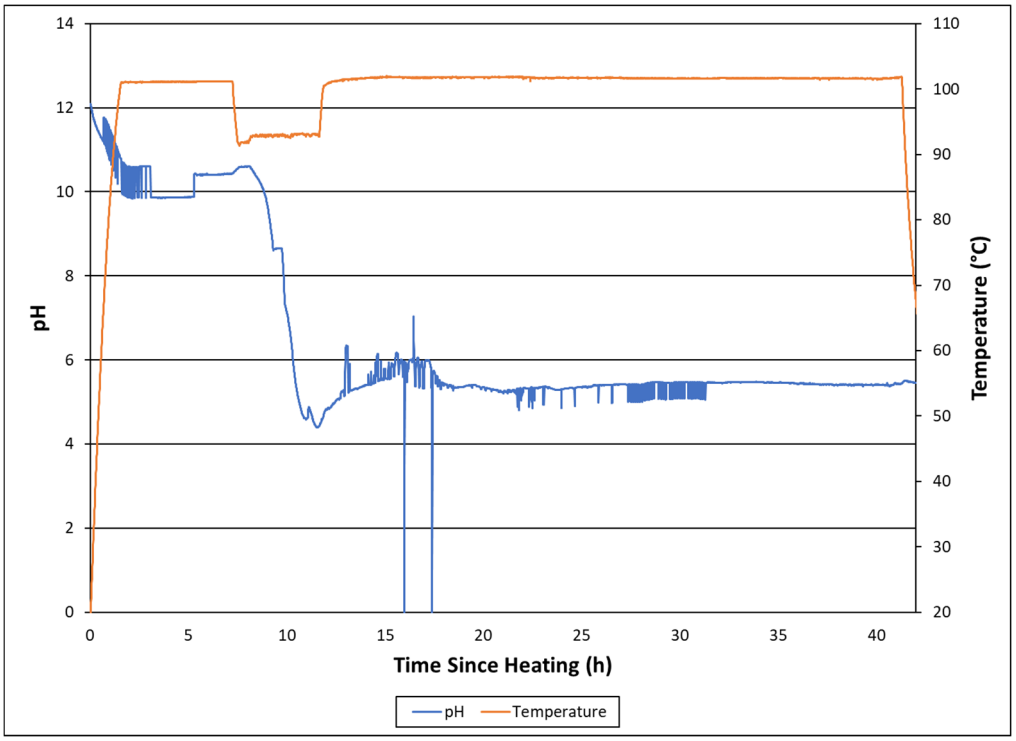

Figure B-3. Tk40-3 pH and Temperature Profiles.

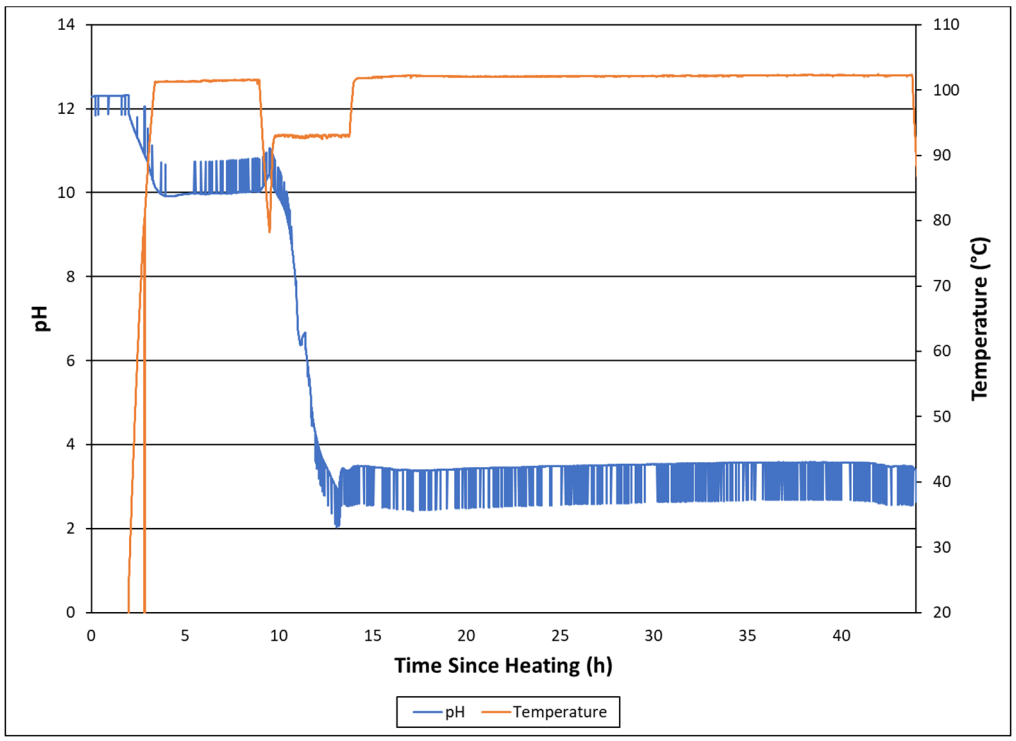

Figure B-4. Tk40-4 pH and Temperature Profiles.

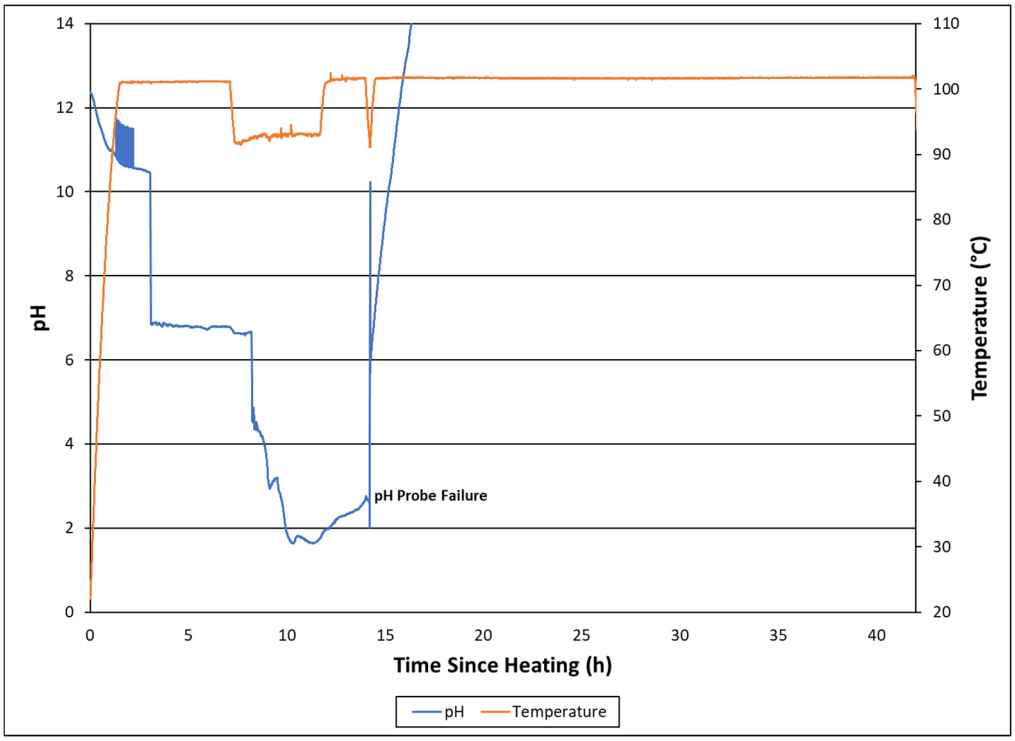

Figure B-5. Tk40-5 pH and Temperature Profiles.

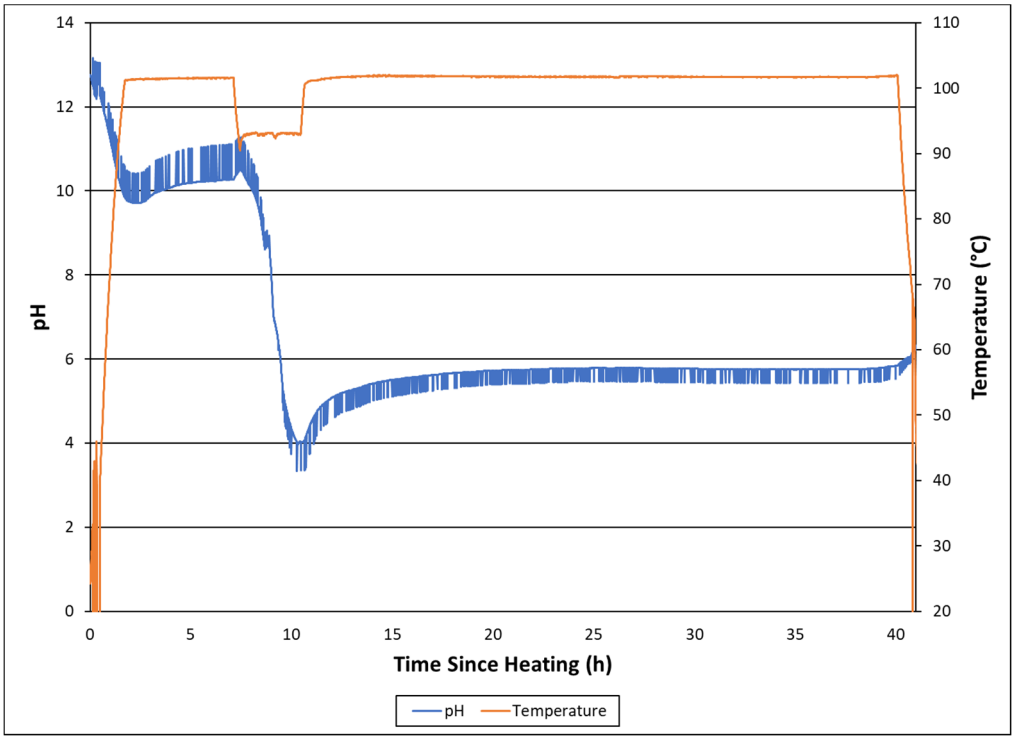

Figure B-6. Tk40-6 pH and Temperature Profiles.

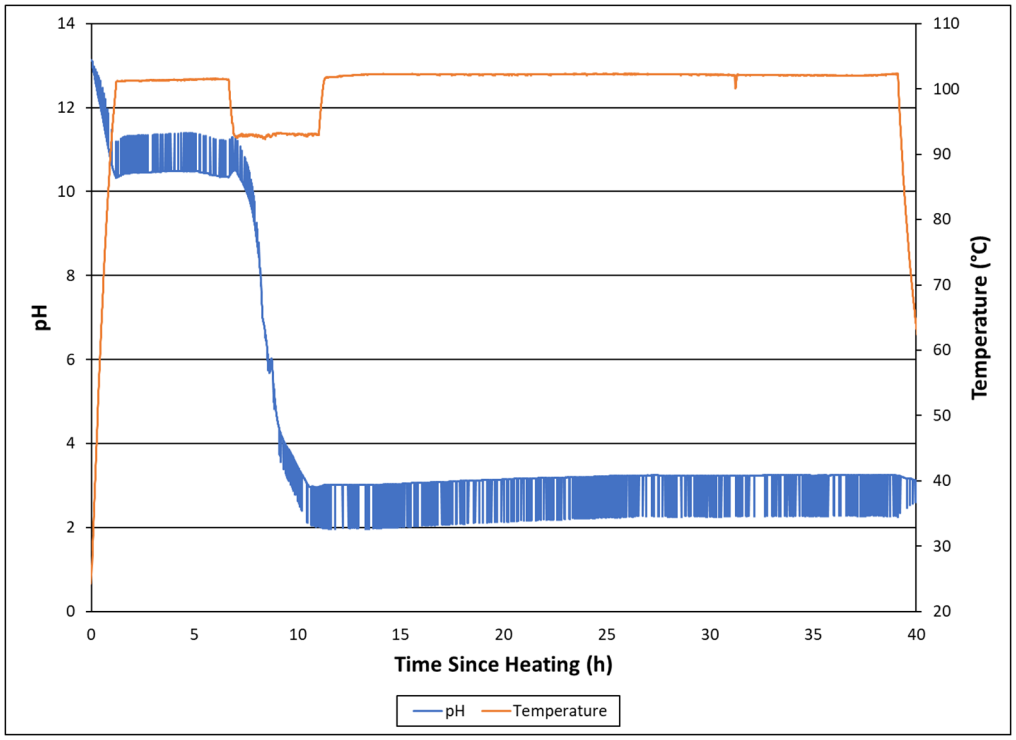

Figure B-7. Tk40-7 pH and Temperature Profiles.

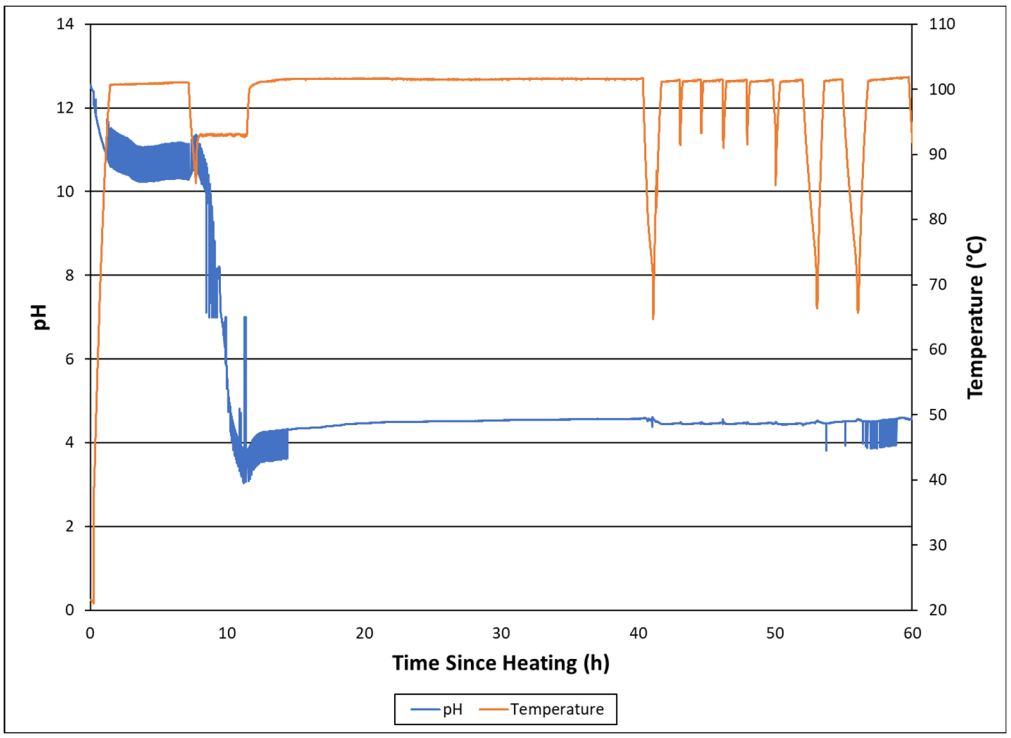

Figure B-8. Tk40-8 pH and Temperature Profiles.

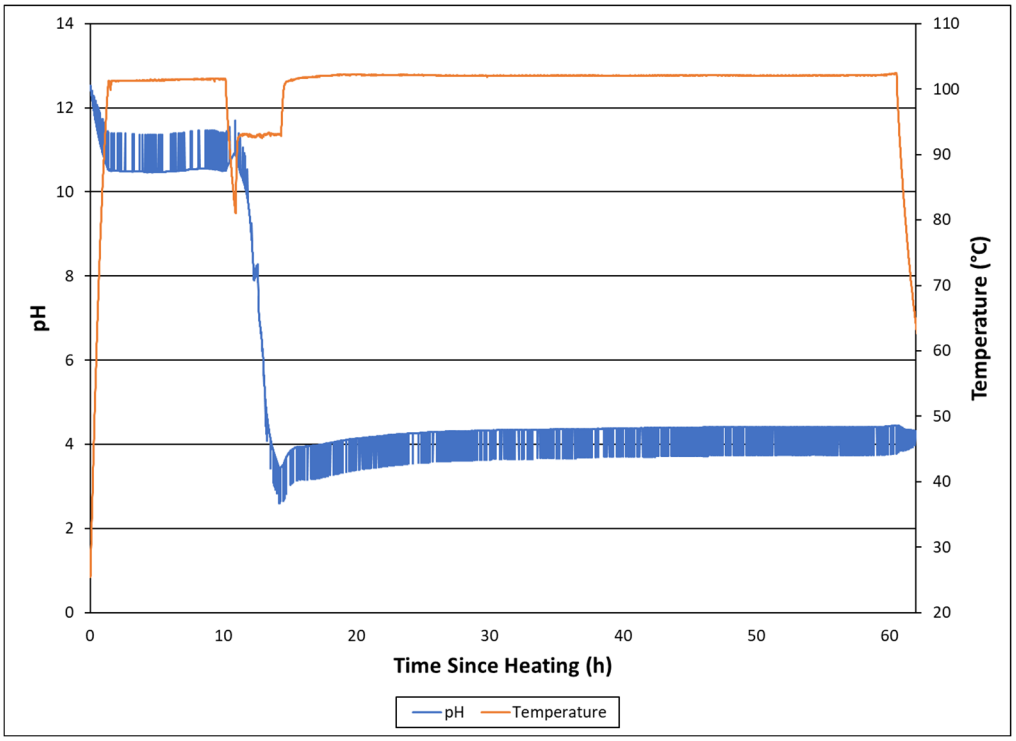

Figure B-9. Tk40-9 SRAT Cycle pH and Temperature Profiles.

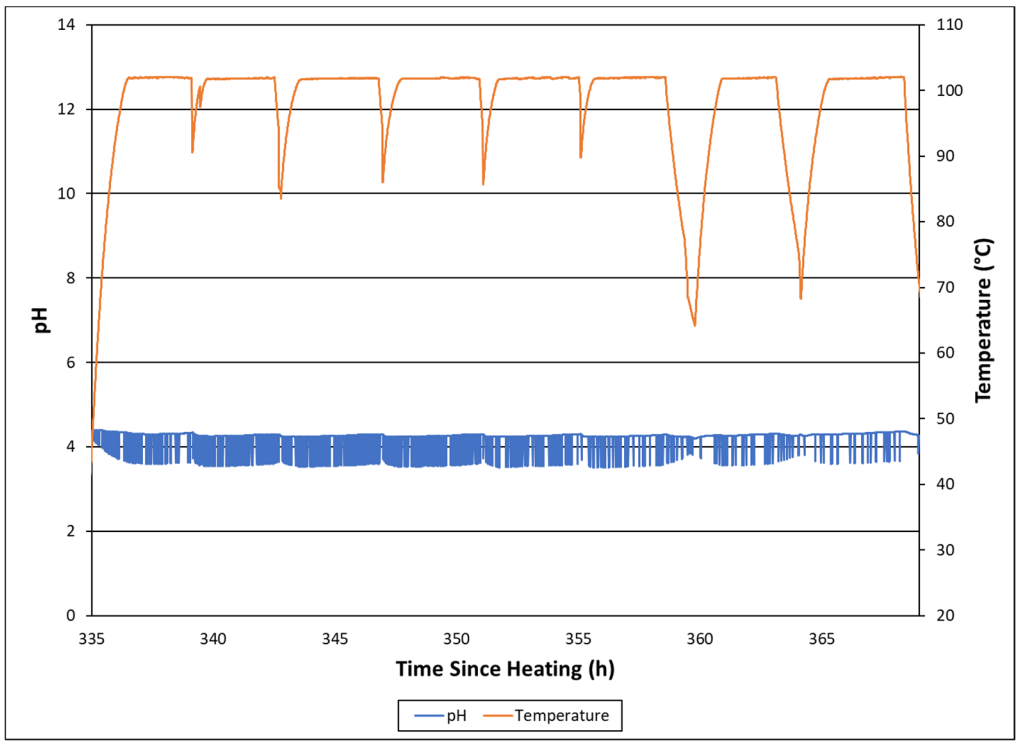

Figure B-10. Tk40-9 SME Cycle pH and Temperature Profiles.

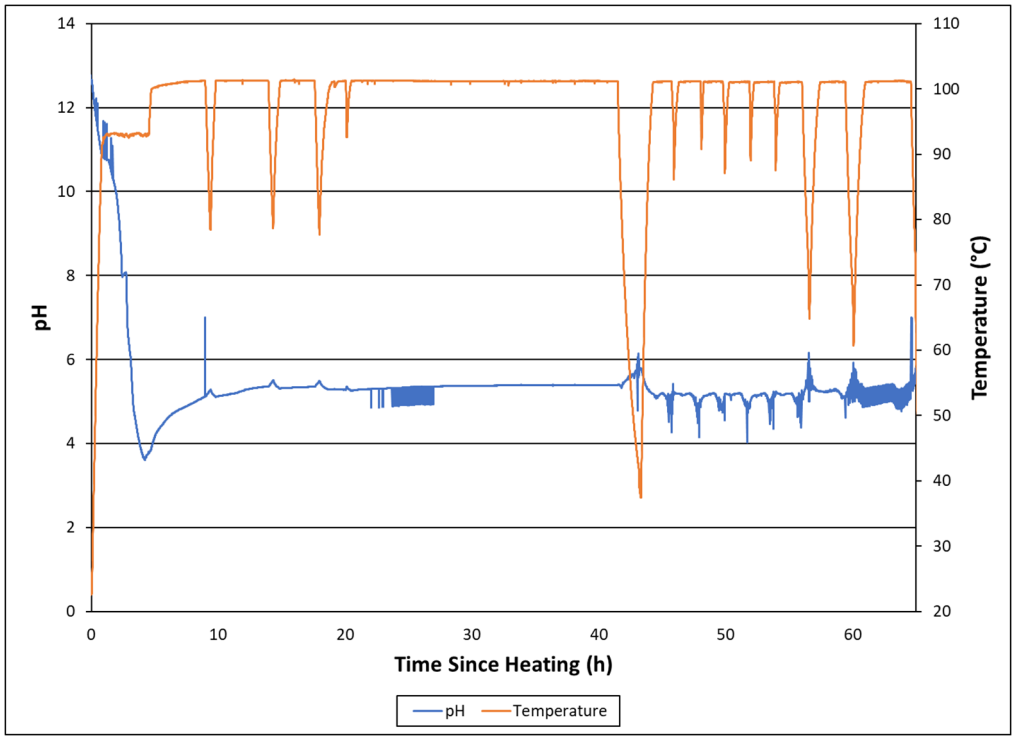

Figure B-11. Tk40-10 pH and Temperature Profiles.

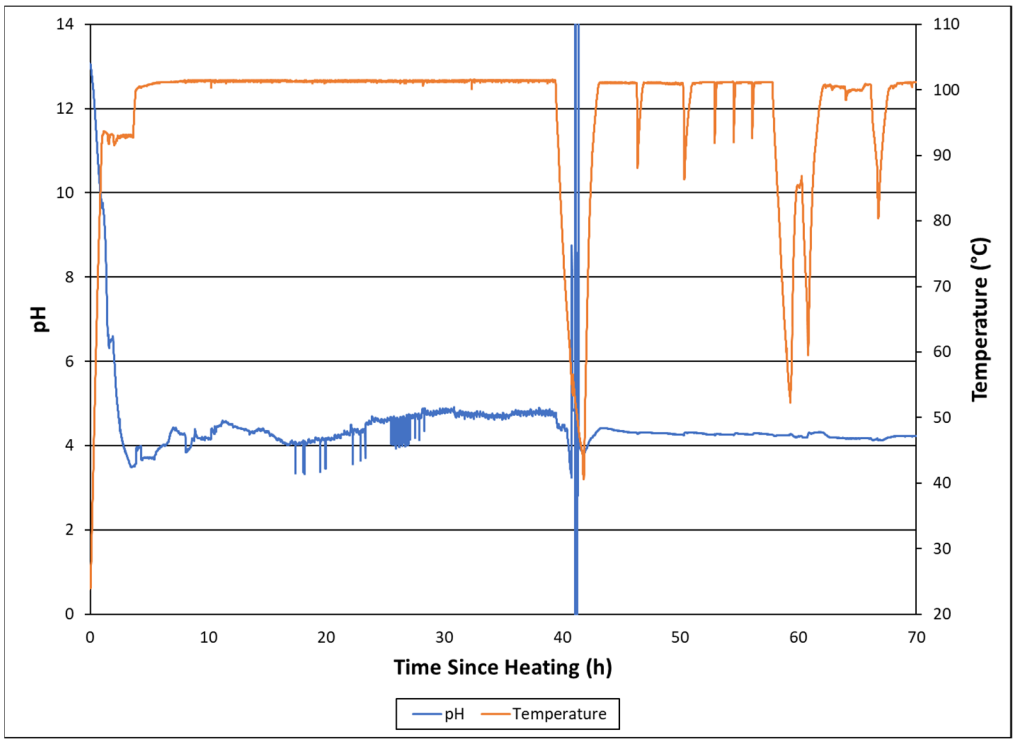

Figure B-12. Tk51-2 pH and Temperature Profiles.

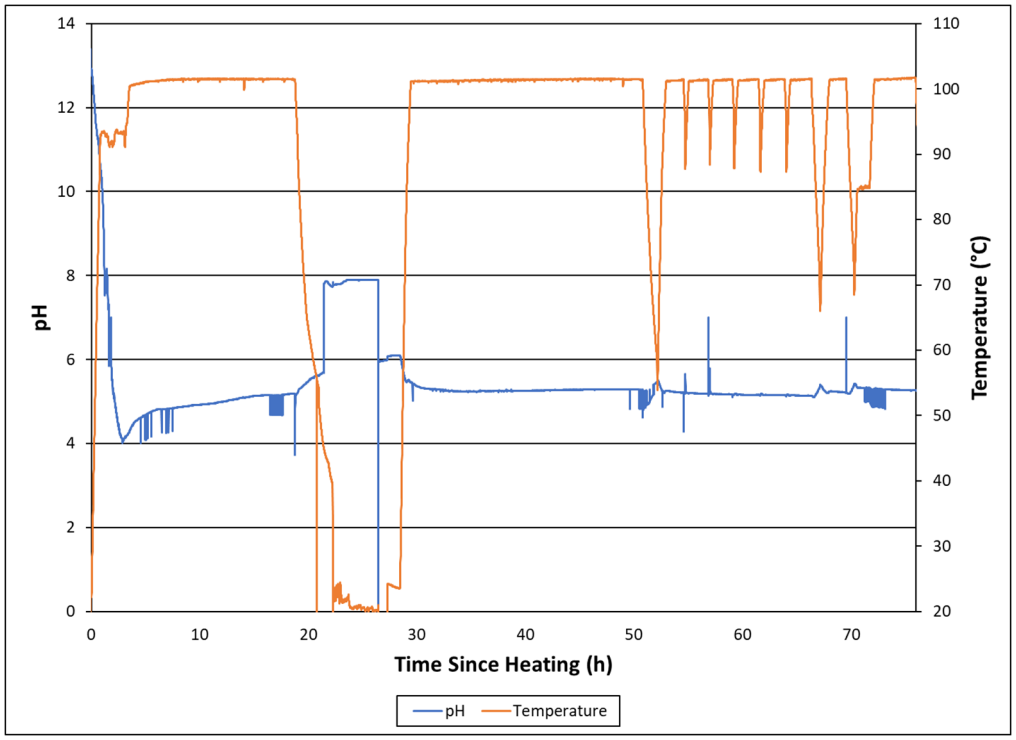

Figure B-13. Tk51-3 pH and Temperature Profiles.

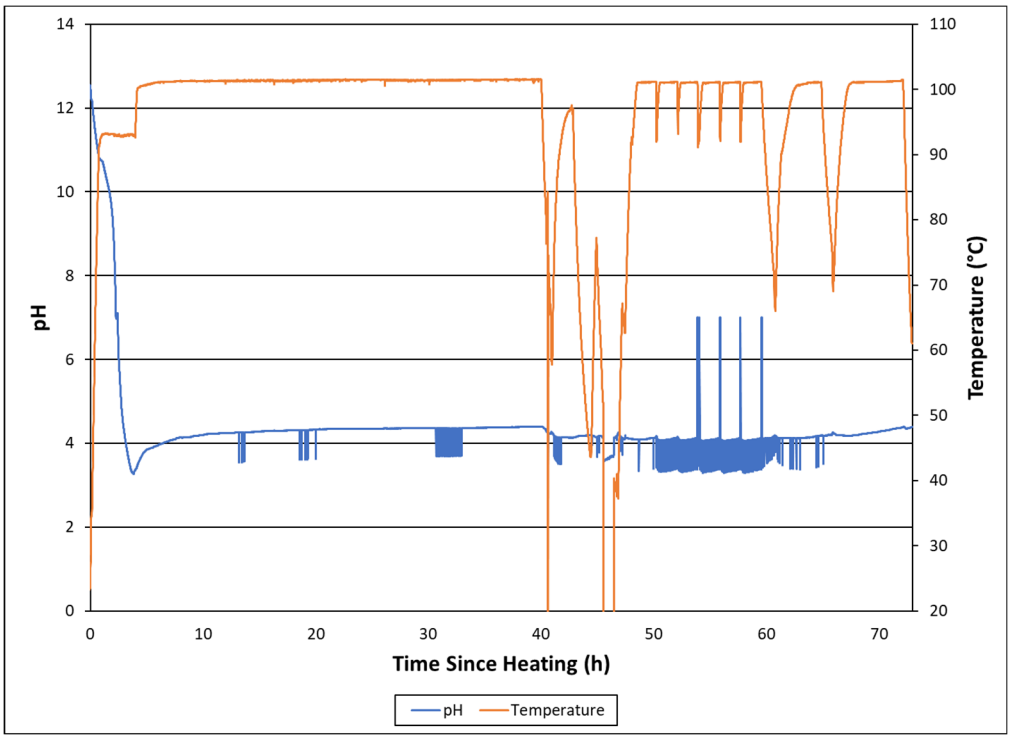

Figure B-14. Tk51-4 pH and Temperature Profiles.

Appendix C. Flow Diagrams from Rheological Measurements

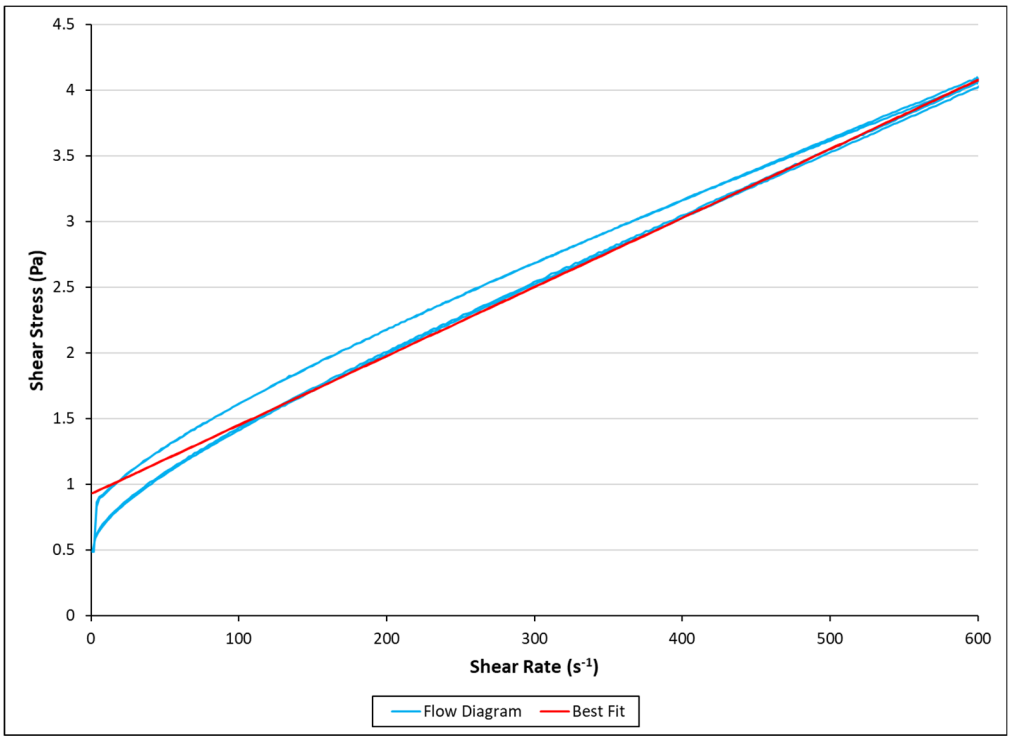

Figure C-1. Tk40 Receipt Flow Diagram and Bingham Plastic Fit.

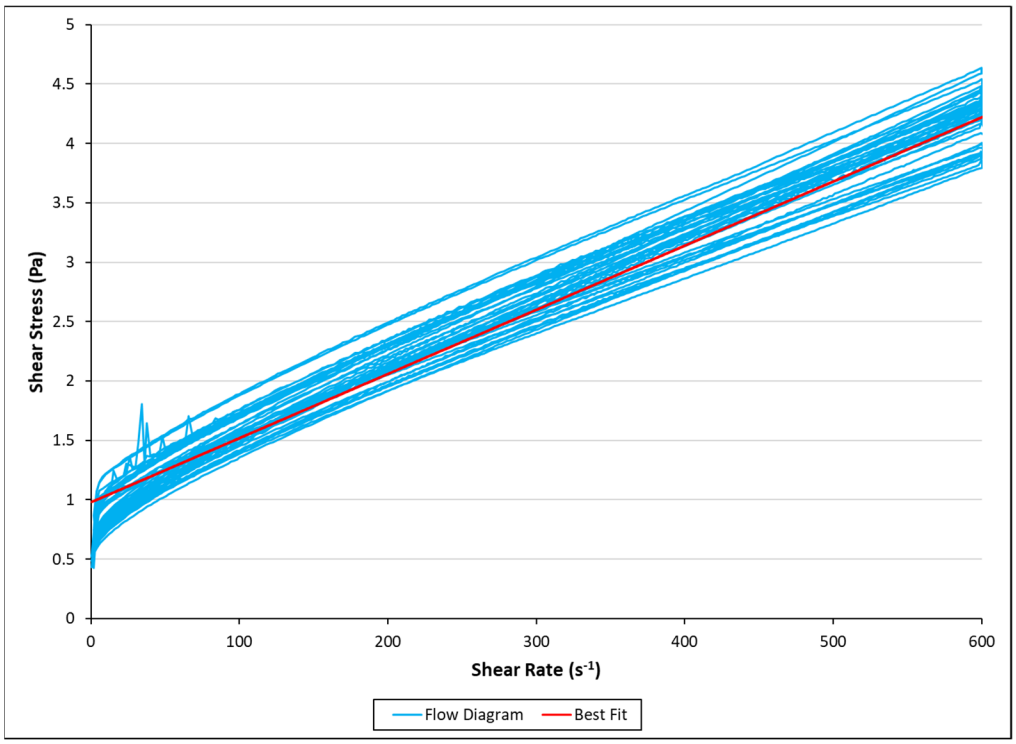

Figure C-2. Tk40 Receipt with Added MST Flow Diagrams and Bingham Plastic Fit. Measurements taken from Tk40-1 through Tk40-9.

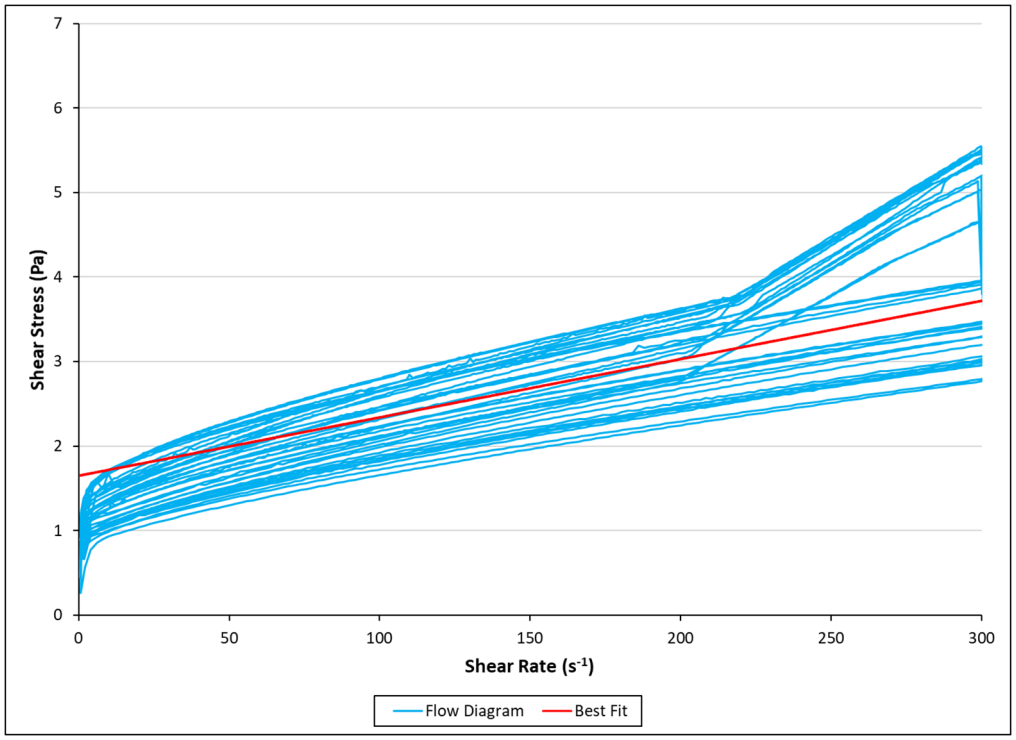

Figure C-3. Tk40 Post Caustic Boiling Flow Diagrams and Bingham Plastic Fit. Measurements taken from Tk40-1 through Tk40-9.

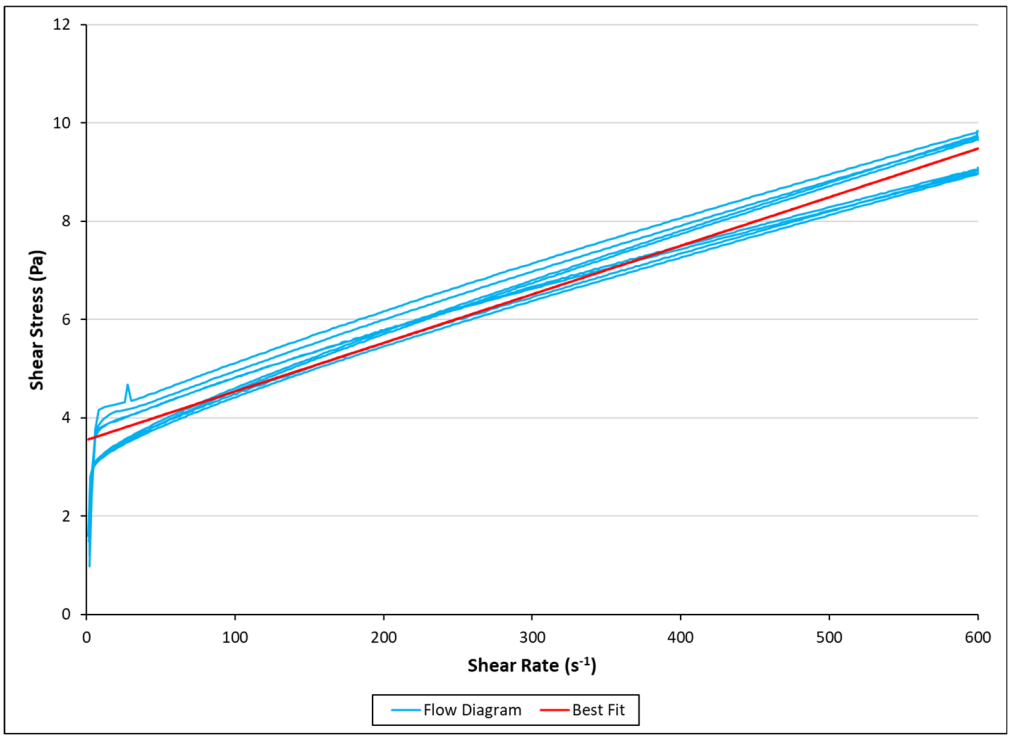

Figure C-4. Tk51 Receipt Flow Diagrams and Bingham Plastic Fit. Measurements taken from Tk51-2 and Tk51-4.

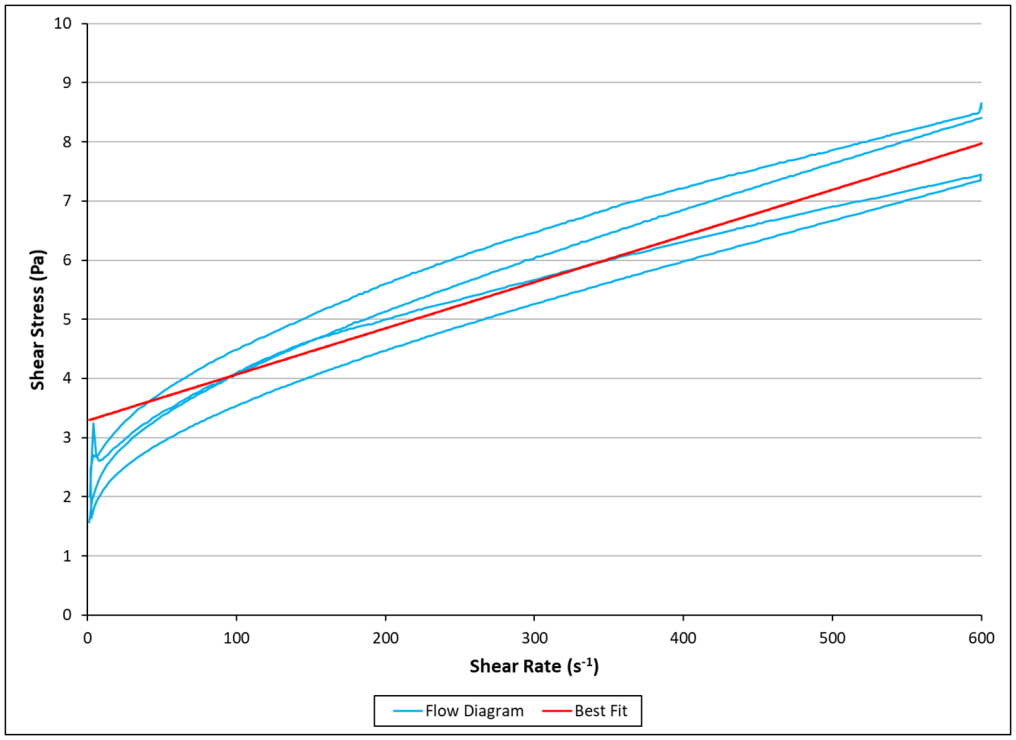

Figure C-5. Tk40-1 SRAT Product Flow Diagram and Bingham Plastic Fit.

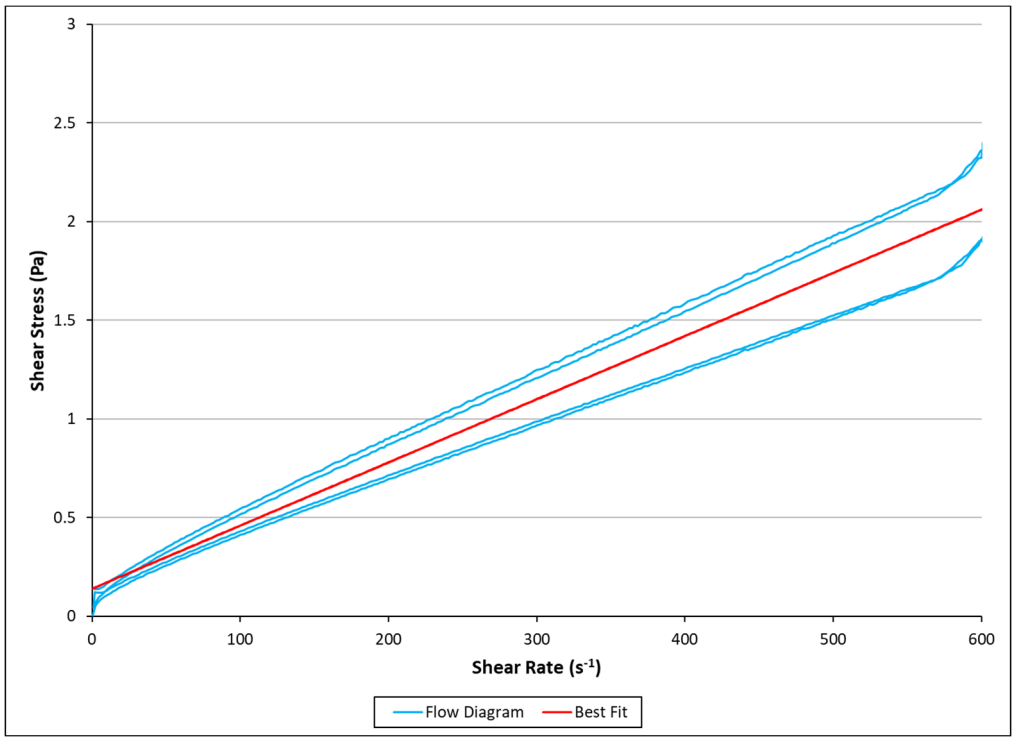

Figure C-6. Tk40-2 SRAT Product Flow Diagram and Bingham Plastic Fit.

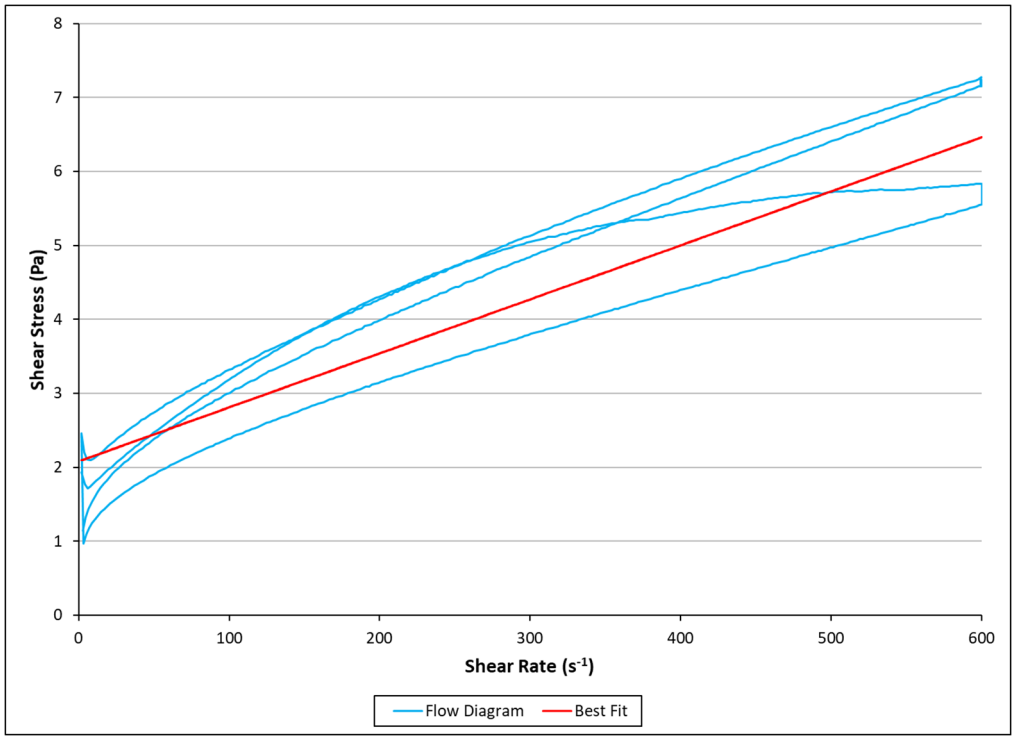

Figure C-7. Tk40-3 SRAT Product Flow Diagram and Bingham Plastic Fit.

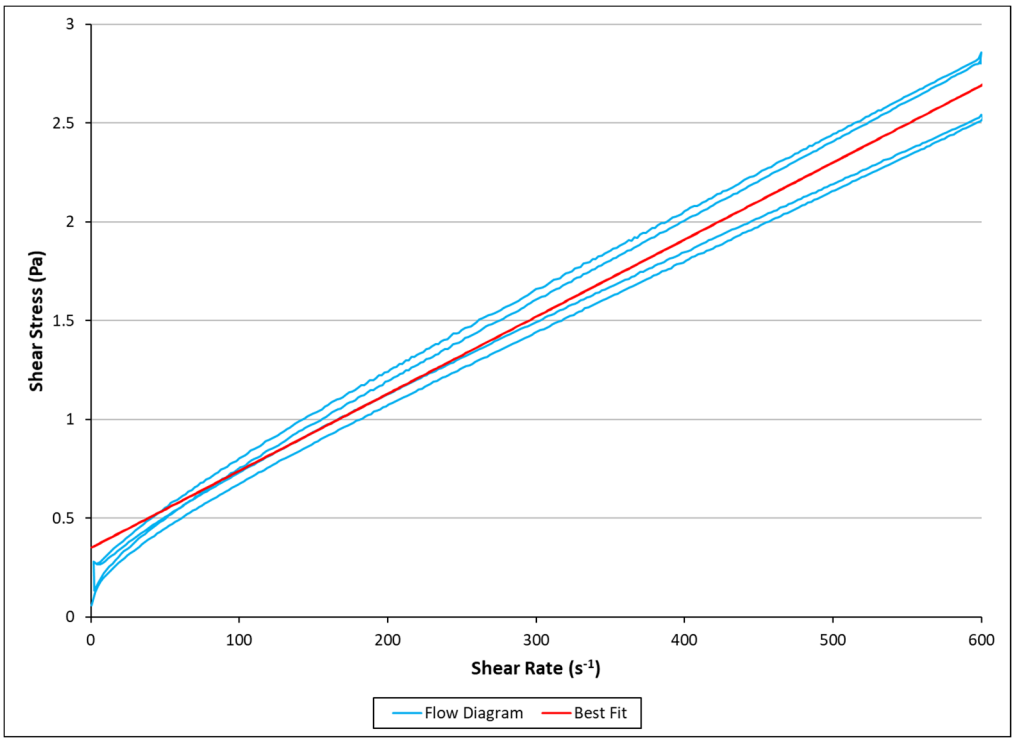

Figure C-8. Tk40-4 SRAT Product Flow Diagram and Bingham Plastic Fit.

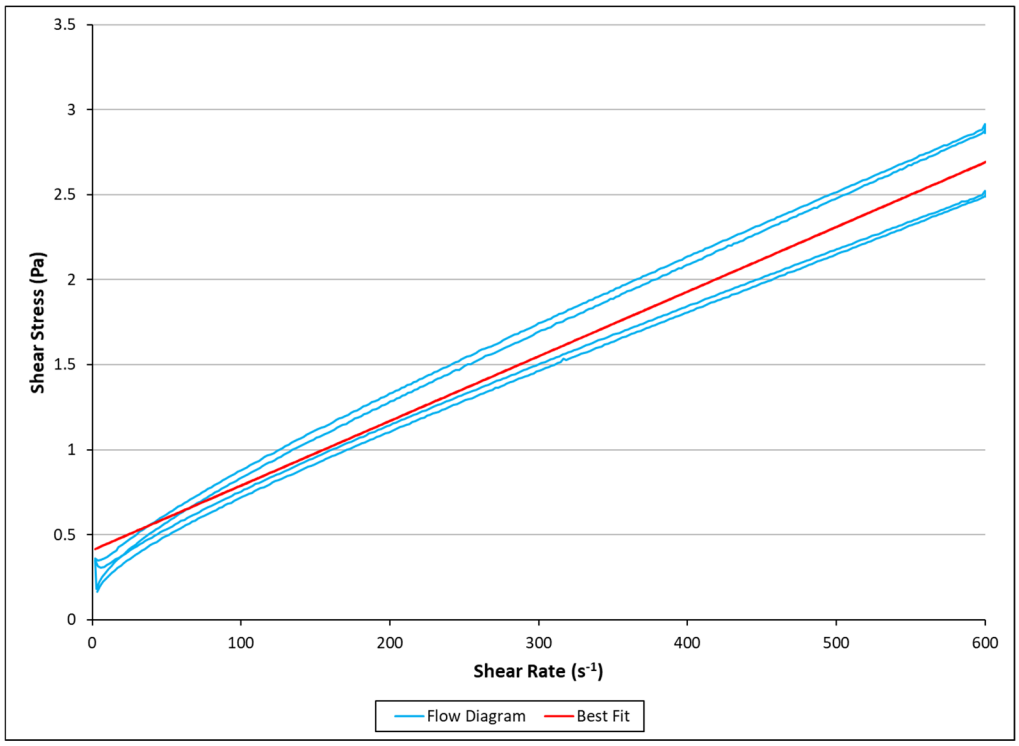

Figure C-9. Tk40-5 SRAT Product Flow Diagram and Bingham Plastic Fit.

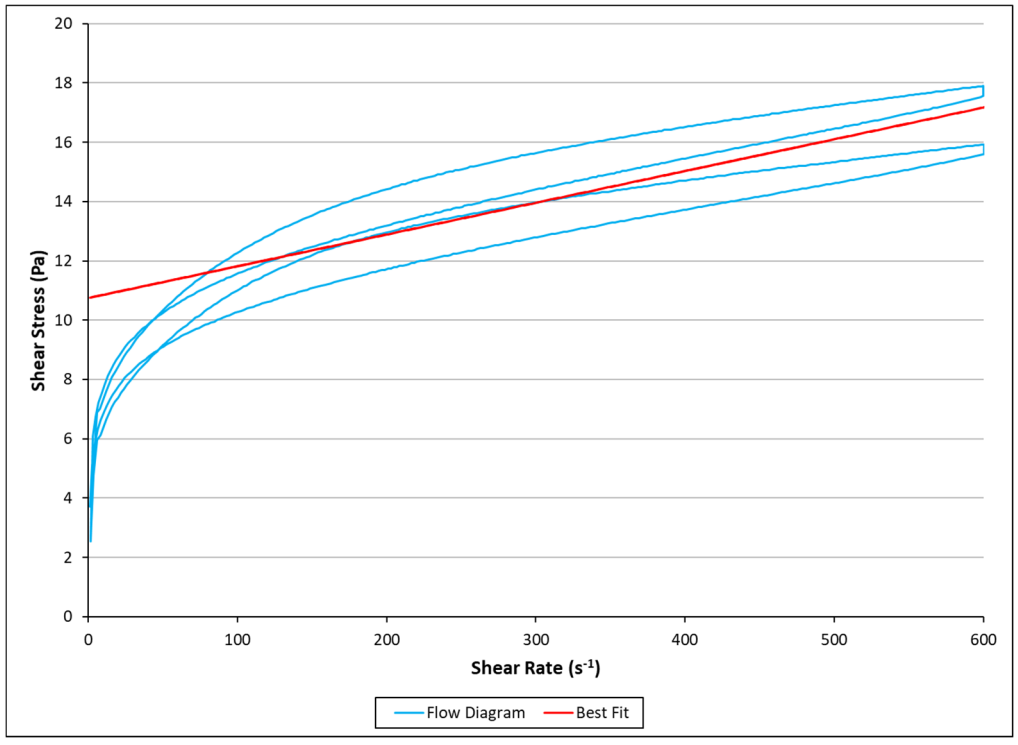

Figure C-10. Tk40-6 SRAT Product Flow Diagram and Bingham Plastic Fit.

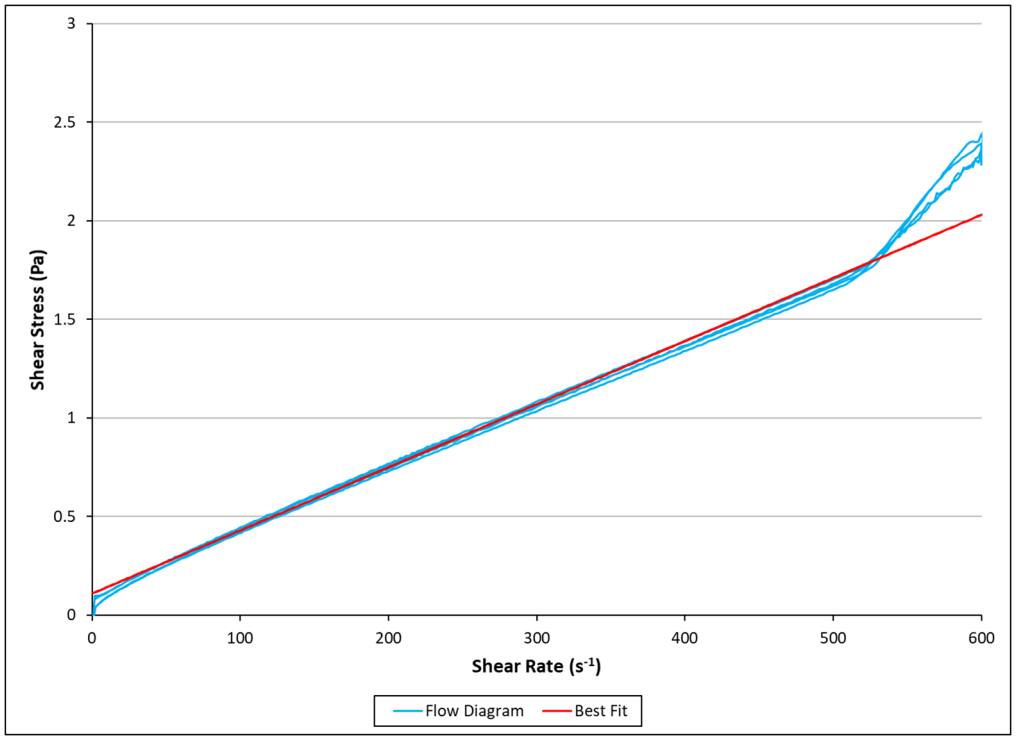

Figure C-11. Tk40-7 SRAT Product Flow Diagram and Bingham Plastic Fit.

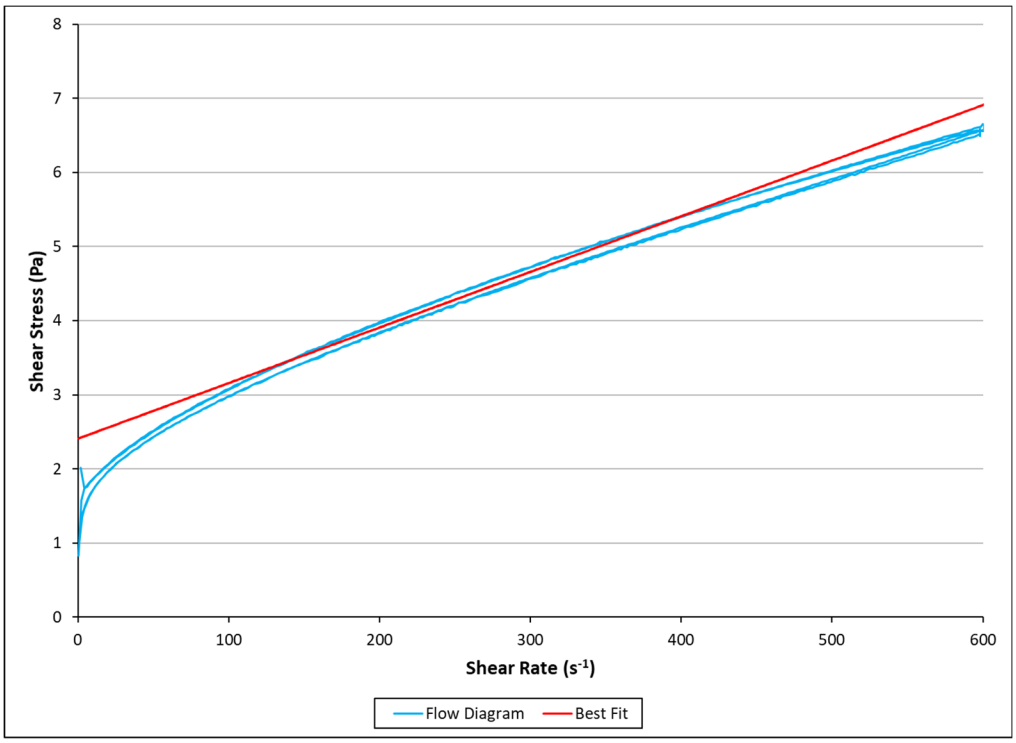

Figure C-12. Tk40-8 SRAT Product Flow Diagram and Bingham Plastic Fit.

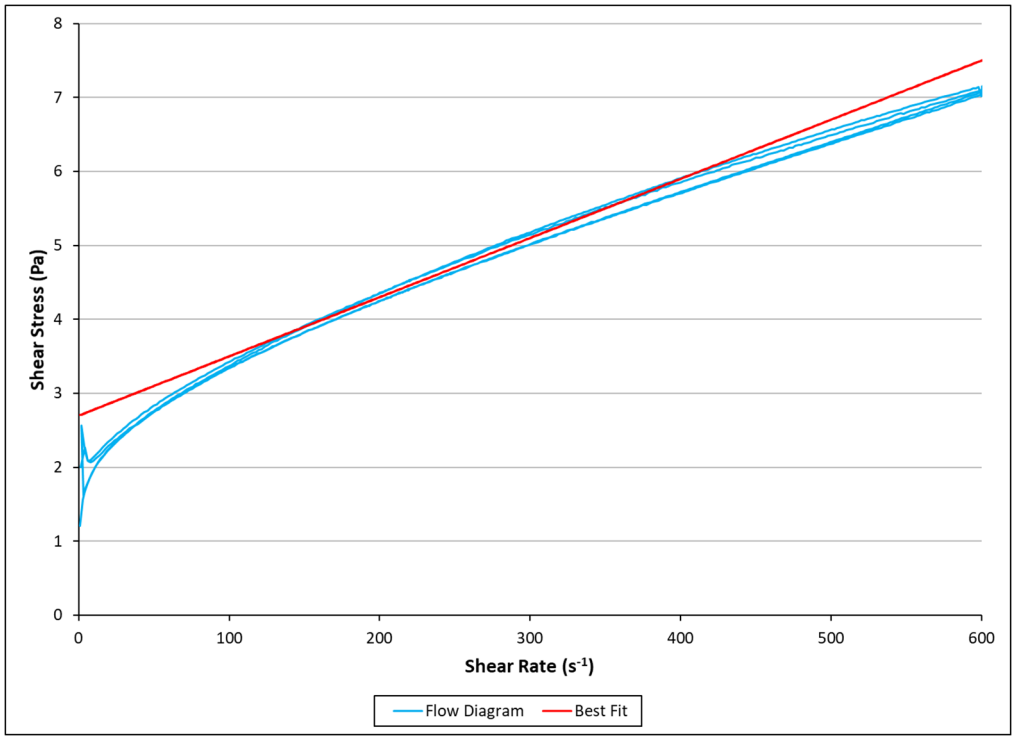

Figure C-13. Tk40-9 SRAT Product Flow Diagram and Bingham Plastic Fit.

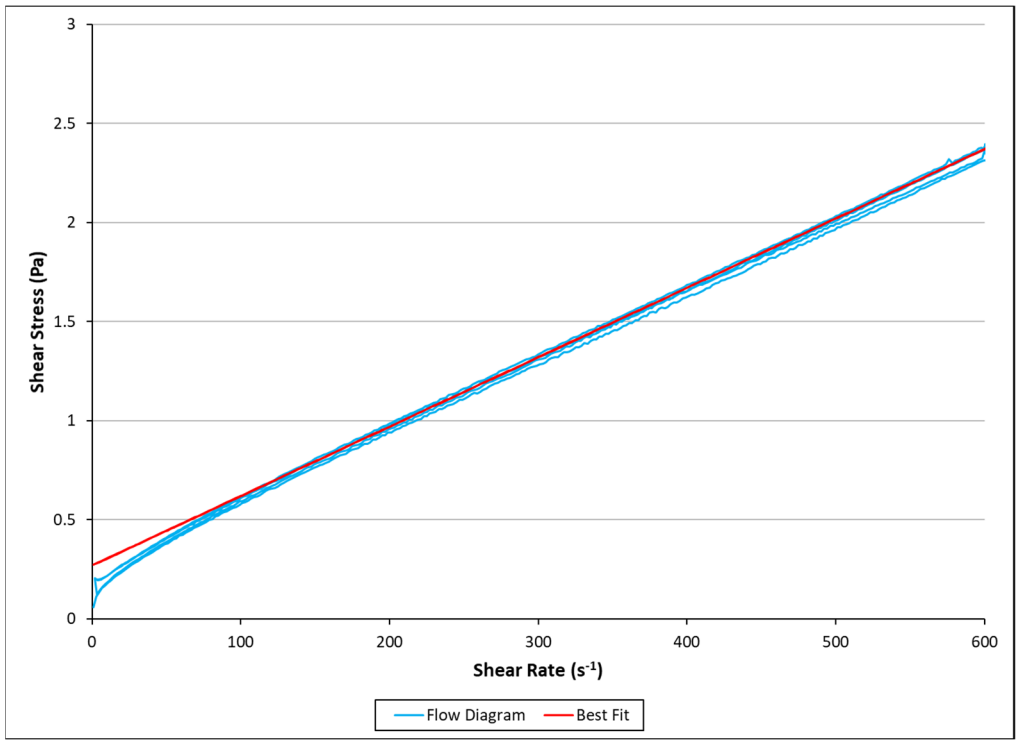

Figure C-14. Tk40-10 SRAT Product Flow Diagram and Bingham Plastic Fit.

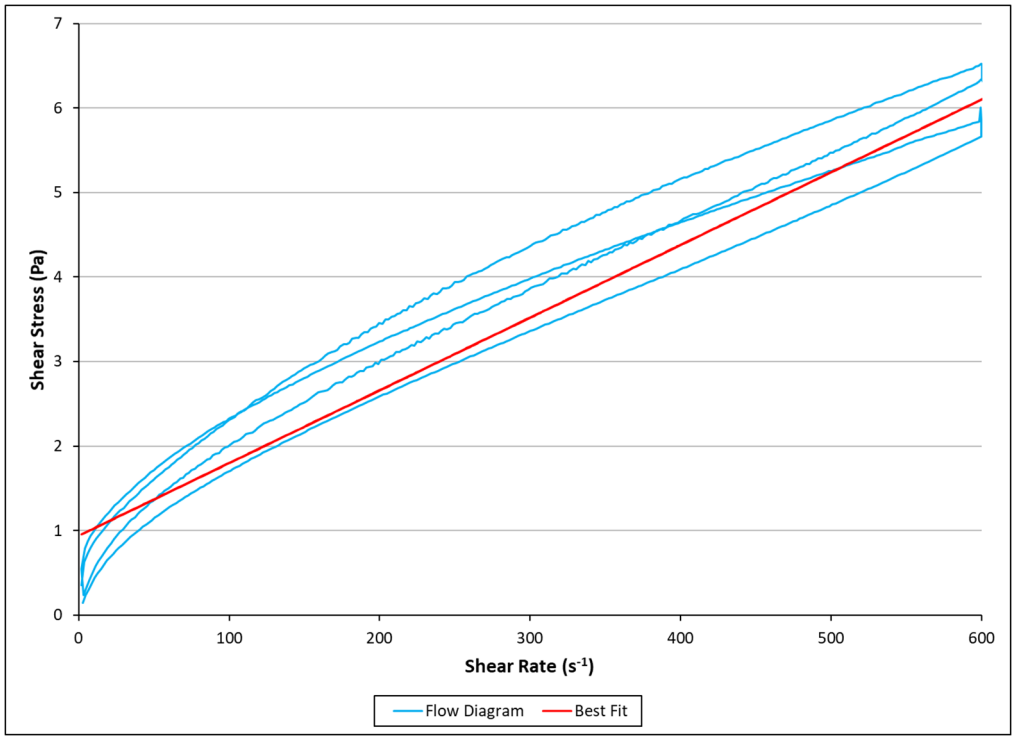

Figure C-15. Tk51-2 SRAT Product Flow Diagram and Bingham Plastic Fit.

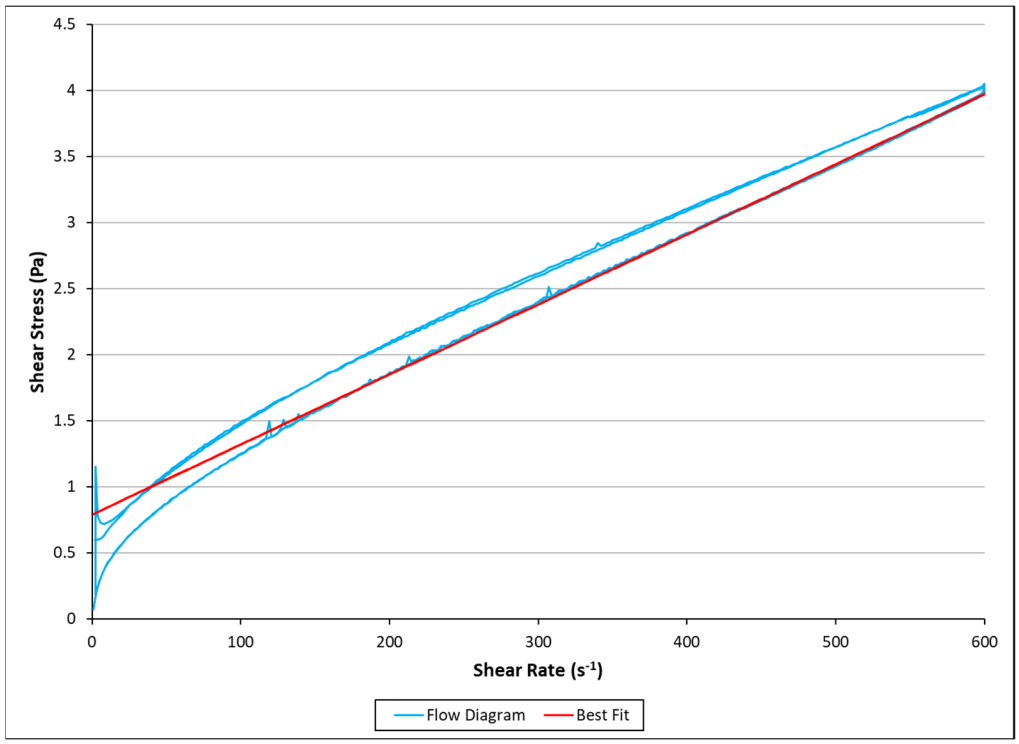

Figure C-16. Tk51-3 SRAT Product Flow Diagram and Bingham Plastic Fit.

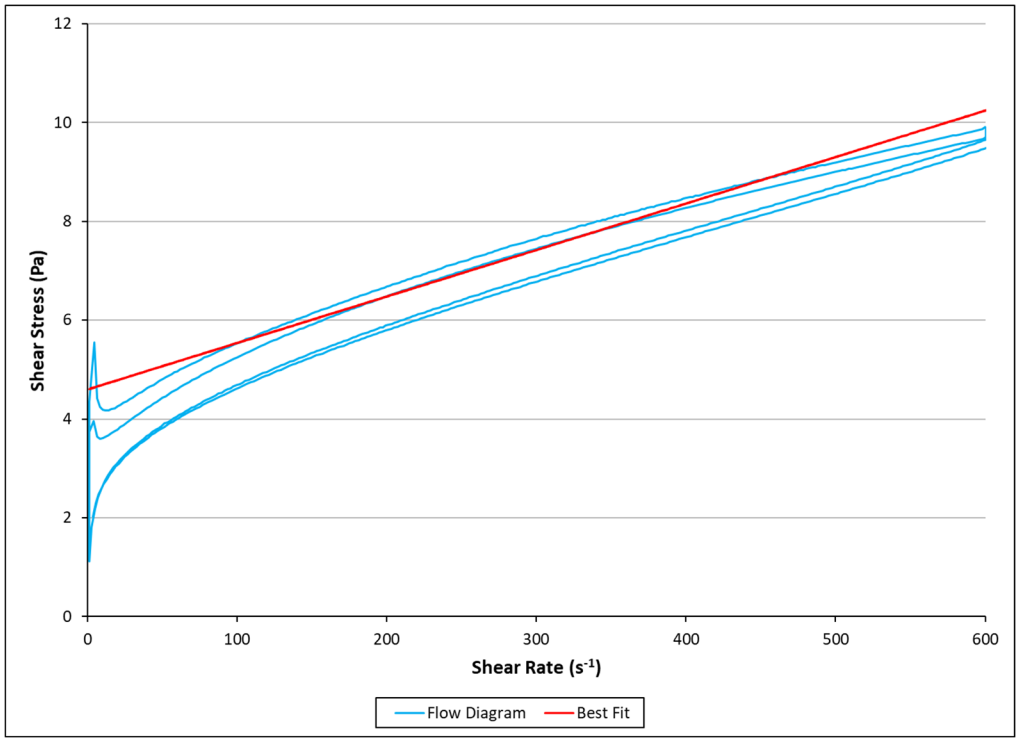

Figure C-17. Tk51-4 SRAT Product Flow Diagram and Bingham Plastic Fit.

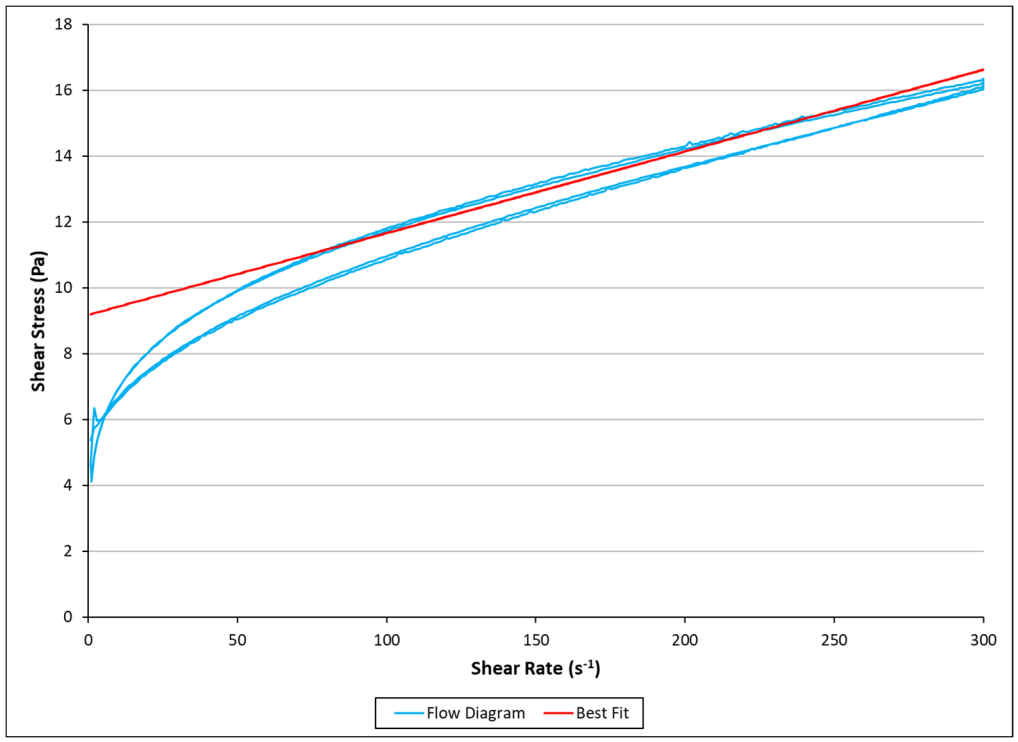

Figure C-18. Tk40-8 SME Product Flow Diagram and Bingham Plastic Fit.

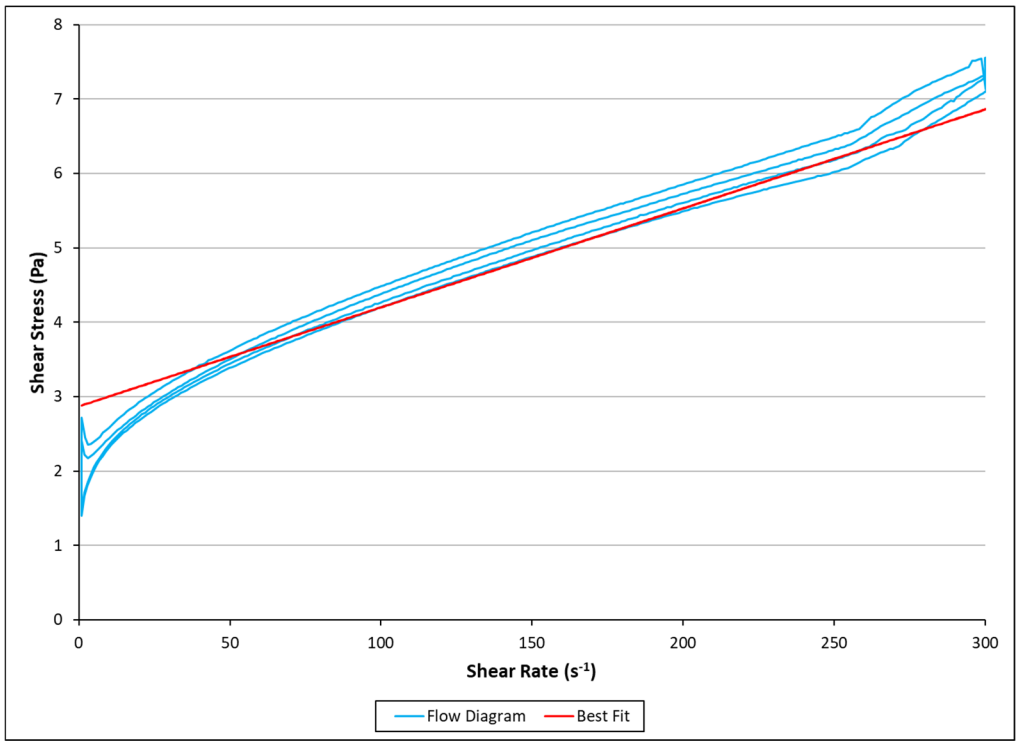

Figure C-19. Tk40-9 SME Product Flow Diagram and Bingham Plastic Fit.

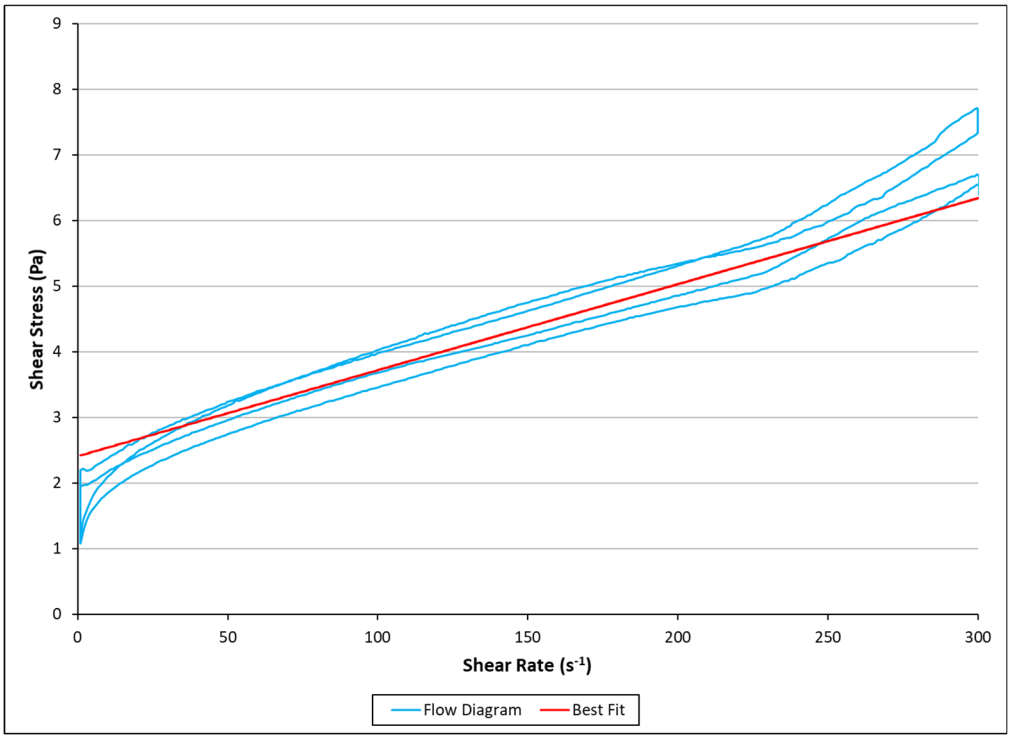

Figure C-20. Tk40-10 SME Product Flow Diagram and Bingham Plastic Fit.

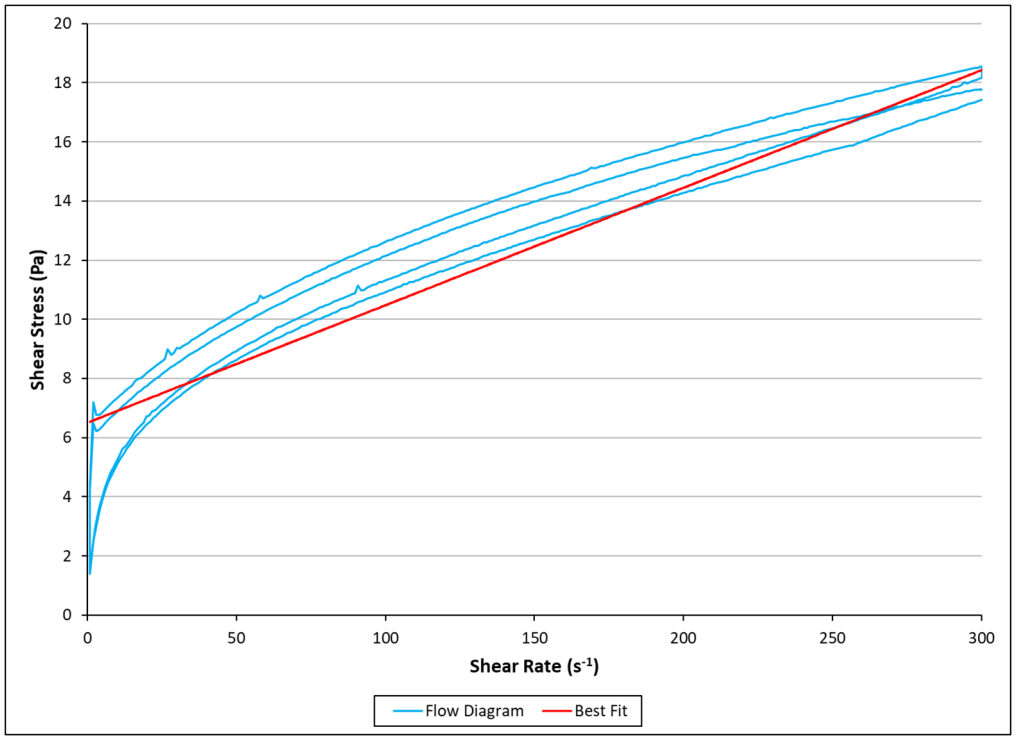

Figure C-21. Tk51-2 SME Product Flow Diagram and Bingham Plastic Fit.

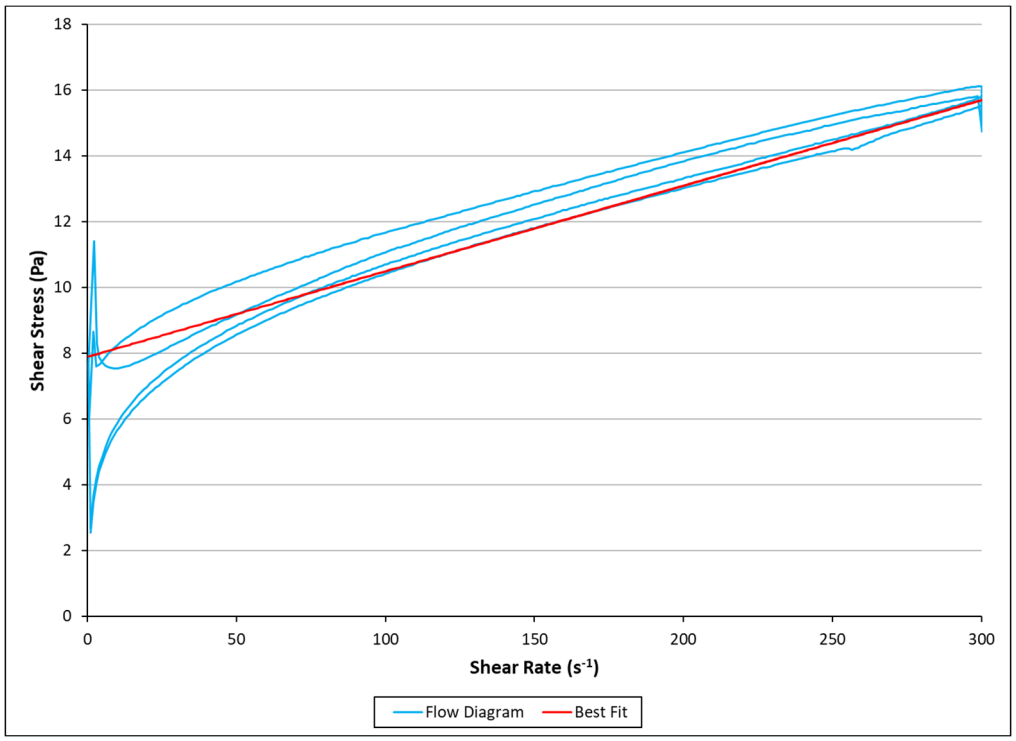

Figure C-22. Tk51-3 SME Product Flow Diagram and Bingham Plastic Fit.

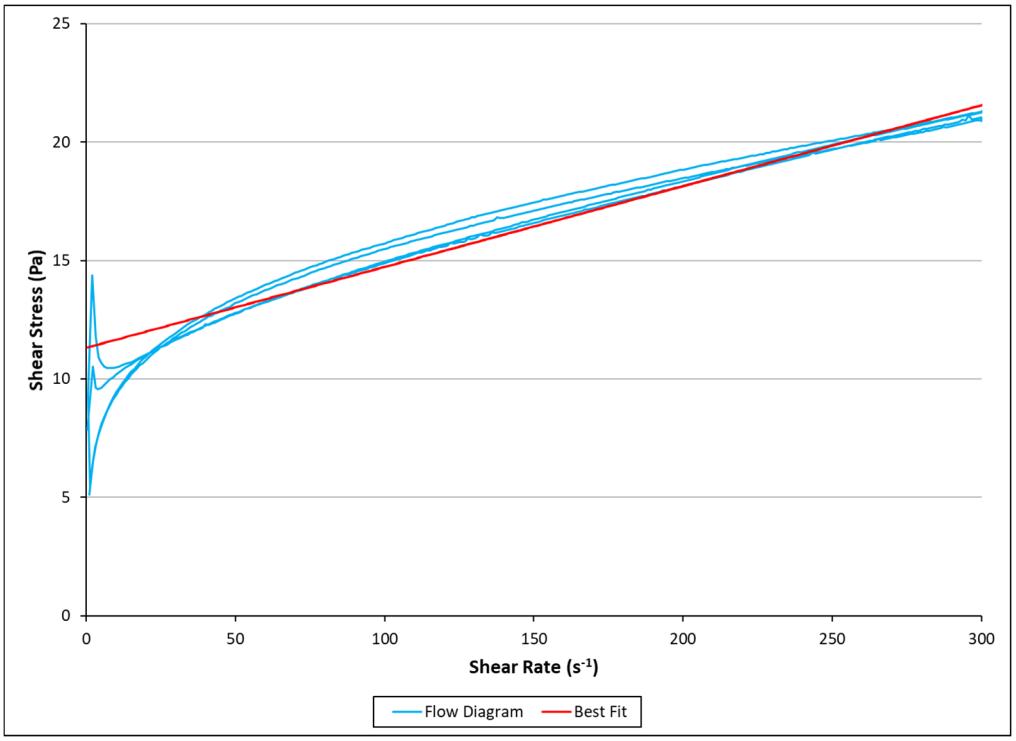

Figure C-23. Tk51-4 SME Product Flow Diagram and Bingham Plastic Fit.

Appendix D. Off-gas Profiles from SB 10 Simulant Experiments

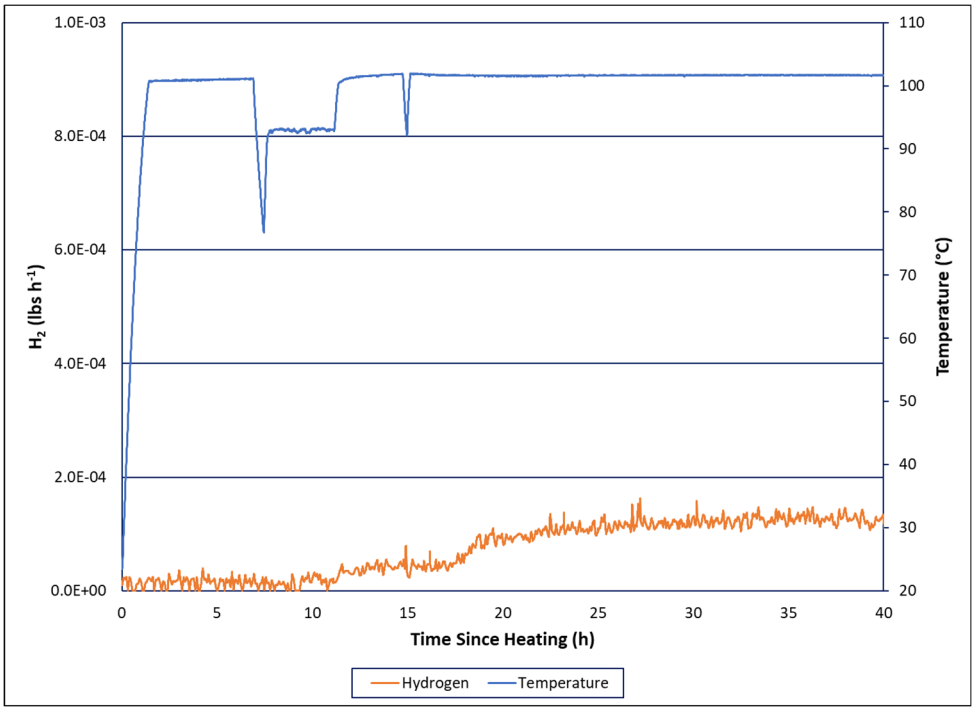

Figure D-1. Tk40-1 Hydrogen Generation Profile (lb/hr). Slurry temperature is given in blue.

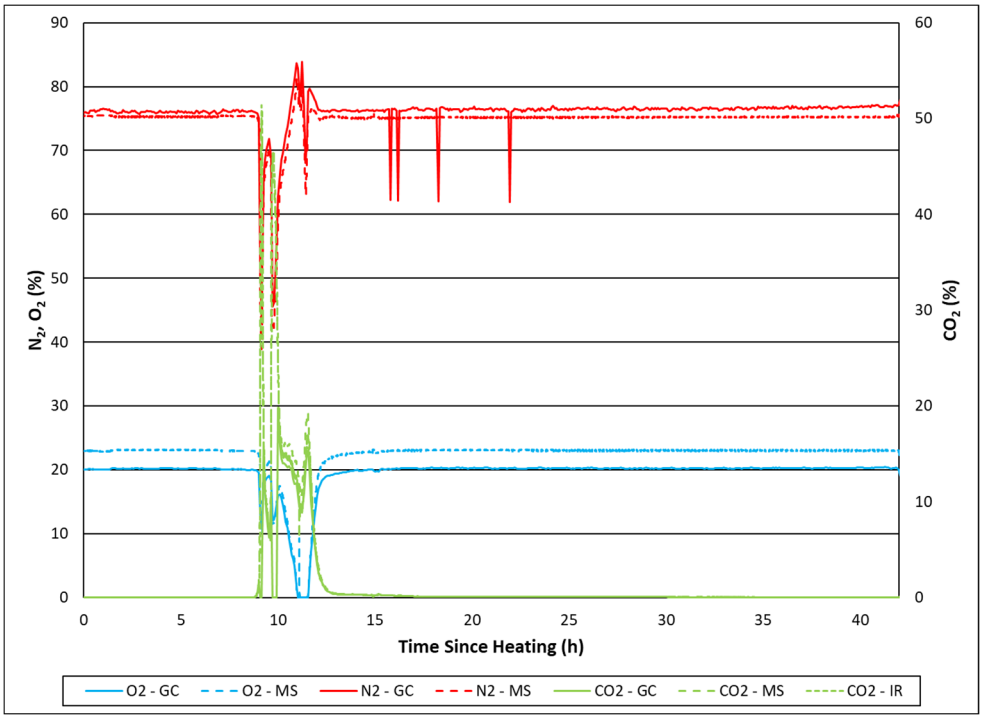

Figure D-2. Tk40-1 N_2 (red), O_2 (blue), and CO_2 (green) profiles (%).

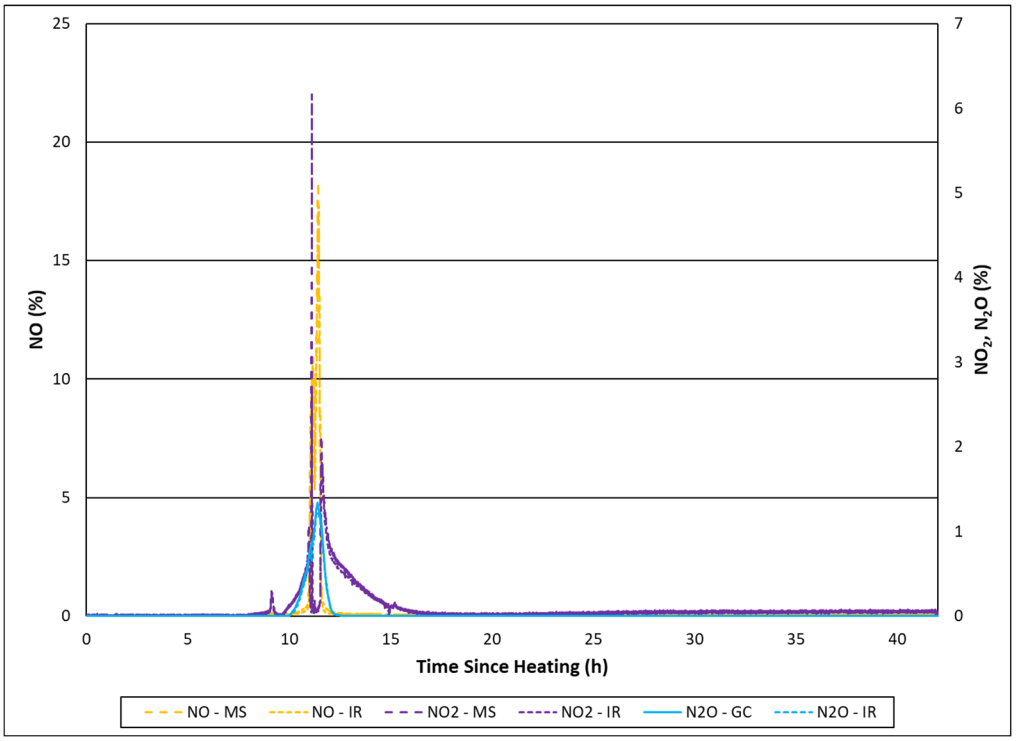

Figure D-3. Tk40-1 NO (orange), NO_2 (purple), and N_2O (blue) profiles (%).

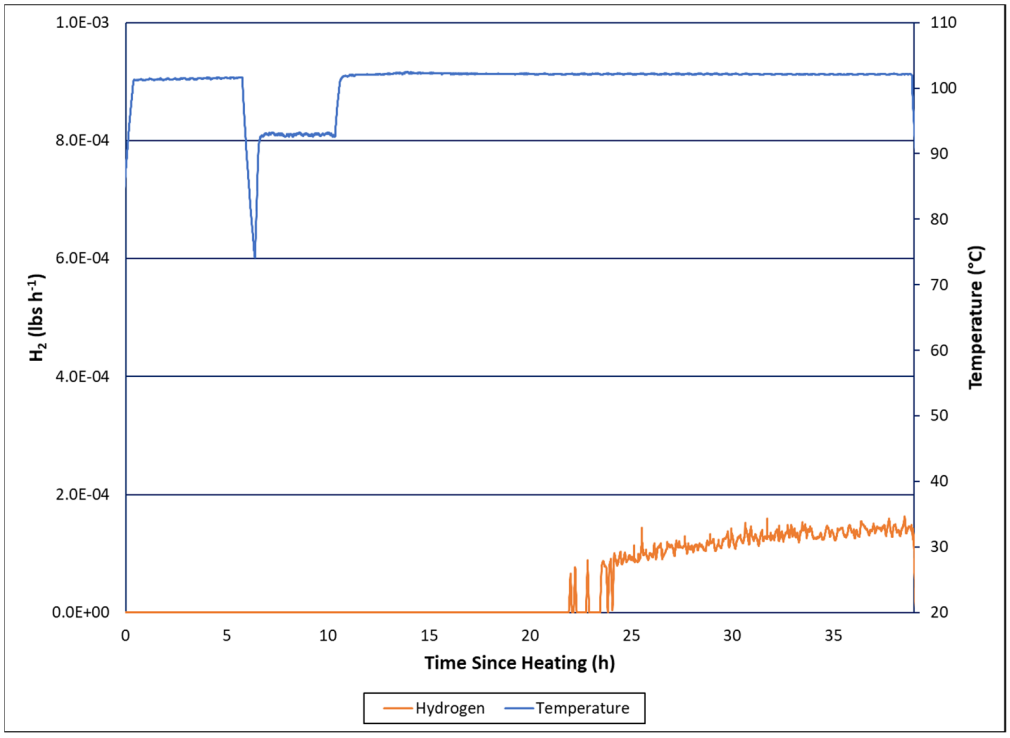

Figure D-4. Tk40-2 Hydrogen Generation Profile (lb/hr). Slurry temperature is given in blue.

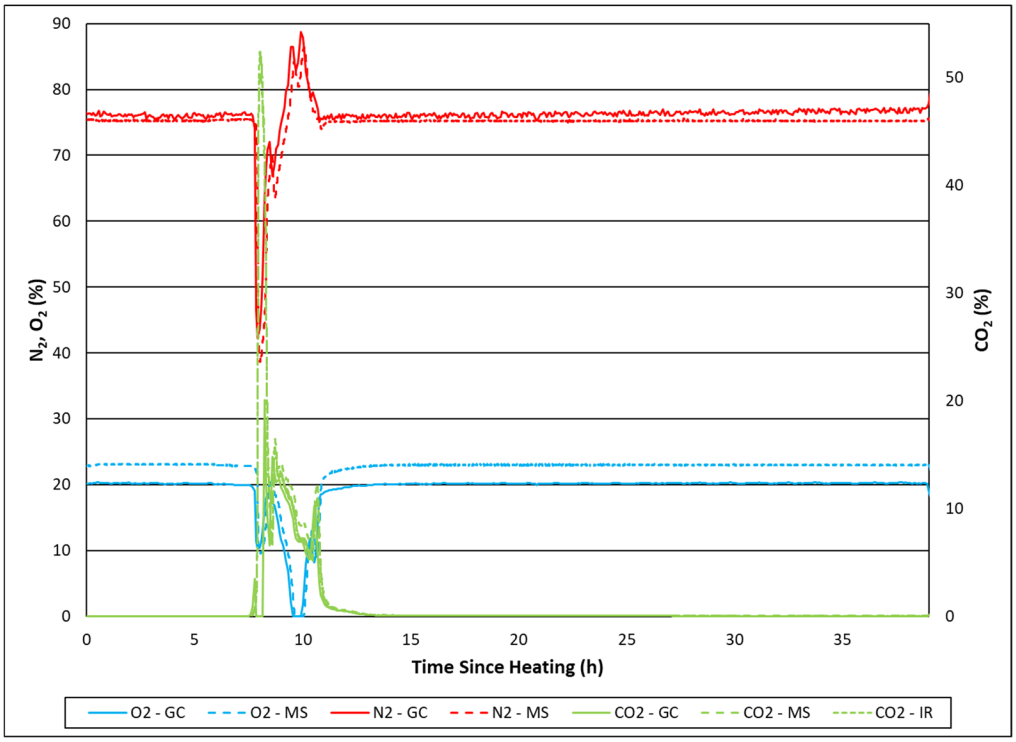

Figure D-5. Tk40-2 N_2 (red), O_2 (blue), and CO_2 (green) profiles (%).

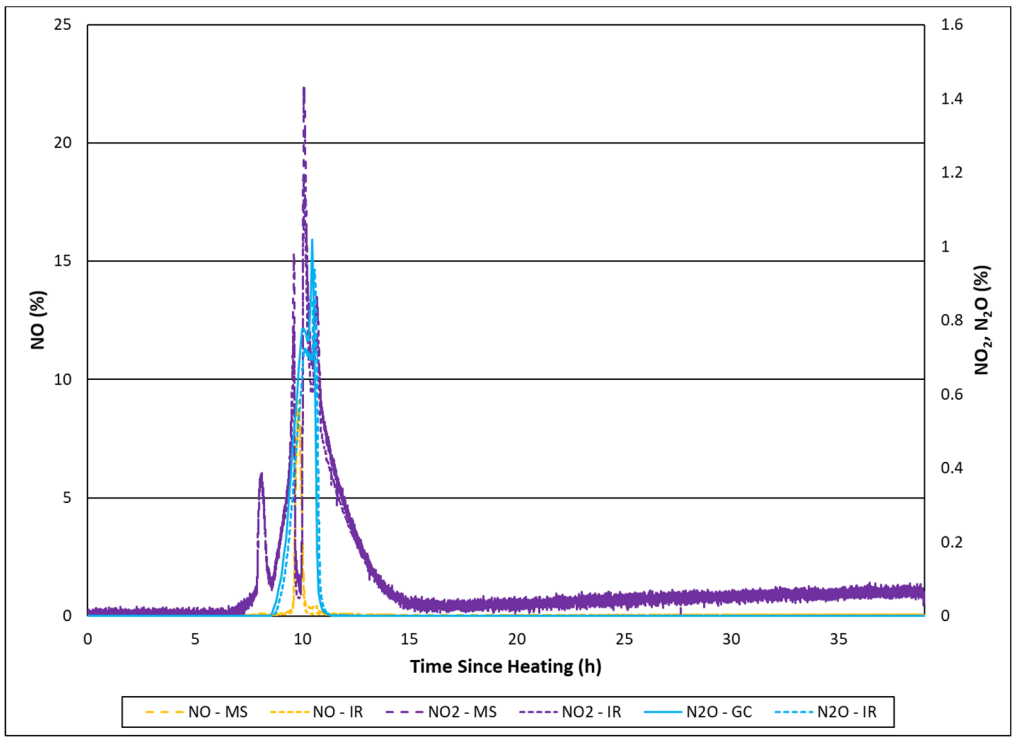

Figure D-6. Tk40-2 NO (orange), NO_2 (purple), and N_2O (blue) profiles (%).

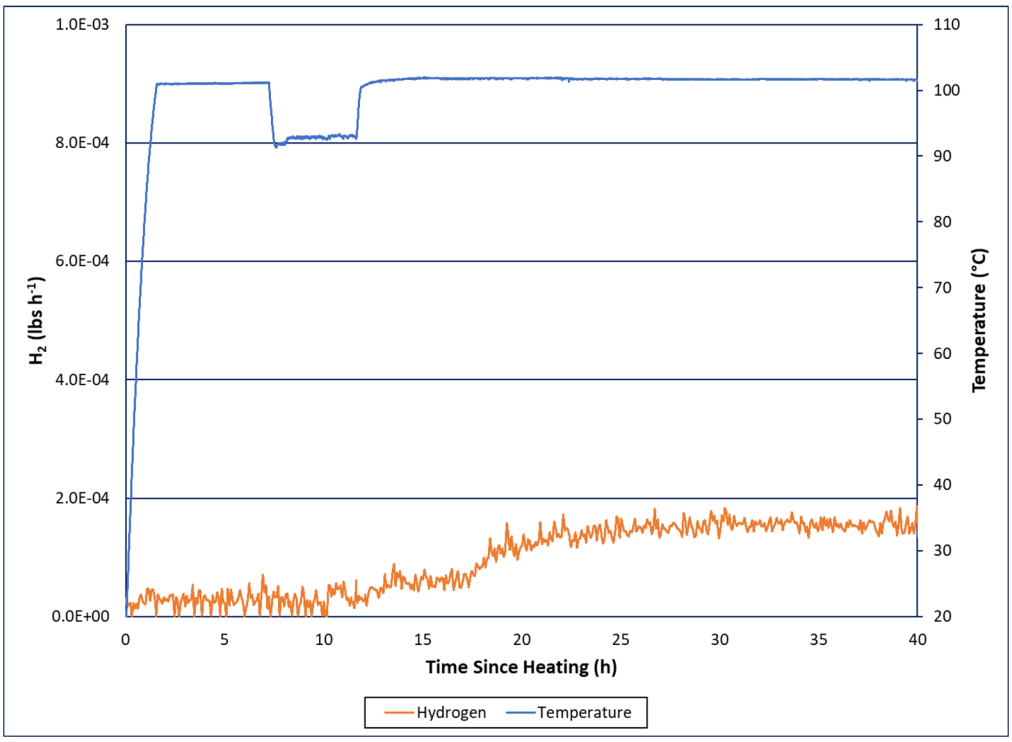

Figure D-7. Tk40-3 Hydrogen Generation Profile (lb/hr). Slurry temperature is given in blue.

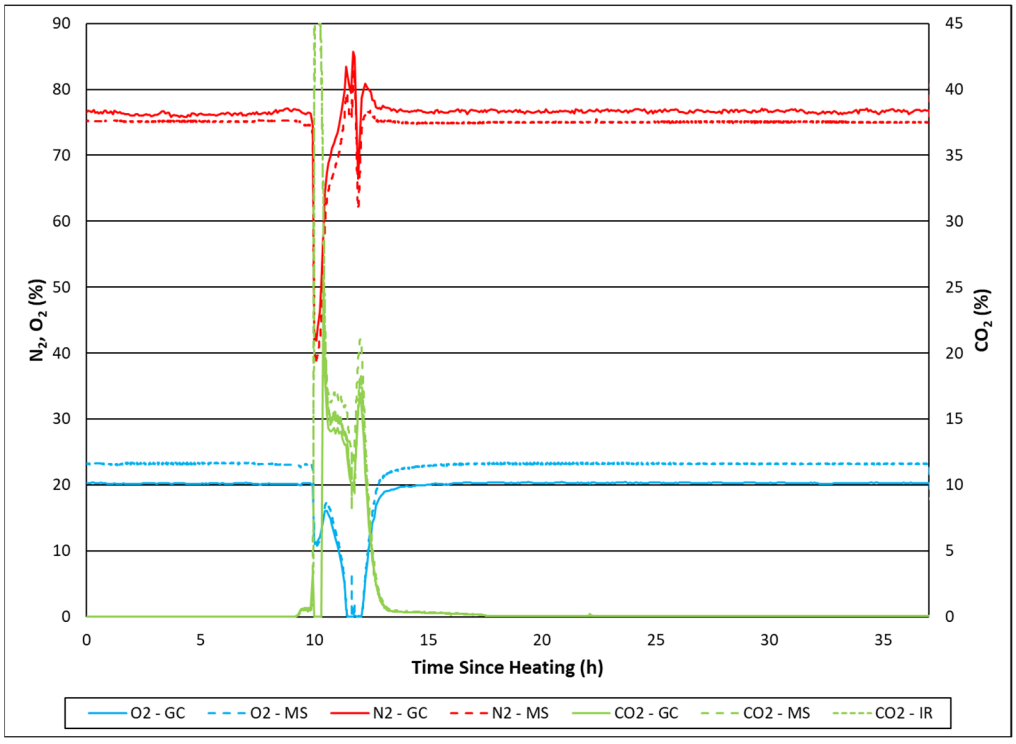

Figure D-8. Tk40-3 N_2 (red), O_2 (blue), and CO_2 (green) profiles (%).

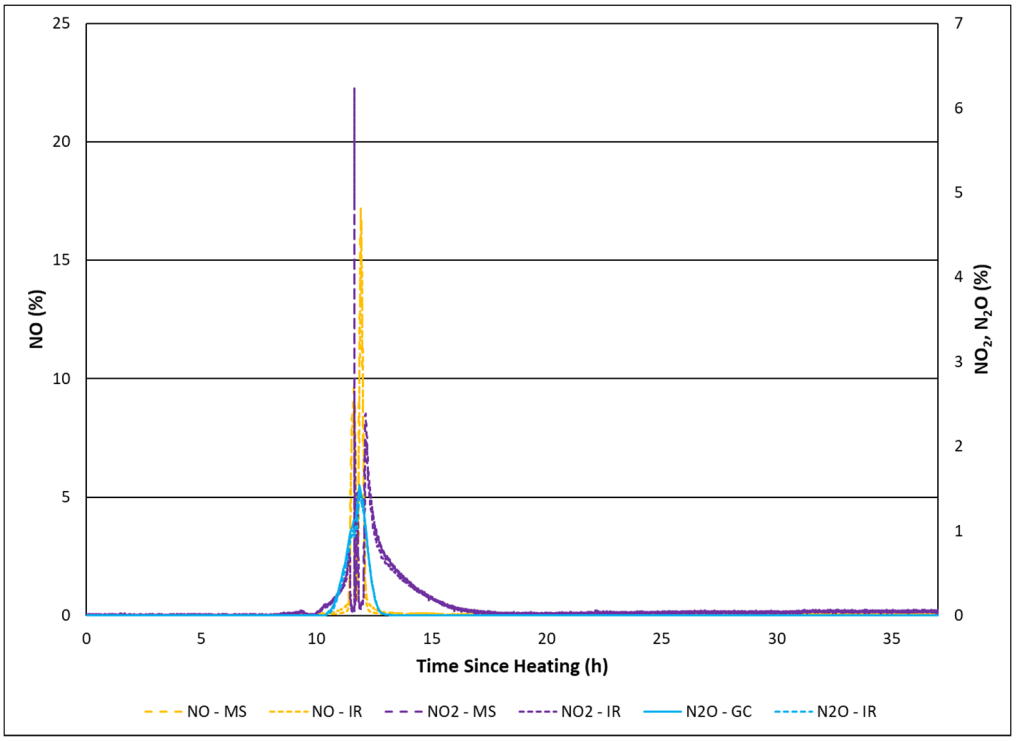

Figure D-9. Tk40-3 NO (orange), NO_2 (purple), and N_2O (blue) profiles (%).

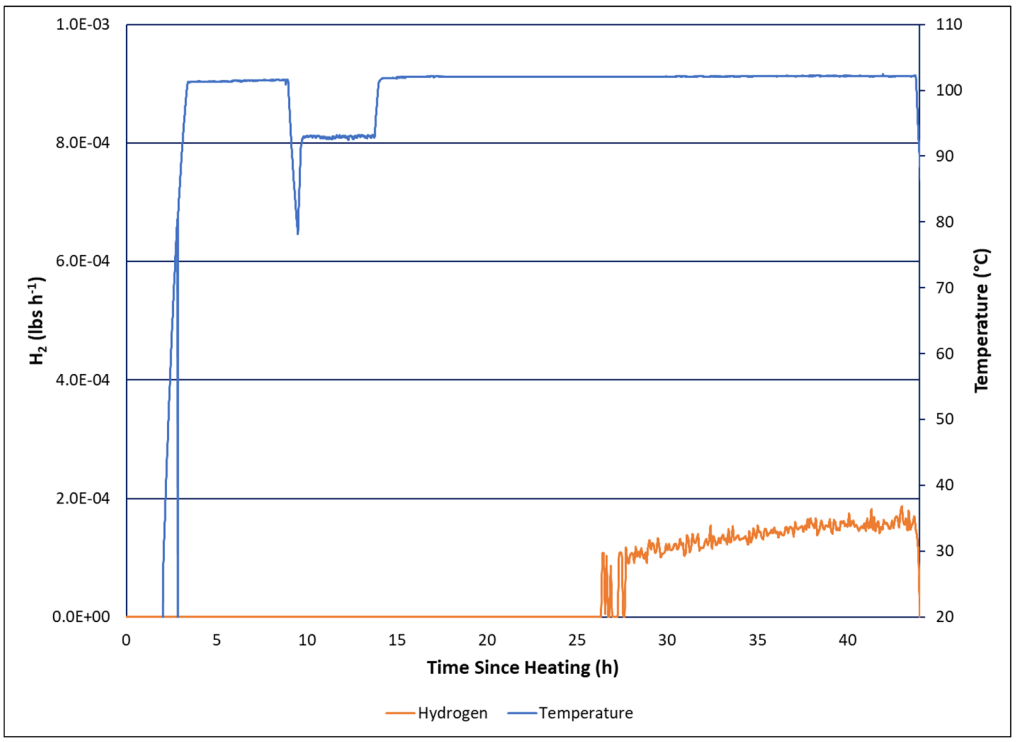

Figure D-10. Tk40-4 Hydrogen Generation Profile (lb/hr). Slurry temperature is given in blue.

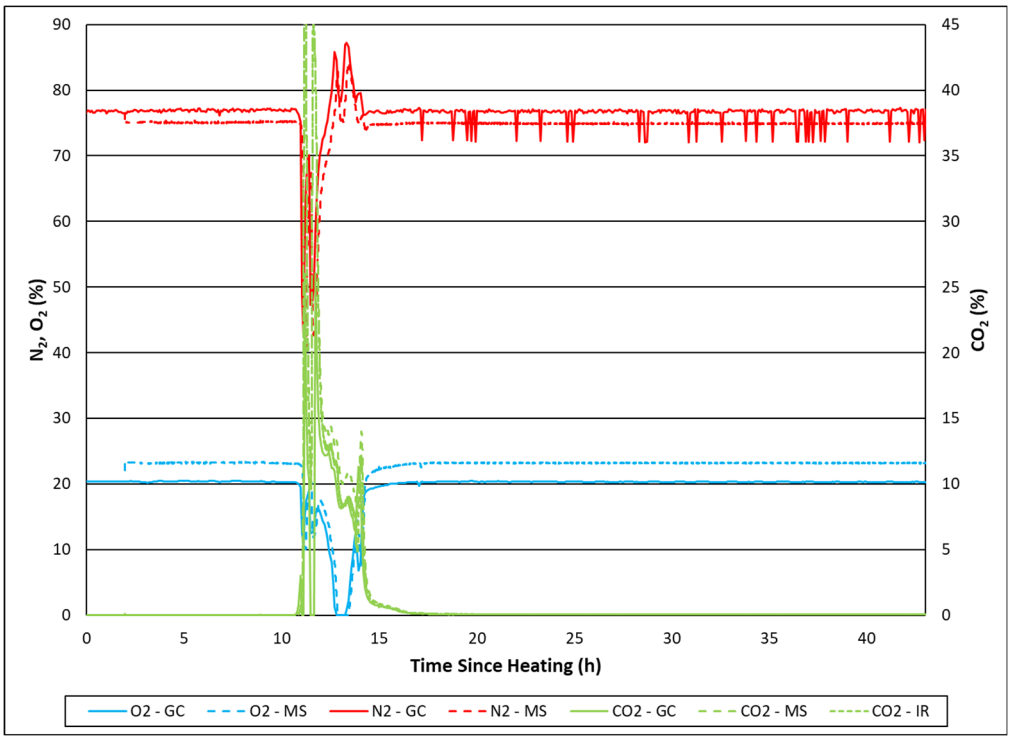

Figure D-11. Tk40-4 N_2 (red), O_2 (blue), and CO_2 (green) profiles (%).

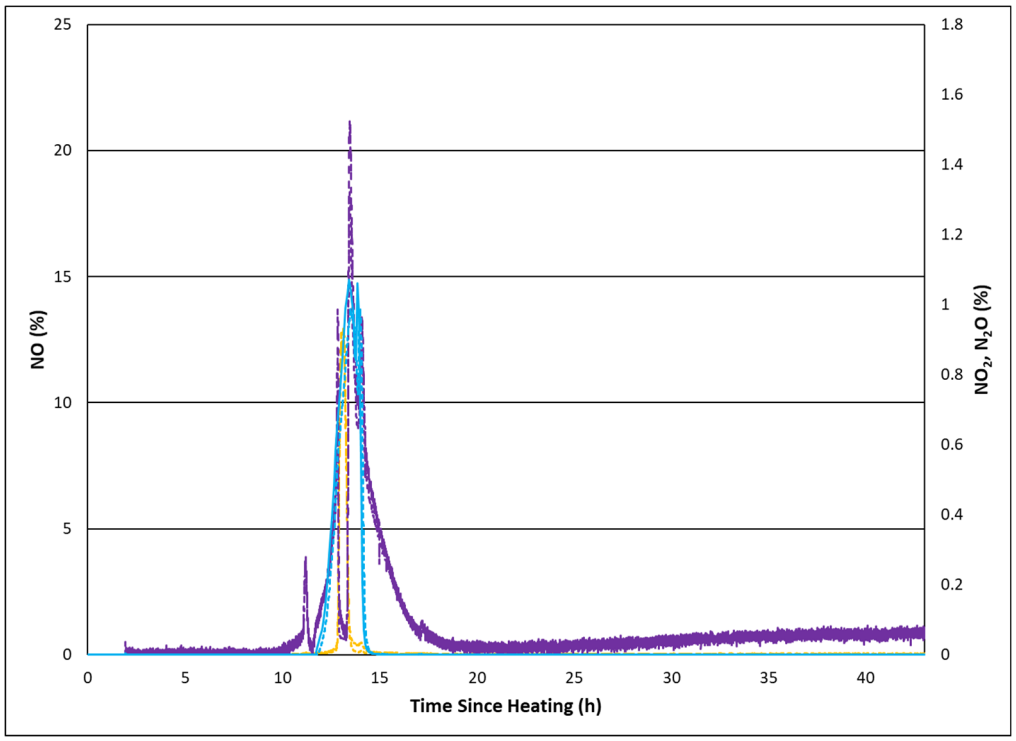

Figure D-12. Tk40-4 NO (orange), NO_2 (purple), and N_2O (blue) profiles (%).

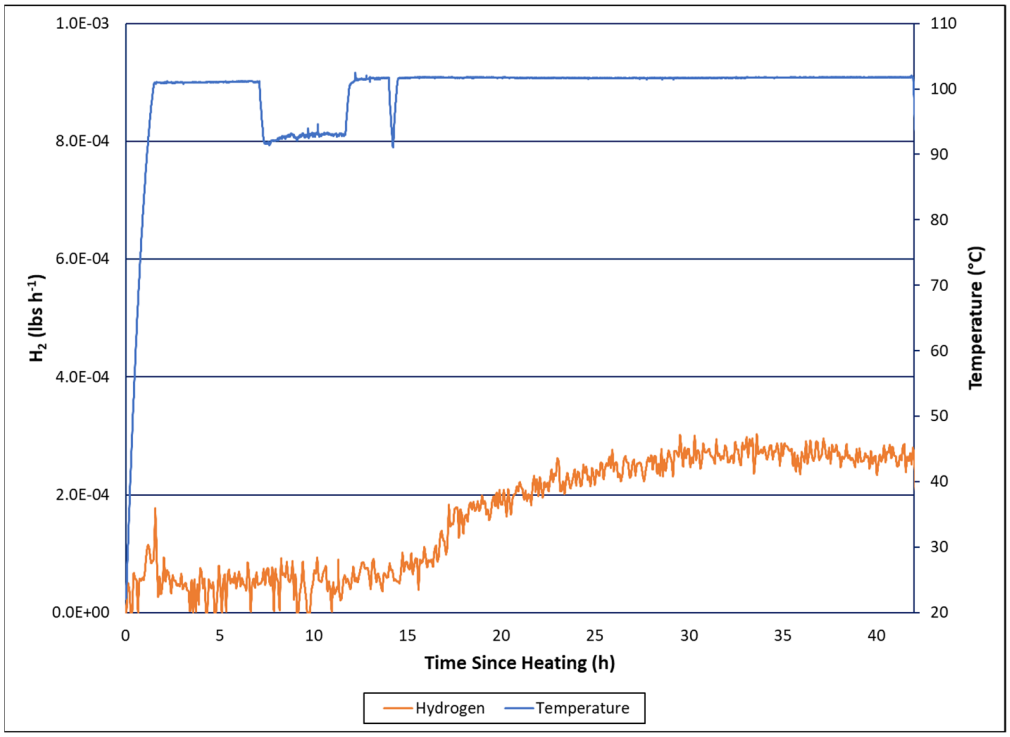

Figure D-13. Tk40-5 Hydrogen Generation Profile (lb/hr). Slurry temperature is given in blue.

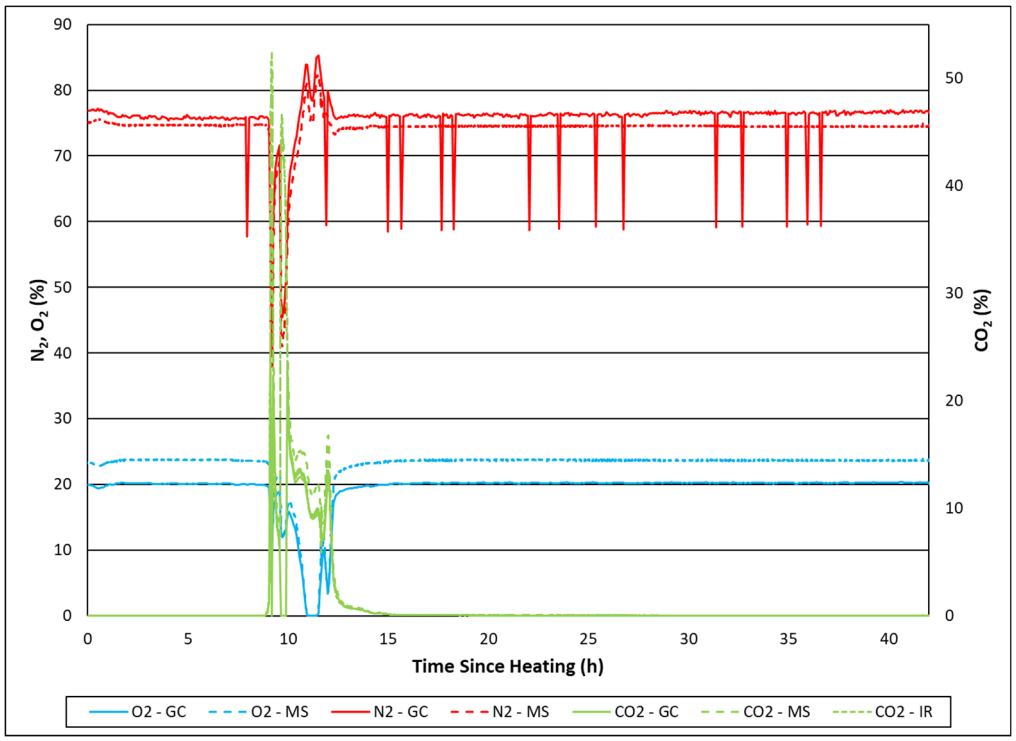

Figure D-14. Tk40-5 N_2 (red), O_2 (blue), and CO_2 (green) profiles (%).

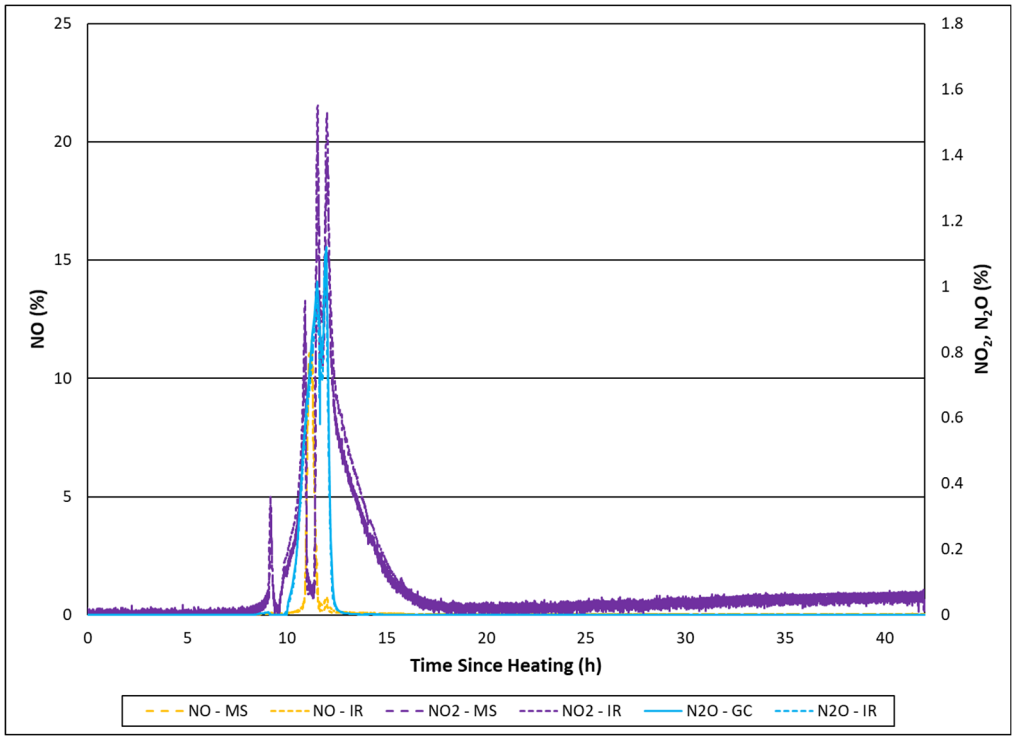

Figure D-15. Tk40-5 NO (orange), NO_2 (purple), and N_2O (blue) profiles (%).

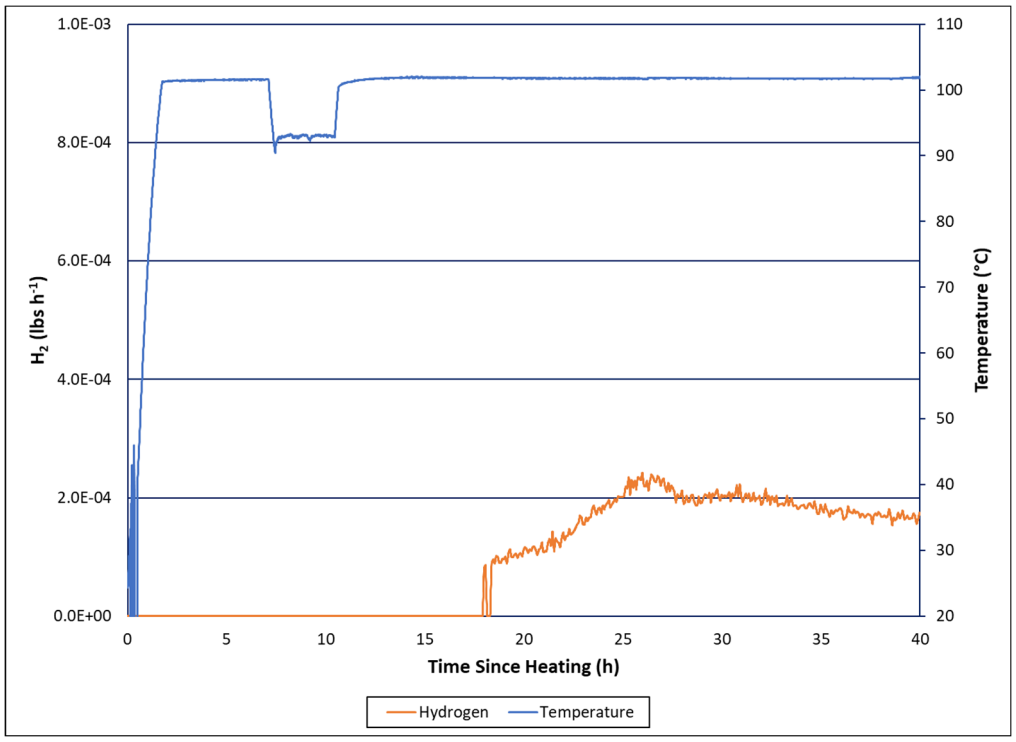

Figure D-16. Tk40-6 Hydrogen Generation Profile (lb/hr). Slurry temperature is given in blue.

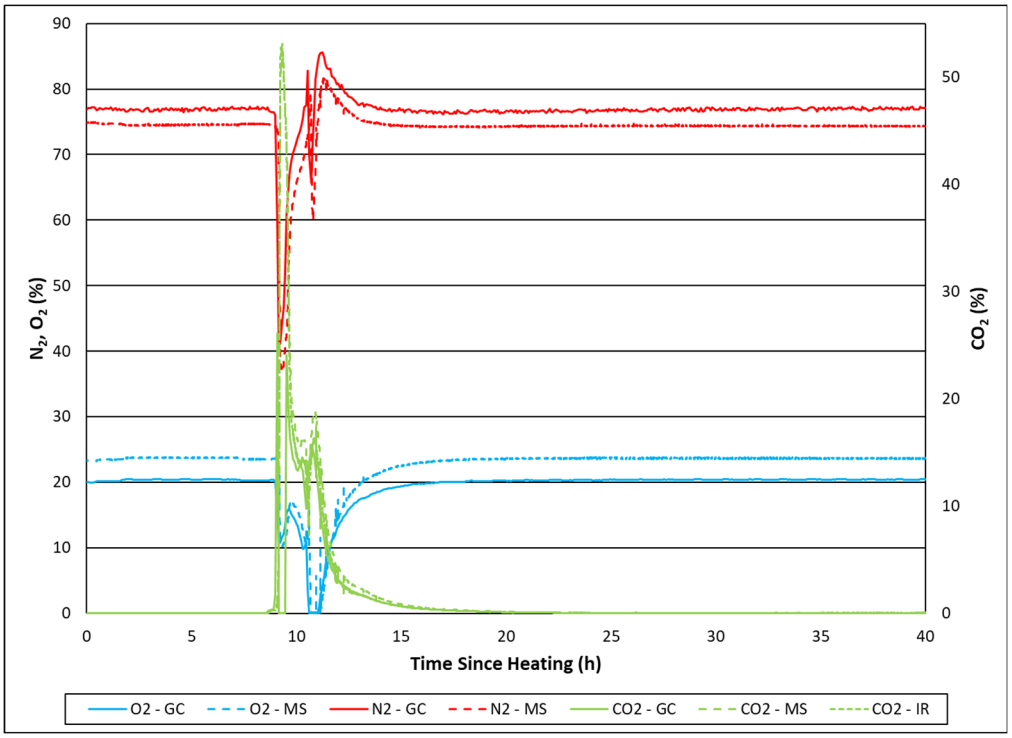

Figure D-17. Tk40-6 N_2 (red), O_2 (blue), and CO_2 (green) profiles (%).

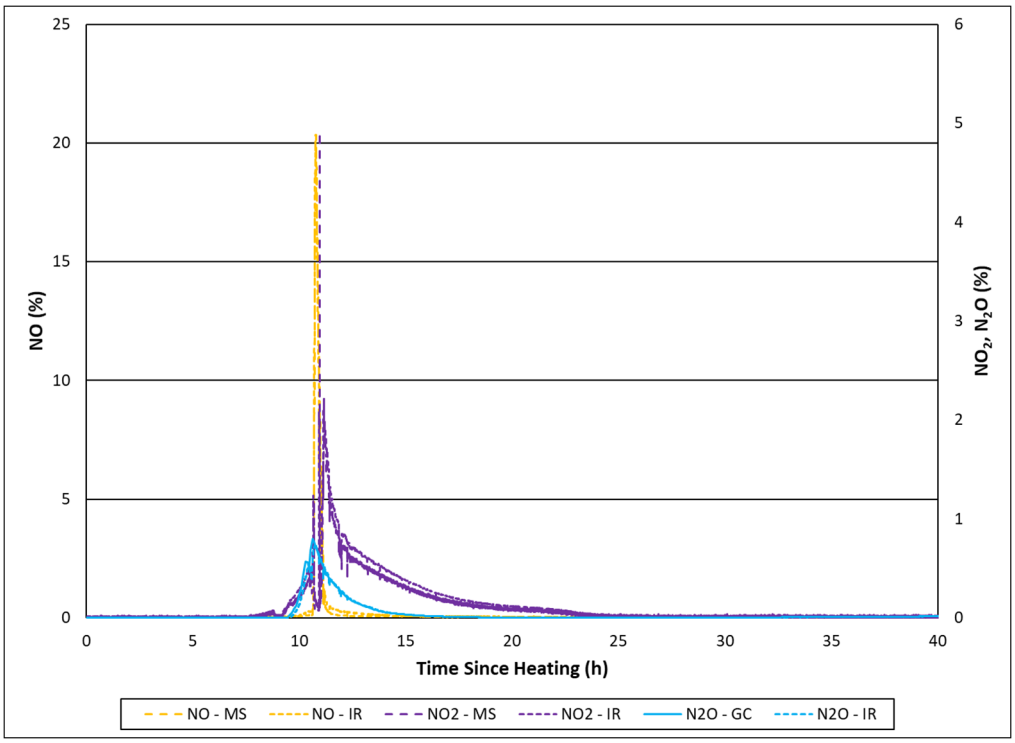

Figure D-18. Tk40-6 NO (orange), NO_2 (purple), and N_2O (blue) profiles (%).

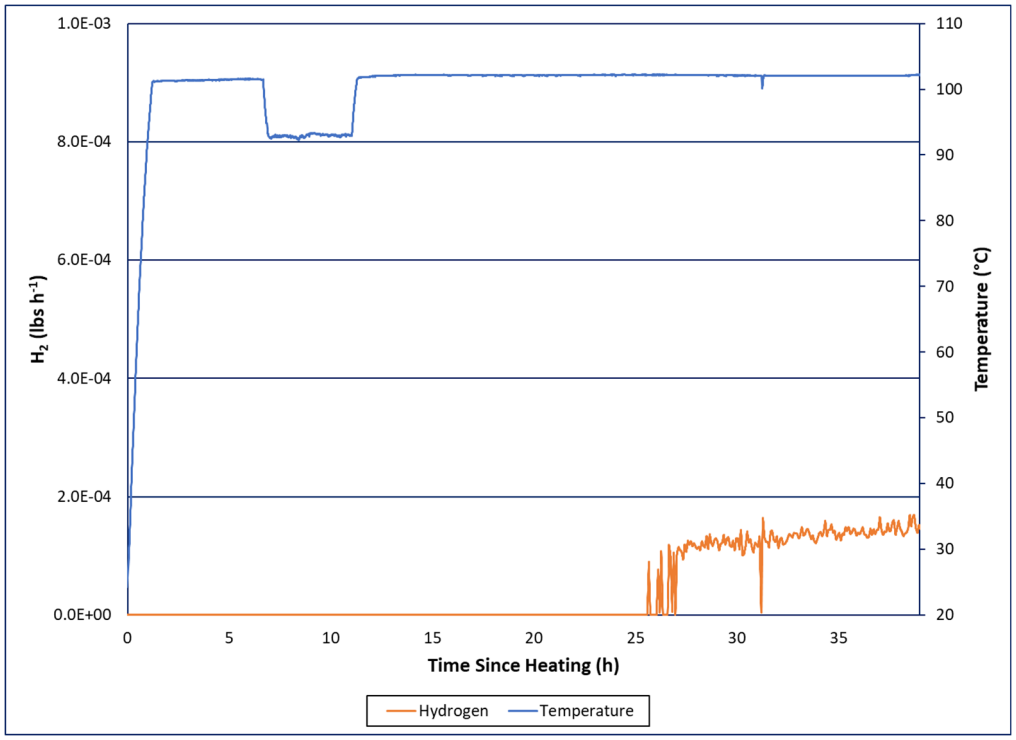

Figure D-19. Tk40-7 Hydrogen Generation Profile (lb/hr). Slurry temperature is given in blue.

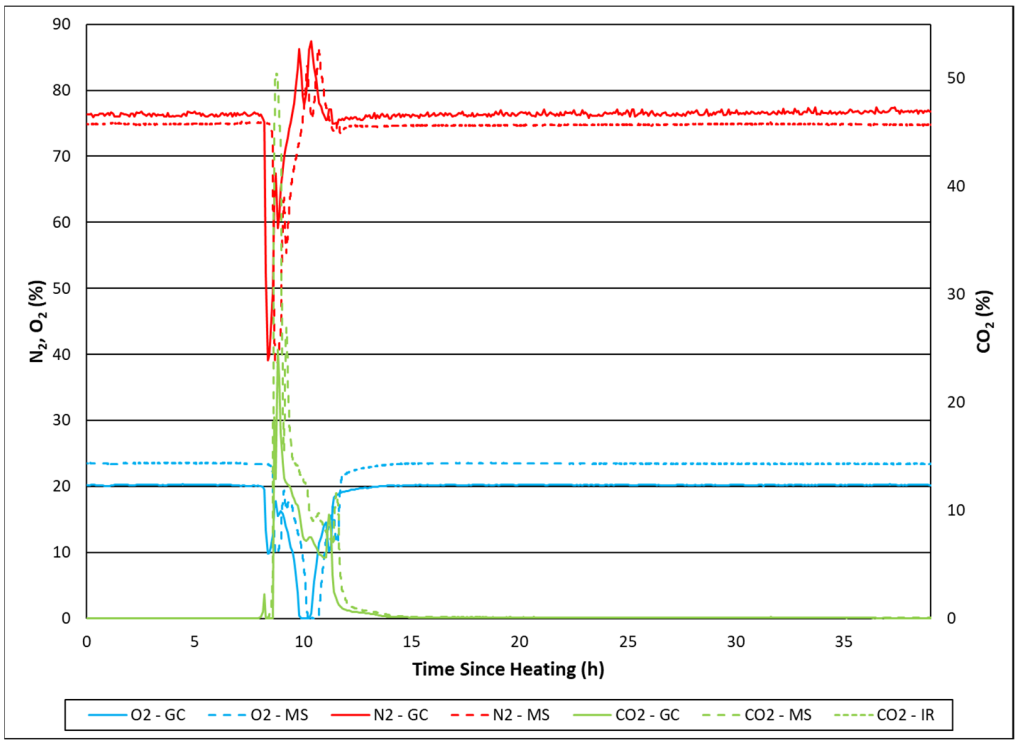

Figure D-20. Tk40-7 N_2 (red), O_2 (blue), and CO_2 (green) profiles (%).

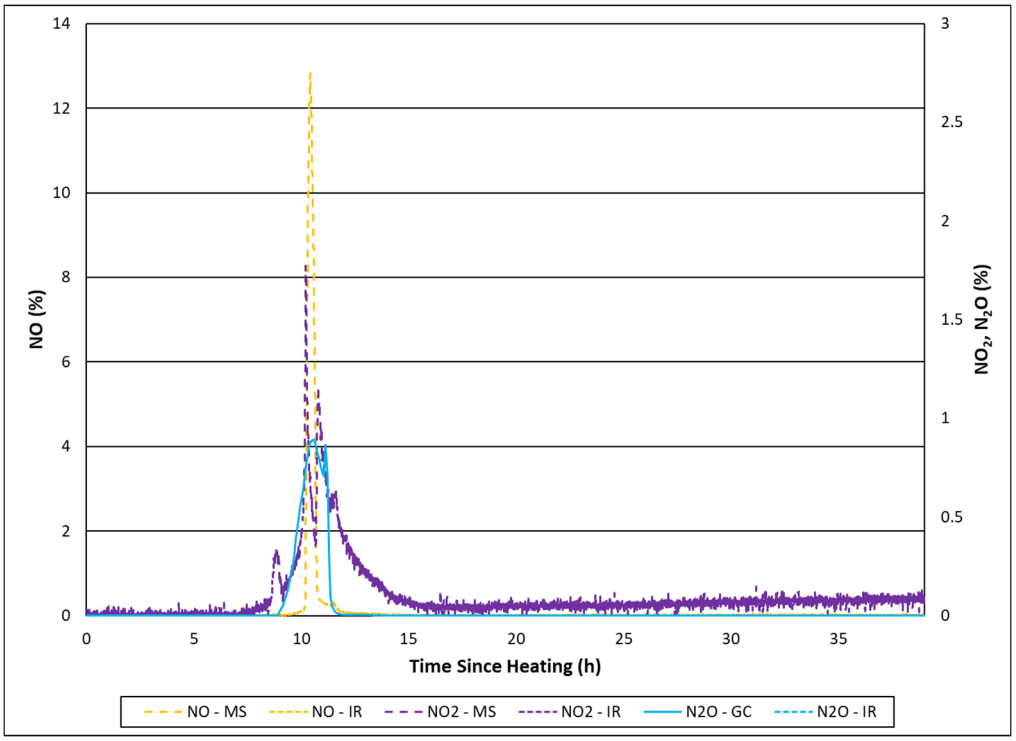

Figure D-21. Tk40-7 NO (orange), NO_2 (purple), and N_2O (blue) profiles (%).

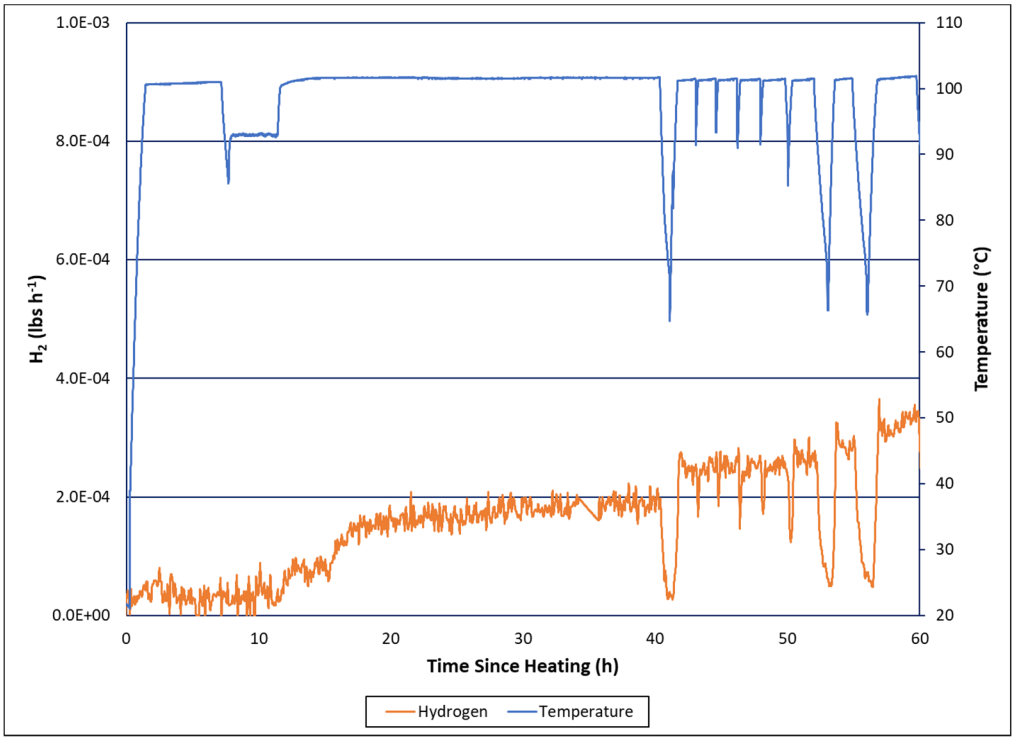

Figure D-22. Tk40-8 Hydrogen Generation Profile (lb/hr). Slurry temperature is given in blue.

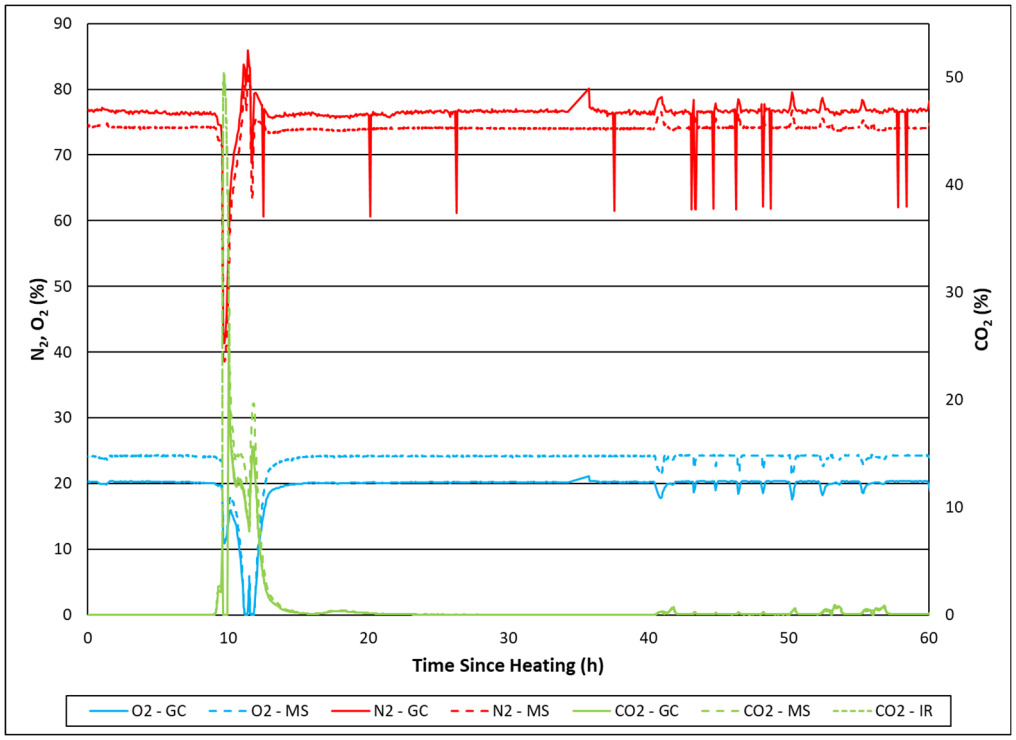

Figure D-23. Tk40-8 N_2 (red), O_2 (blue), and CO_2 (green) profiles (%).

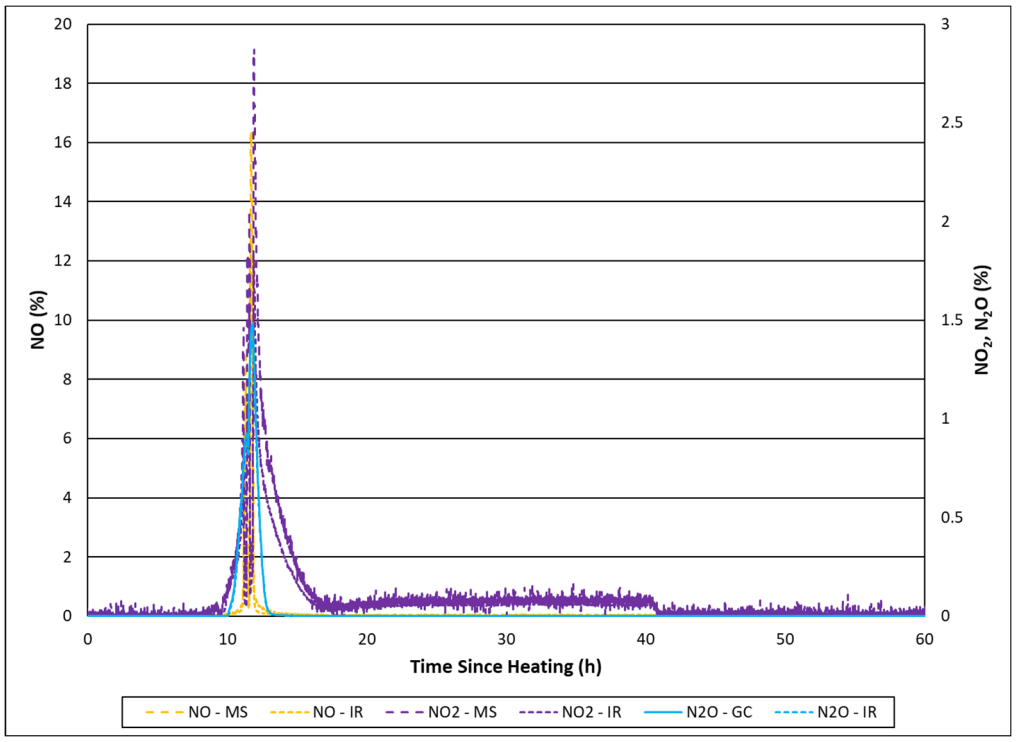

Figure D-24. Tk40-8 NO (orange), NO_2 (purple), and N_2O (blue) profiles (%).

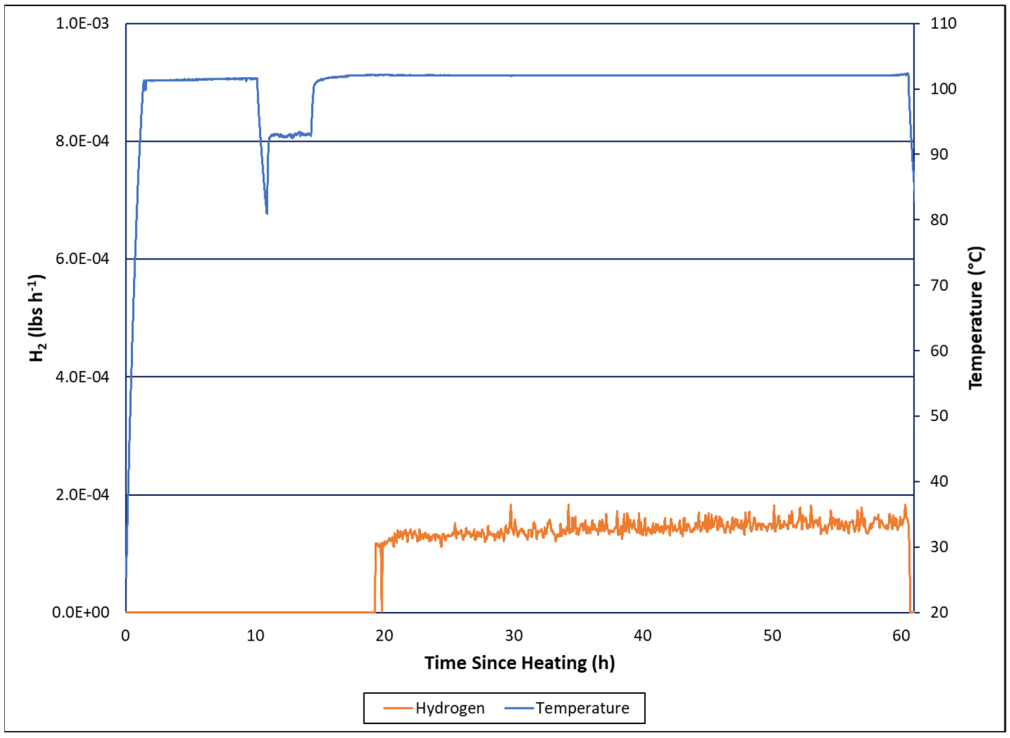

Figure D-25. Tk40-9 SRAT Cycle Hydrogen Generation Profile (lb/hr). Slurry temperature is given in blue.

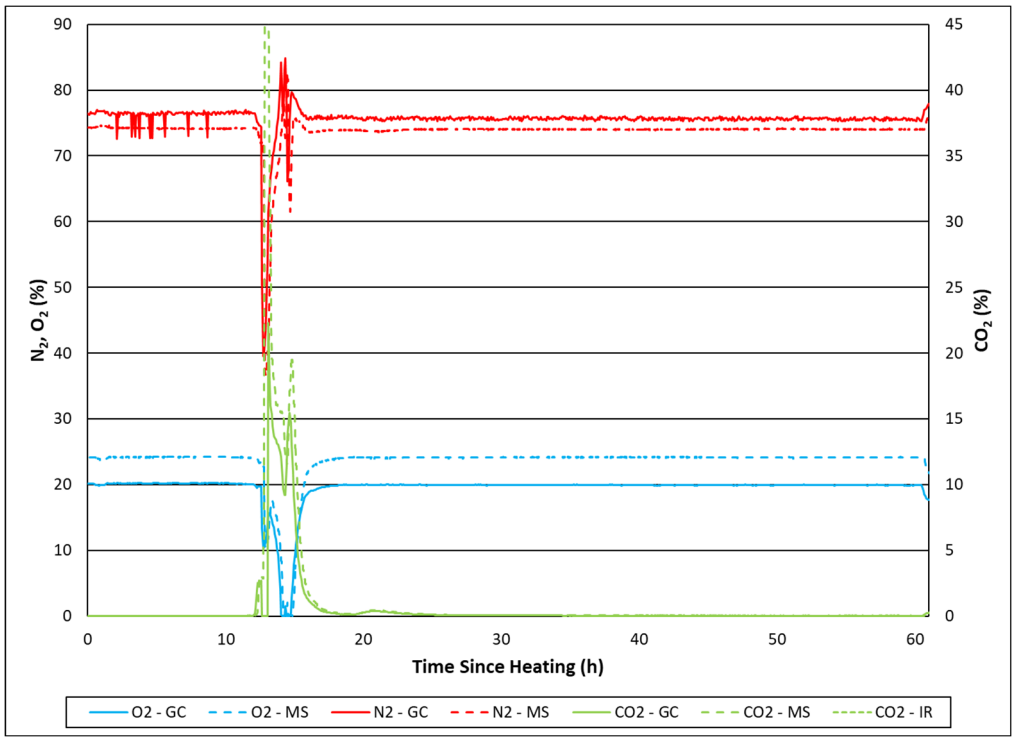

Figure D-26. Tk40-9 SRAT Cycle N_2 (red), O_2 (blue), and CO_2 (green) profiles (%).

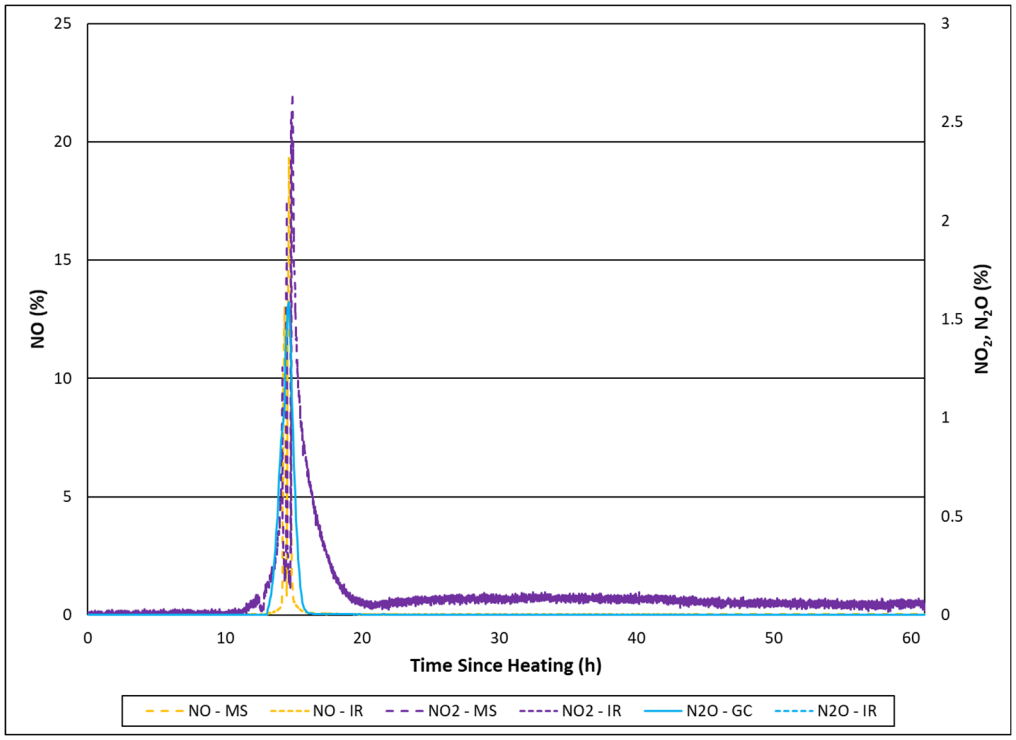

Figure D-27. Tk40-9 SRAT Cycle NO (orange), NO_2 (purple), and N_2O (blue) profiles (%).

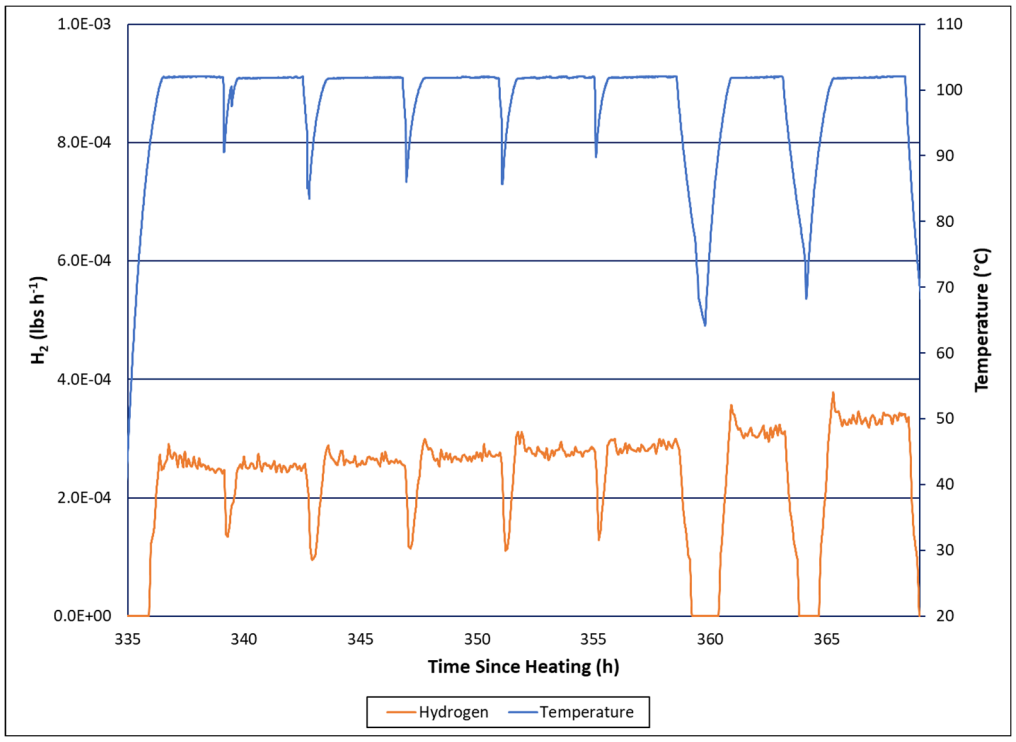

Figure D-28. Tk40-9 SME Cycle Hydrogen Generation Profile (lb/hr). Slurry temperature is given in blue.

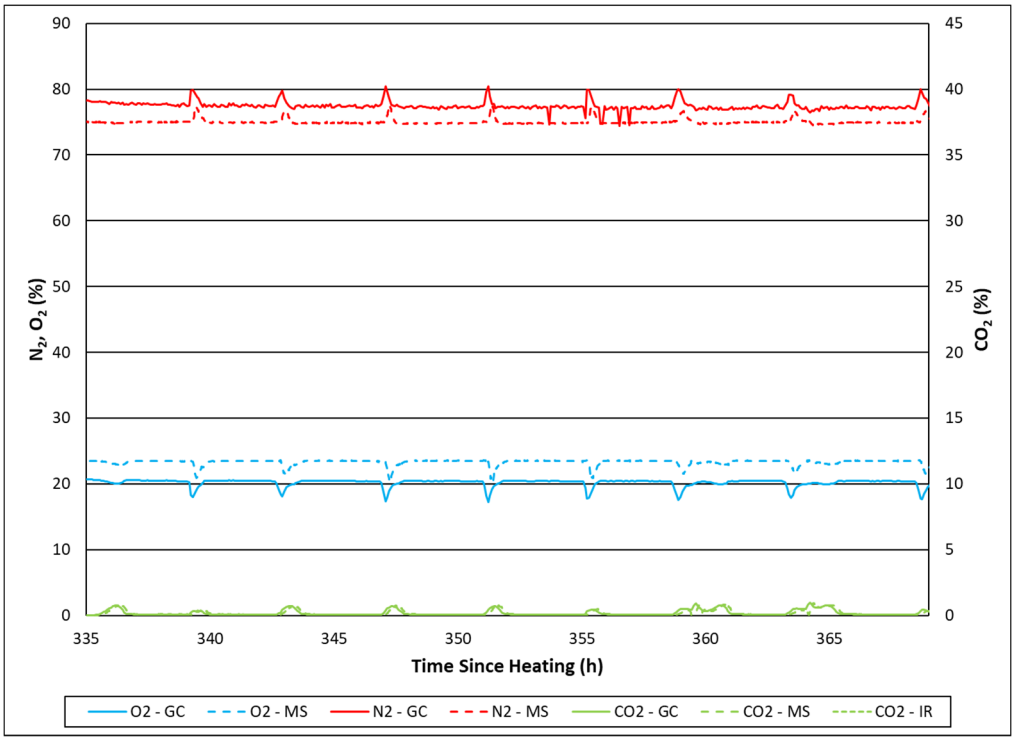

Figure D-29. Tk40-9 SME Cycle N_2 (red), O_2 (blue), and CO_2 (green) profiles (%).

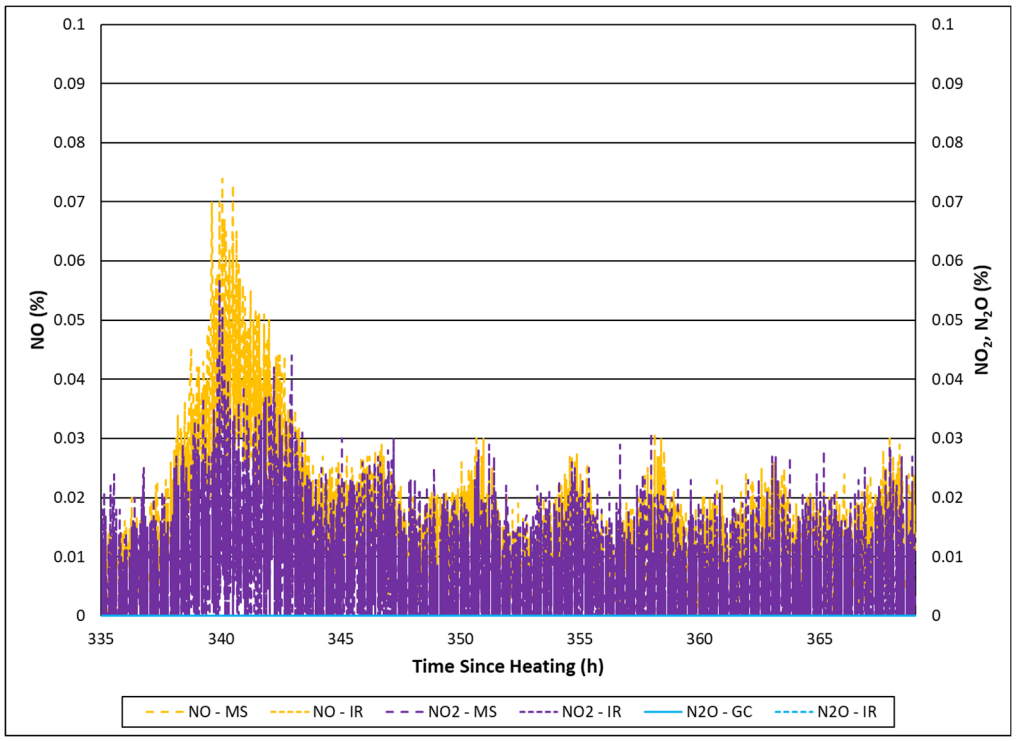

Figure D-30. Tk40-9 SME Cycle NO (orange), NO_2 (purple), and N_2O (blue) profiles (%).

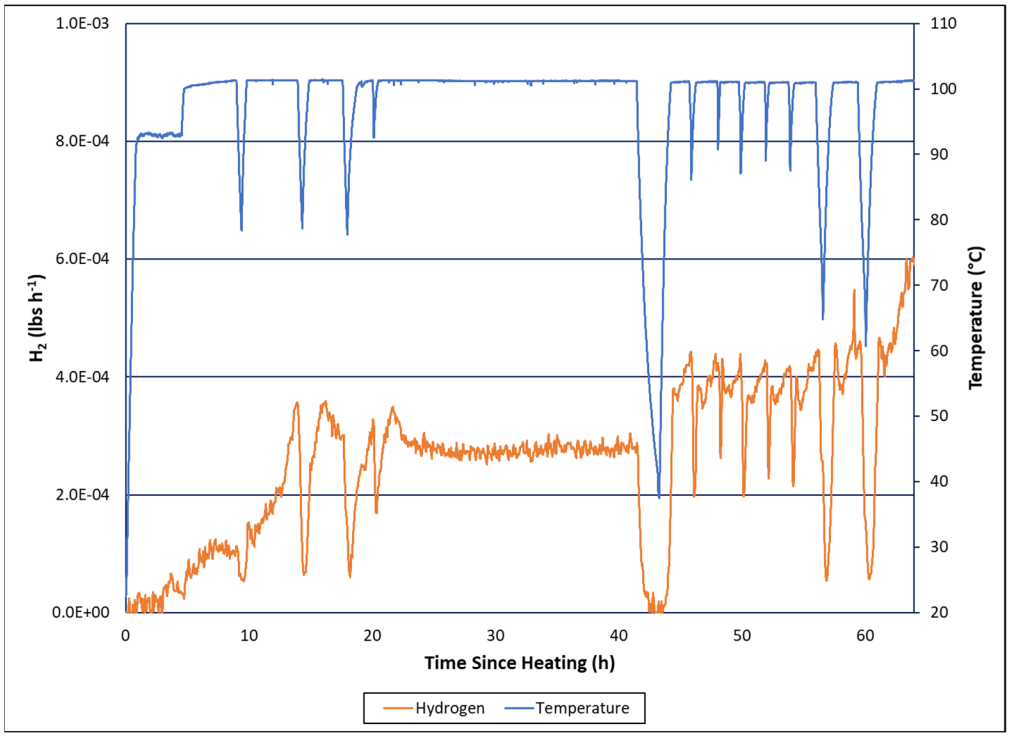

Figure D-31. Tk40-10 Hydrogen Generation Profile (lb/hr). Slurry temperature is given in blue.

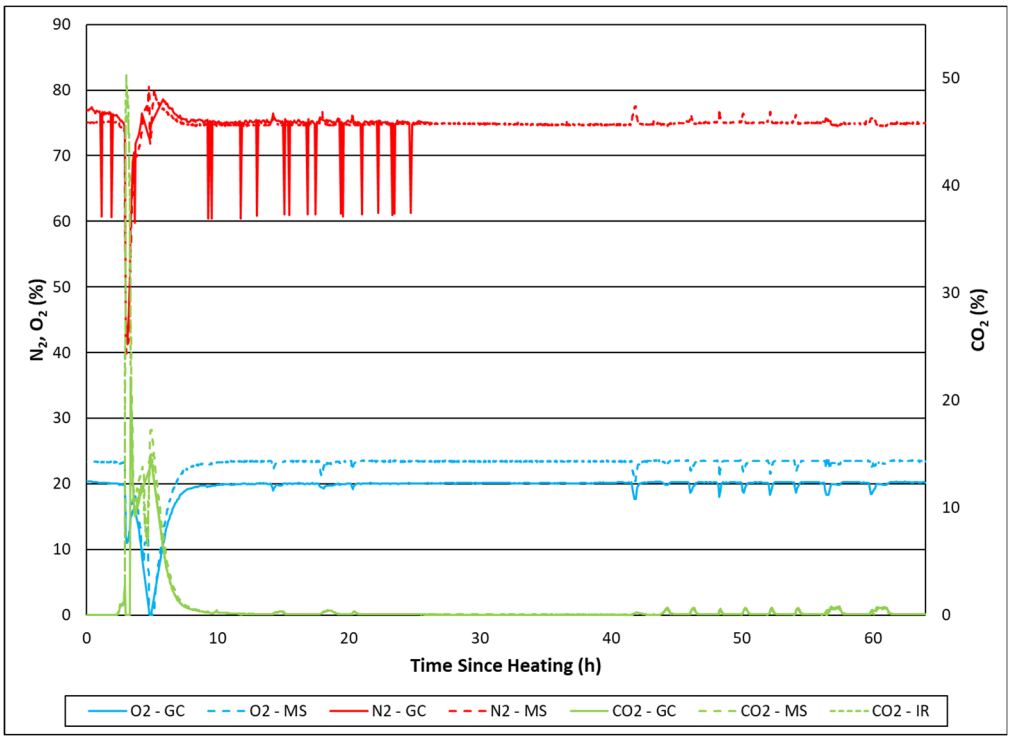

Figure D-32. Tk40-10 N_2 (red), O_2 (blue), and CO_2 (green) profiles (%).

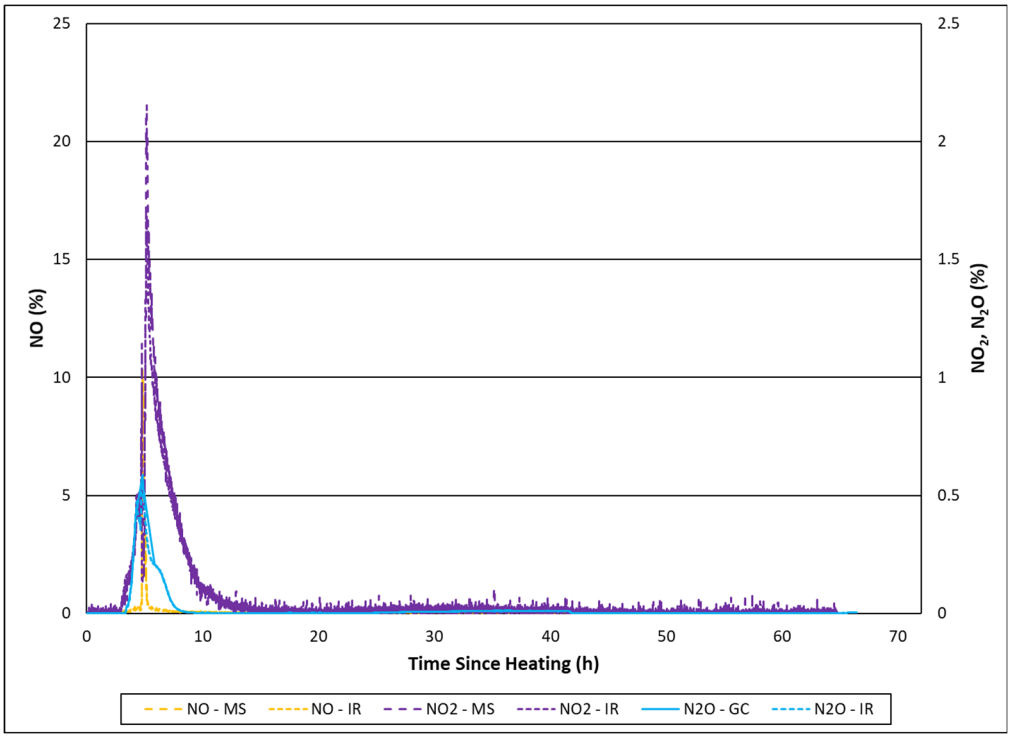

Figure D-33. Tk40-10 NO (orange), NO_2 (purple), and N_2O (blue) profiles (%).

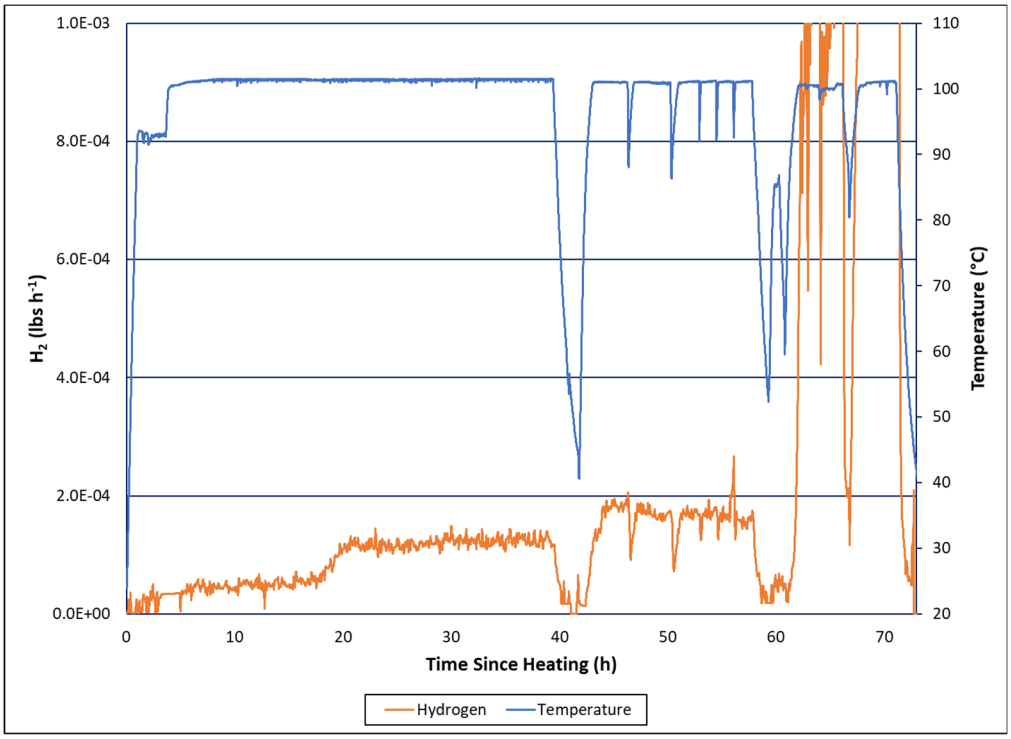

Figure D-34. Tk51-2 Hydrogen Generation Profile (lb/hr). Slurry temperature is given in blue.

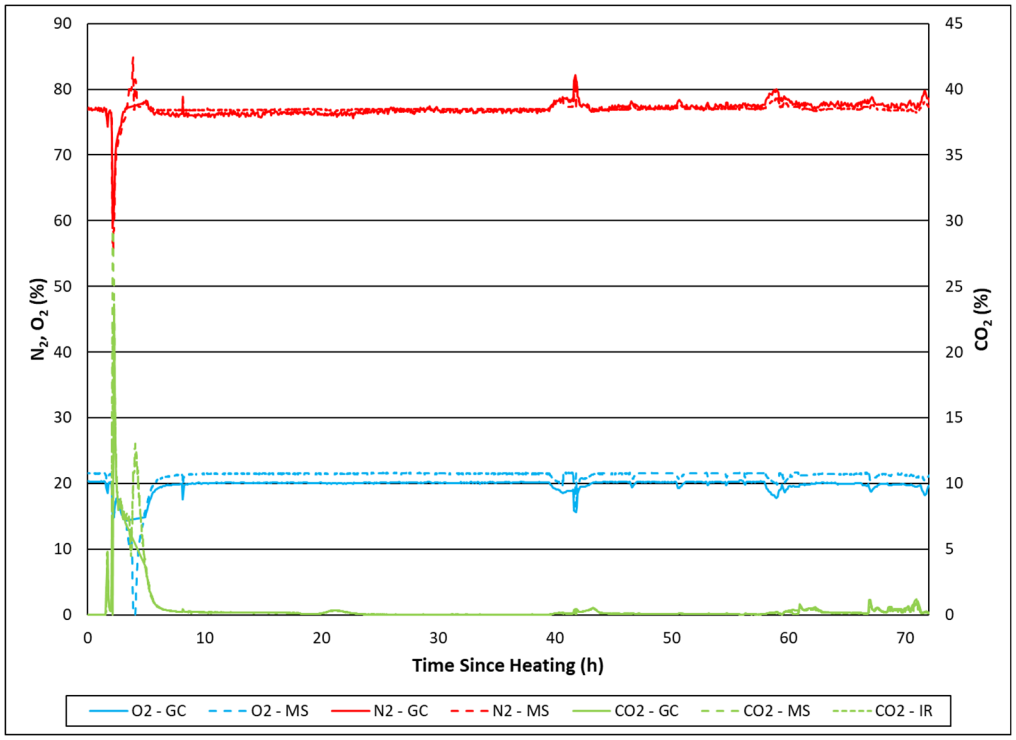

Figure D-35. Tk51-2 N_2 (red), O_2 (blue), and CO_2 (green) profiles (%).

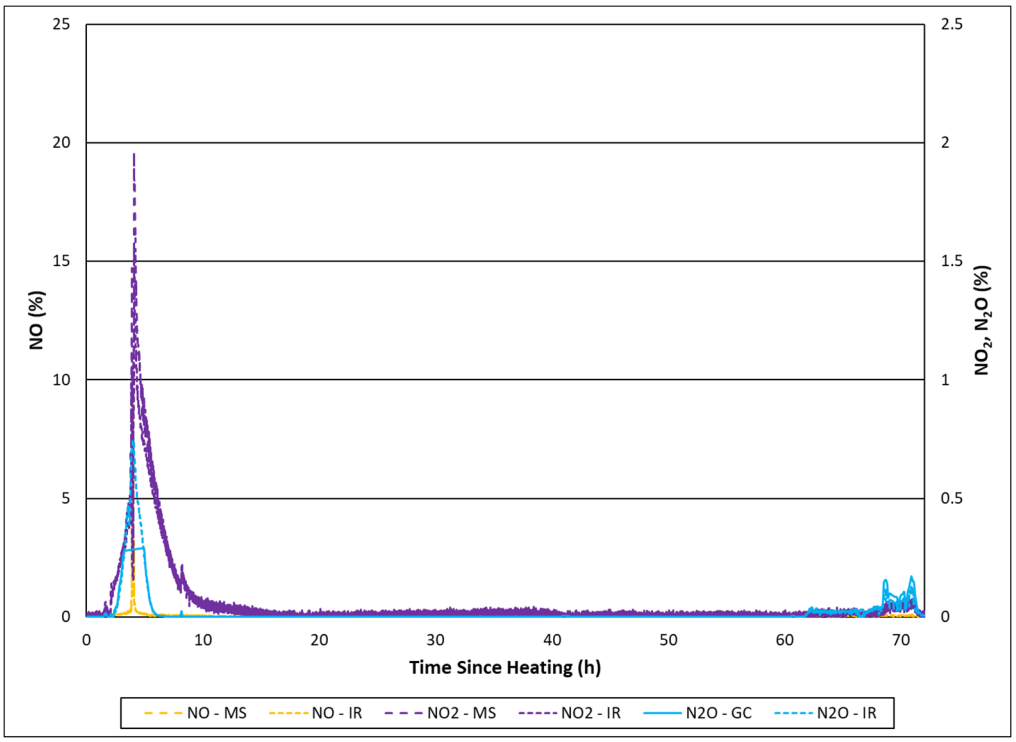

Figure D-36. Tk51-2 NO (orange), NO_2 (purple), and N_2O (blue) profiles (%).

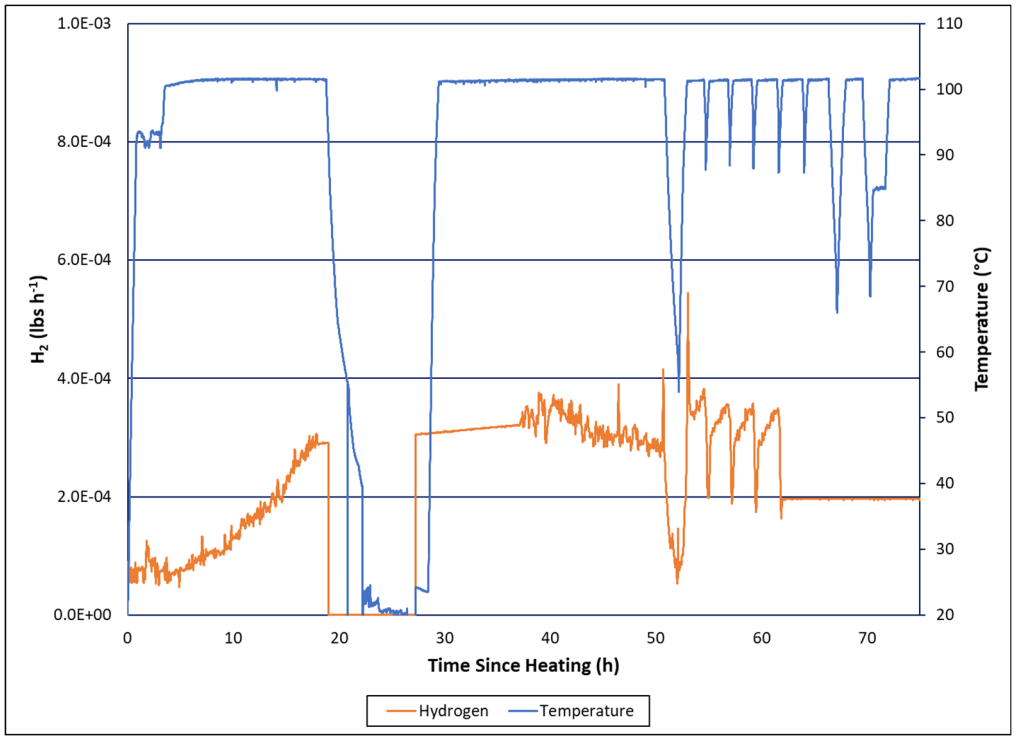

Figure D-37. Tk51-3 Hydrogen Generation Profile (lb/hr). Slurry temperature is given in blue.

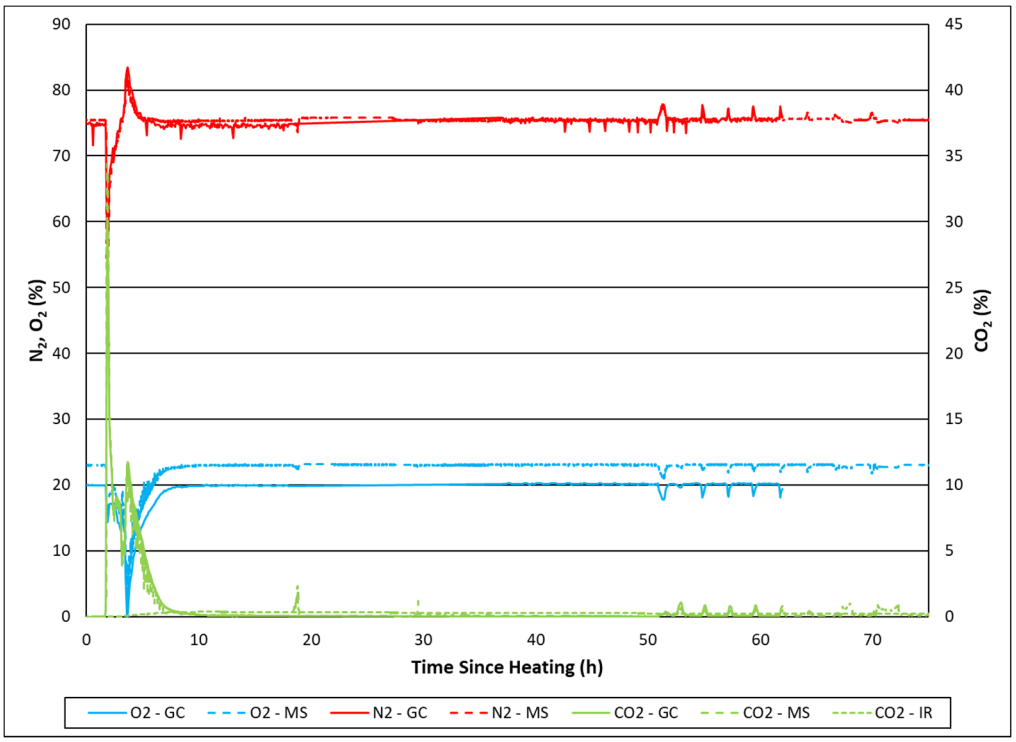

Figure D-38. Tk51-3 N_2 (red), O_2 (blue), and CO_2 (green) profiles (%).

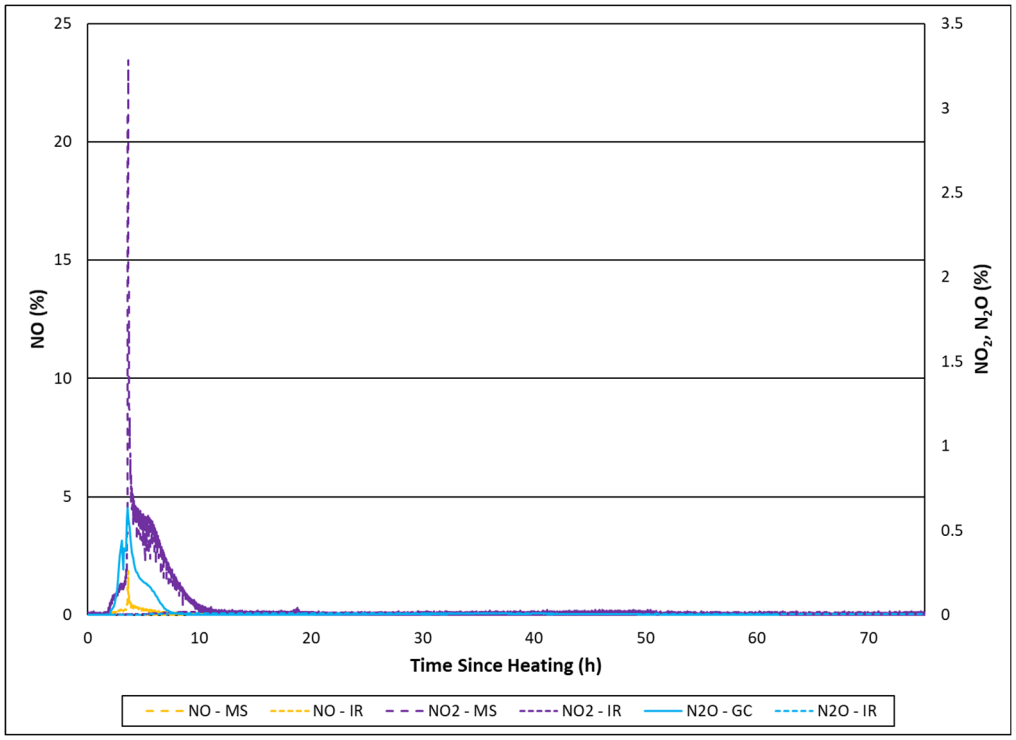

Figure D-39. Tk51-3 NO (orange), NO_2 (purple), and N_2O (blue) profiles (%).

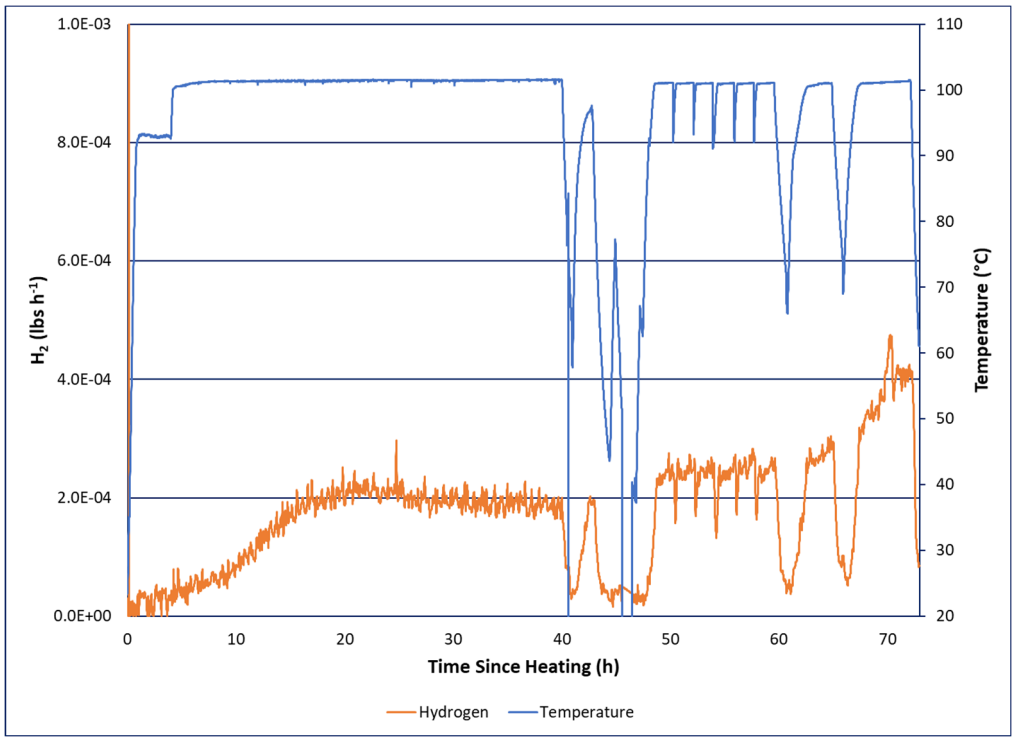

Figure D-40. Tk51-4 Hydrogen Generation Profile (lb/hr). Slurry temperature is given in blue.

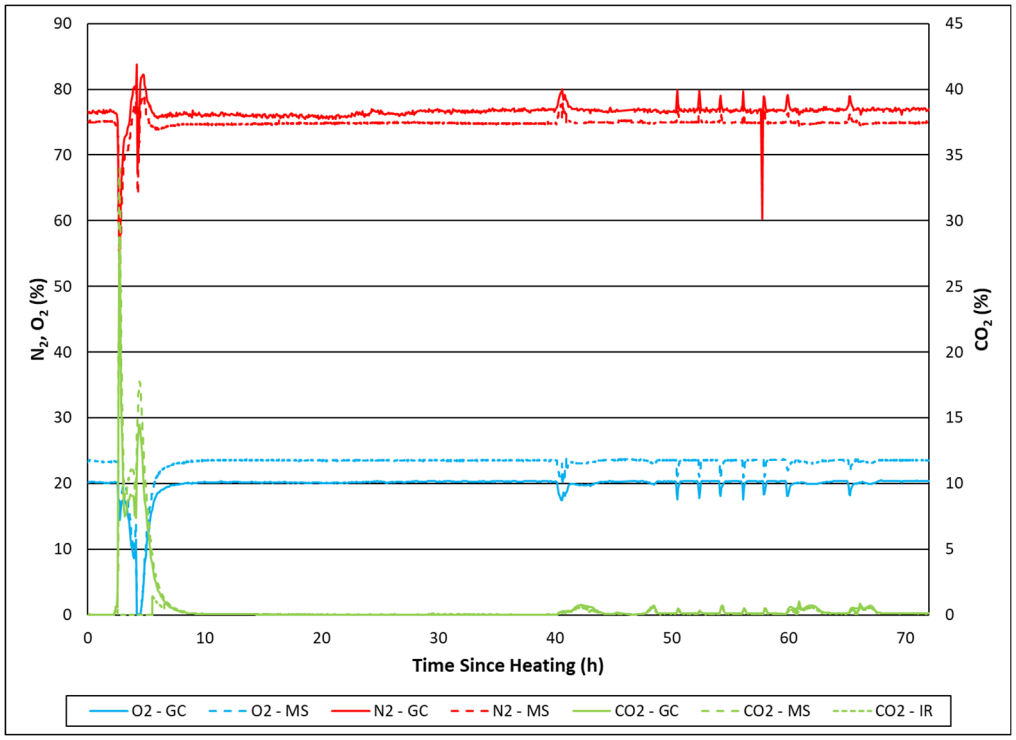

Figure D-41. Tk51-4 N_2 (red), O_2 (blue), and CO_2 (green) profiles (%).

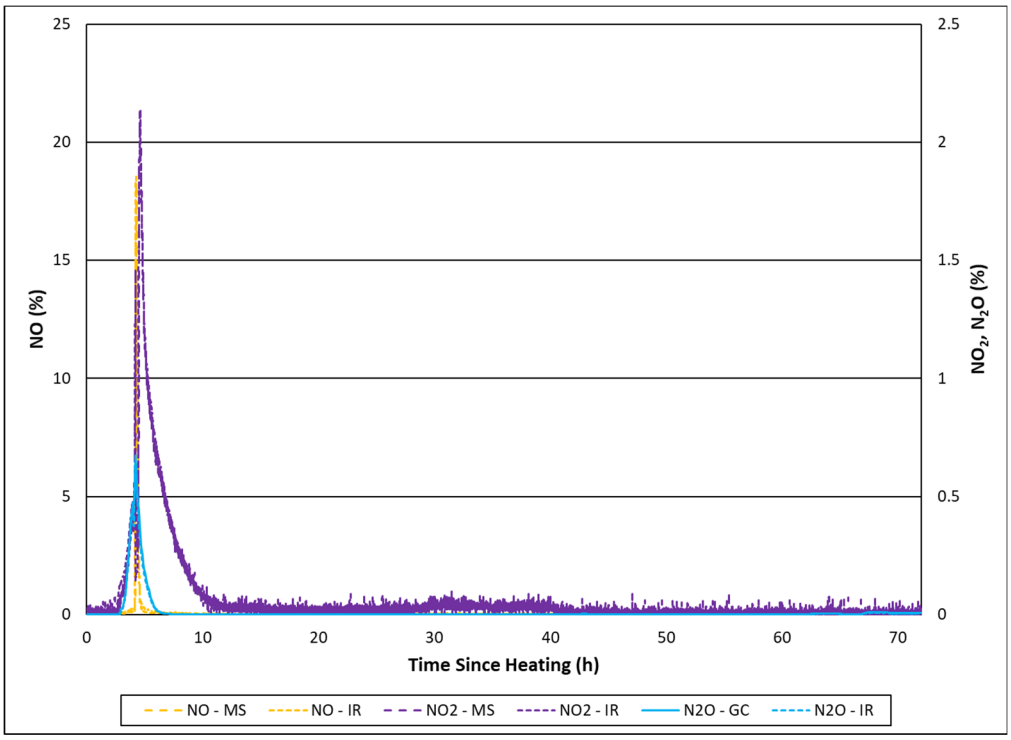

Figure D-42. Tk51-4 NO (orange), NO_2 (purple), and N_2O (blue) profiles (%).

Distribution:

a.fellinger@srnl.doe.gov
aaron.staub@srs.gov
alex.cozzi@srnl.doe.gov
amy.ramsey@srnl.doe.gov
anna.murphy@srs.gov
anthony.robinson@srs.gov
azadeh.samadi-dezfouli@srs.gov
barbara.hamm@srs.gov
bill.clark@srs.gov
bill.holtzscheiter@srs.gov
boyd.wiedenman@srnl.doe.gov
c.diprete@srnl.doe.gov
chris.martino@srnl.doe.gov
connie.herman@srnl.doe.gov
curtis.gardner@srs.gov
daniel.mccabe@srnl.doe.gov
david.crowley@srnl.doe.gov
eric.freed@srs.gov
erich.hansen@srnl.doe.gov
frank.pennebaker@srnl.doe.gov
gregg.morgan@srnl.doe.gov
hasmukh.shah@srs.gov
james.folk@srs.gov
jeff.ray@srs.gov
jeffrey.crenshaw@srs.gov
jeffrey.gillam@srs.gov
jeremiah.ledbetter@srs.gov
john.iaukea@srs.gov
john.mayer@srnl.doe.gov
joseph.manna@srnl.doe.gov
kevin.brotherton@srs.gov
maria.rios-armstrong@srs.gov
mark-a.smith@srs.gov
michael.stone@srnl.doe.gov
nancy.halverson@srnl.doe.gov
patricia.lee@srnl.doe.gov
patricia.suggs@srs.gov
paul.ryan@srs.gov
Records Administration (EDWS)
richard.edwards@srs.gov
spencer.isom@srs.gov
terri.fellinger@srs.gov
thomas.colleran@srs.gov
thomas.temple@srs.gov
tony.polk@srs.gov
vijay.jain@srs.gov
william.ramsey@srnl.doe.gov
helen.boyd@srs.gov
ben.dean@srs.gov
aubrey.silker@srs.gov
kirk.russell@srs.gov
thomas.huff@srs.gov
robert.hoeppel@srs.gov